

ICRR
ANNUAL
REPORT

APRIL 2006 — MARCH 2007

Institute for Cosmic Ray Research
University of Tokyo

INSTITUTE
FOR
COSMIC RAY RESEARCH
UNIVERSITY OF TOKYO

ANNUAL REPORT
(APRIL 2006 – MARCH 2007)

Editorial Board

MORI, Masaki

OBAYASHI, Yoshihisa

YASUDA, Naoki

KANEYUKI, Kenji

ITOH, Hideo

©Institute for Cosmic Ray Research, University of Tokyo

5-1-5, Kashiwanoha, Kashiwa, Chiba 277-8582 Japan

Telephone: (81) 4-7136-3102

Facsimile: (81) 4-7136-3115

WWW URL: <http://www.icrr.u-tokyo.ac.jp/>

TABLE OF CONTENTS

Preface	
Research Divisions	1
Neutrino and Astroparticle Division	2
High Energy Cosmic Ray Division	15
Astrophysics and Gravity Division	31
Observatories and a Research Center	46
Norikura Observatory	47
Akeno Observatory	51
Kamioka Observatory	53
Research Center for Cosmic Neutrinos	54
Appendix A. ICRR International Workshops	56
Appendix B. ICRR Seminars	56
Appendix C. List of Publications — 2006 fiscal year	58
(a) Papers Published in Journals	
(b) Conference Papers	
(c) ICRR Report	
Appendix D. Doctoral Theses	63
Appendix E. Public Relations	63
(a) ICRR News	
(b) Public Lectures	
(c) Visitors	
Appendix F. Inter-University Researches	65
Appendix G. List of Committee Members	68
(a) Board of Councillors	
(b) Advisory Committee	
(c) User's Committee	
Appendix H. List of Personnel	69

PREFACE

The Institute for Cosmic Ray Research, the inter-university institute, is closely associated with Japanese universities and foreign institutes. The experimental facilities located at the institute are jointly established and used by about 350 physicists in the community. We hope that we will continue to keep good collaborations and to keep providing important results on cosmic rays physics and related subjects although the national university system has been drastically changed in 2004.

The study of cosmic rays has often played a leading role when the particle physics has made a rapid progress. Pions and muons were discovered in the cosmic rays and those discoveries have yielded a fruitful outcome of the elementary particles using particle accelerators subsequently. The discovery of the neutrino mass has again brought a triumph of the cosmic ray research and it has opened up a new field.

The institute has three research divisions; Neutrino and Astro-particle Division, High Energy Cosmic Ray Division, and Astrophysics and Gravity Division. In each division, a few different types of experiments are conducted.

At Kamioka underground observatory, the Super-Kamiokande experiment is continuously producing interesting results. There are some other projects in Kamioka, for example, dark matter experiments and geo-physics experiments, which make use of advantages of the underground environments. A new experiment to study dark matter, XMASS, has been funded in 2007 and we expect to start the experiment in two years from now.

The construction of the prototype gravitational wave antenna is also in progress. The next big project of the institute is the gravitational wave detector (LCGT), by which the direct detection of the gravitational wave (GW) is aimed. The detection of the GW will proof the Einstein's theory of general relativity and can unveil dynamic features of the universe.

The Telescope Array project has almost been completed in November, 2007 and will produce interesting data soon. There is a steady flow of data from the experiment at Yangbajing (Tibet), and from the cosmic gamma-ray telescope (CANGAROO) deployed over the desert of Woomera (Australia).

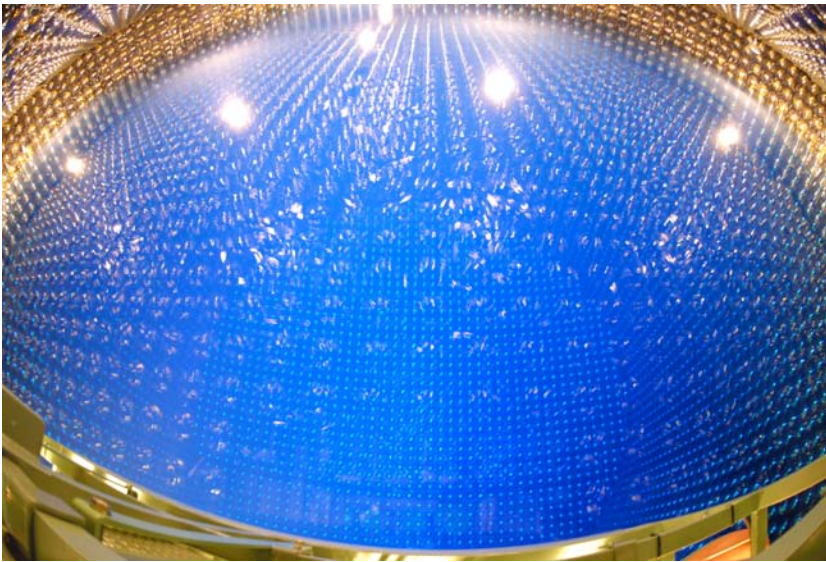
The underground physics and the ground based cosmic ray measurements overseas are the back-born of the institute.



Yoichiro Suzuki,
Director,
Institute for Cosmic Ray Research,
The University of Tokyo



The ICRR building at Kashiwa, Chiba, Japan.



The inner detector of Super-Kamiokande-III during the full reconstruction. The purified water is under filling.



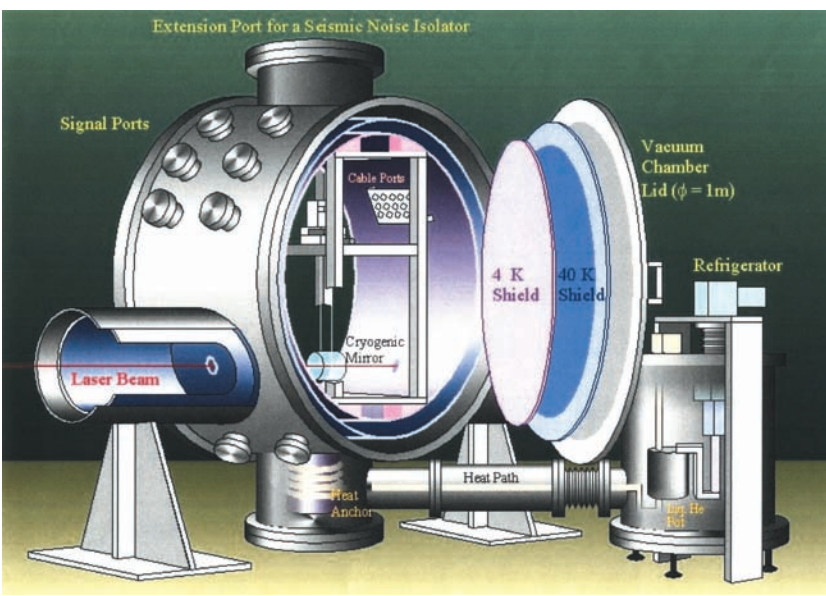
The system of four imaging atmospheric Cherenkov telescopes of 10m diameter of CANGAROO project for detection of very high energy gamma-rays. The whole system is in operation since March 2004 in Woomera, South Australia.



Tibet-III air shower array (37000 m²) at Yangbajing, Tibet (4300 m in altitude).



Air fluorescence telescopes (left) and a scintillator surface detector (right) of the Telescope Array experiment under construction in Utah, USA for the study of extremely high energy cosmic rays.



Cryogenic mirror suspension system for Large Scale Cryogenic Gravitational Wave Telescope.

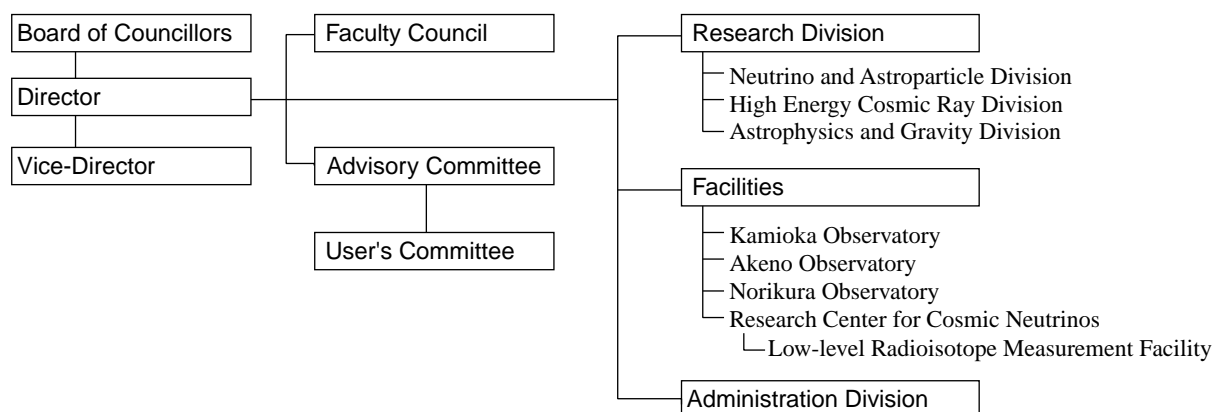


Wide-view telescope of 2.5 m diameter (left telescope) in Arizona, USA for the Sloan Digital Sky Survey project.



A public lecture held by Research Center for Cosmic Neutrinos.

Organization



Number of Staff Members in 2006

	Scientific Staff	Technical Staff	Research Fellows	Administrators and Secretaries	
Neutrino and Astroparticle Div.	18	5	5	13	41
High Energy Cosmic Ray Div.	14	14	11	4	43
Astrophysics and Gravity Div.	8	0	4	1	13
Administration	0	0	1	12	13
Total	40	19	21	30	110

FY 2001–2006 Budget

	2001	2002	2003	2004	2005	2006
Personnel expenses	418 475	460 332	434 874	539 000	465 000	566 000
Non-personnel expenses	1 518 584	1 518 065	1 785 449	1 902 000	1 822 000	812 000
Total	1 937 059	1 978 397	2 220 323	2 441 000	2 287 000	1 378 000

(in 1 000 yen)

RESEARCH DIVISIONS

Neutrino and Astroparticle Division

Overview

Super-Kamiokande Experiment

K2K Experiment

T2K Experiment

XMASS Experiment

High Energy Cosmic Ray Division

Overview

CANGAROO-III Project

TA: Telescope Array Experiment

Tibet AS γ Project

Ashra Project

Astrophysics and Gravity Division

Overview

TAMA Project

LCGT Project

Status of CLIO at Kamioka

Sloan Digital Sky Survey

Theory Group

CMB constraints on the fine structure constant

Cosmological Constraints on Gravitino LSP Scenario with Sneutrino NLSP

Graviton emission from a Gauss-Bonnet brane

New Two-loop Contributions to Hadronic EDMs in the MSSM

Electric Dipole Moments in PseudoDirac Gauginos

Non-perturbative effect on thermal relic abundance of dark matter

Late-time Affleck-Dine baryogenesis after thermal inflation

Affleck-Dine baryogenesis in anomaly-mediated supersymmetry breaking

Increasing the effective number of neutrinos with decaying particles

Implication of Dark Energy Parametrizations on the Determination of the Curvature of the Universe

Dark matter in universal extra dimension model

Power Spectrum of the Density Perturbations From Smooth Hybrid New Inflation Model

Baryogenesis via left-right asymmetry generation by Affleck-Dine mechanism in Dirac neutrino model

NEUTRINO AND ASTROPARTICLE DIVISION

Overview

This division aims to study particle physics that is not accessible within accelerator facilities, with prime interests in physics of neutrinos and proton decay, and astroparticle physics with the use of underground experimental facilities.

Our most important facility is the Super-Kamiokande (SK) that is a 50 kton water Cherenkov detector. SK took data from April 1996 to July 2001 (SK-I phase) using 11,146 50cm-diameter photomultipliers (PMTs) for its inner detector and 1,885 20cm-diameter PMTs for its outer detector. The most important physics results are the discovery of neutrino oscillation in the atmospheric neutrino in 1998, demonstrating that neutrinos have a finite mass, and the accurate measurement of the solar neutrino flux from the decay of ^8B which served to confirm the long-conjectured neutrino oscillation hypothesis in solar neutrinos beyond doubt. The search for nucleon decay at SK gives the current severest limit, which constrains strongly the grand unification scenario of particle interactions. SK has been monitoring neutrinos from supernova burst. If a supernova burst occurs at the distance to the center of our galaxy, SK is able to detect about 8,000 neutrino events. A high intensity neutrino beam experiment using J-PARC (T2K) is expected to start in 2009 and SK detector will be the far detector of the experiment. High precision measurement of oscillation parameters and the third oscillation pattern (the effect of the mixing angle θ_{13}) will be investigated by T2K. After the accident in 2001, SK detector had been running using about 5,200 50cm-diameter PMTs until October 2005 (called as the SK-II data taking period). Mounting about 6000 PMTs in order to fully reconstruct the detector was performed from October 2005 through April 2006 and fully recovered detector has been running since July 2006 (called as SK-III data taking period).

Another activity of the Neutrino and Astroparticle division is a multi-purpose experiment using liquid xenon aiming at the detection of cold dark matter, neutrino absolute mass using neutrinoless double beta decay, and low energy solar neutrinos. An R&D study for the liquid xenon detector had been performed at the underground laboratory and the construction of the 800kg detector will be started from 2007.

Recent progress of research activities in the Neutrino and Astroparticle division is presented here.

Super-Kamiokande Experiment

[Spokesperson : Yoichiro Suzuki]

Kamioka Observatory, ICRR, Univ. of Tokyo, Gifu, 506-1205

In collaboration with the members of:

Kamioka Observatory, ICRR, Univ. of Tokyo, Japan; RCCN, ICRR, Univ. of Tokyo, Japan; Boston Univ., USA; BNL, USA; Univ. of California, Irvine, USA; California State

Univ., Dominguez Hills, USA; Chonnam National Univ., Korea; Duke Univ., USA; George Mason Univ., USA; Gifu Univ., Japan; Univ. of Hawaii, USA; Indiana Univ., USA; KEK, Japan; Kobe Univ., Japan; Kyoto Univ., Japan; LANL, USA; Louisiana State Univ., USA; Univ. of Maryland, USA; Univ. of Minnesota, USA; Miyagi Univ. of Education, Japan; SUNY, Stony Brook, Japan; Nagoya Univ., Japan; Niigata Univ., Japan; Okayama Univ., Japan; Osaka Univ., Japan; Seoul National Univ., Japan; Shizuoka Seika College, Japan; Shizuoka Univ., Japan; Sungkyunkwan Univ., Korea; Tohoku Univ., Japan; Univ. of Tokyo, Japan; Tokai Univ., Japan; Tokyo Inst. of Tech., Japan; Inst. of Experimental Physics, Poland; Univ. of Washington, USA.

Introduction

Super-Kamiokande (SK) is a large water Cherenkov detector, located 1000 m underground in Kamioka mine, Japan. 50 kton of pure water is contained in a stainless steel tank of 39.3 meters in diameter and 41.4 m in height. SK took data from April 1996 to July 2001 (SK-I phase) using 11,146 20-inch photomultipliers (PMTs) for inner detector and 1,885 8-inch PMTs for outer detector. After the accident in November 2001, the detector was reconstructed in 2002 using about 5200 20-inch PMTs. The detector has been running as the second phase of the experiment (SK-II) since December 2002.

In this report, those results are described.

SK Full Reconstruction

The full reconstruction of the Super-Kamiokande detector occurred throughout 2005 and 2006. About 60% of the detector PMTs were lost in the 2001 accident, and the remainder were re-mounted in 2002. These tubes and about 6000 new PMTs produced from 2003 to 2005, were then mounted and installed again from July 2005 to April 2006.

The PMTs were assembled with acrylic and FRP cases in order to prevent the production of a shockwave in the event of an implosion. (Tubes from in 2002 were similarly encased). Assembly work started July 2005 and finished March 2006. Mounting the PMTs was performed October 2005 through April 2006. Connecting the PMT cables to the electronics huts outside of the tank was done in parallel to the mounting work.

After finishing the reconstruction work, the SK tank was filled with pure water as shown in Figure 1. On July 11, 2006 SK started taking data as "SK-3."

Atmospheric neutrinos

Cosmic ray interactions in the atmosphere produce neutrinos. The prediction of the absolute flux has an uncertainty

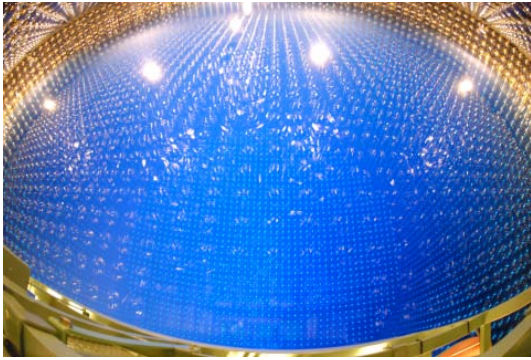


Fig. 1. SK full reconstruction has finished and the tank is almost full of pure water. Photo taken in July 2006.

of at least $\pm 20\%$. However, the flavor ratio of the atmospheric neutrino flux, $(\nu_\mu + \bar{\nu}_\mu)/(\nu_e + \bar{\nu}_e)$, has been calculated to an accuracy of better than 5%. Another important feature of atmospheric neutrinos is that the fluxes of upward and downward going neutrinos are expected to be nearly equal for $E_\nu > (\text{a few GeV})$ where the geomagnetic effect on primary cosmic ray is negligible.

SK-I observed 12,180 fully-contained (FC) events and 911 partially-contained (PC) events during 1489 days of data taking and SK-II observed 6605 FC events and 427 PC events during 804 days. FC events deposit all of their Cherenkov light in the inner detector, while PC events have exiting tracks which deposit some Cherenkov light in the outer detector. The neutrino interaction vertex was required to have been reconstructed within the 22.5 kiloton fiducial volume, defined to be > 2 m from the PMT wall.

The FC events were classified into “sub-GeV” ($E_{vis} < 1330$ MeV) and “multi-GeV” ($E_{vis} > 1330$ MeV) samples. The numbers of observed and predicted events for sub- and multi-GeV energy regions in SK are summarized in Table 1. The prediction is based on the recent precise measurements of primary cosmic rays by BESS and AMS and a three dimensional calculation of the neutrino flux by Honda et al. The hadronic interaction model of cosmic rays is also improved in the calculation.

Among FC events, single-ring events are identified as e -like or μ -like based on a Cherenkov ring pattern. All the PC events were assigned to be multi-GeV μ -like. Using the number of e -like and μ -like events, the ratio of (μ/e) was obtained and it is significantly smaller than the expectation as shown in the table. Momentum resolution for SK-II is slightly worse than SK-I. This is because the number of ID PMTs in SK-II is about a half of SK-I. However, the performance of the vertex reconstruction, the ring counting, and the particle identification in SK-II are almost the same as in SK-I.

The zenith angle distributions for the sub- and multi-GeV samples are shown in Fig. 2. The μ -like data from SK exhibited a strong up-down asymmetry in zenith angle (Θ) while no significant asymmetry was observed in the e -like data. The data were compared with the Monte Carlo expectation without neutrino oscillations and the best-fit expectation for $\nu_\mu \leftrightarrow \nu_\tau$ oscillations. The oscillated Monte Carlo reproduced well the zenith angle distributions of the data. Some fraction of the

Table 1. Summary of the atmospheric $(\mu/e)_{data}/(\mu/e)_{MC} (\equiv R)$ ratio measurement.

	SK-I		SK-II	
	Data	MC	Data	MC
Sub-GeV				
e -like	3353	2879.8	1842	1554.5
μ -like	3227	4212.8	1723	2215.4
R	$0.658 \pm 0.016 \pm 0.035$		$0.656 \pm 0.022 \pm 0.033$	
Multi-GeV				
e -like	746	680.5	417	426.2
μ -like(FC+PC)	1562	2029.5	806	1103.8
R	$0.702^{+0.032}_{-0.030} \pm 0.101$		$0.746^{+0.047}_{-0.044} \pm 0.056$	

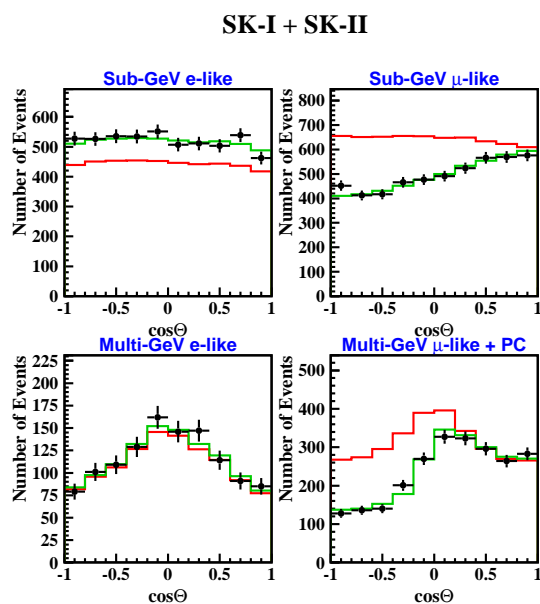


Fig. 2. The zenith angle distributions for sub-GeV e -like, sub-GeV μ -like, multi-GeV e -like and multi-GeV (FC+PC) μ -like events. $\cos\Theta = 1$ means down-going particles. The red histograms show the MC prediction for the no neutrino oscillation case. The green histograms show the Monte Carlo prediction for $\nu_\mu \leftrightarrow \nu_\tau$ oscillations with $\sin^2 2\theta = 1.0$ and $\Delta m^2 = 2.5 \times 10^{-3} \text{eV}^2$.

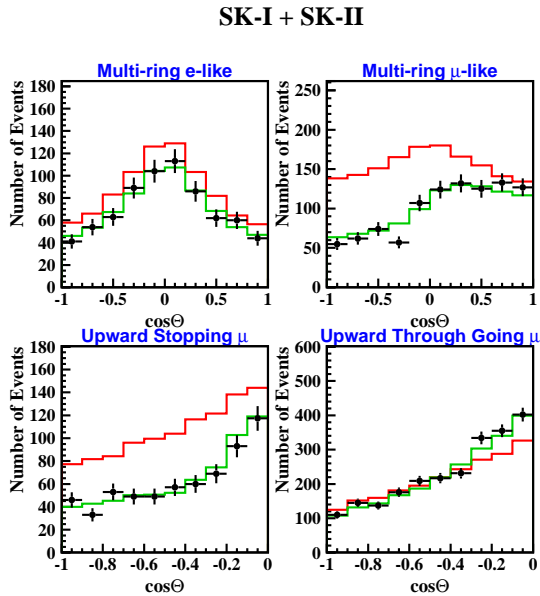


Fig. 3. The zenith angle distributions for multi-ring sub-GeV μ -like (upper left) and multi-ring multi-GeV μ -like (lower left) samples. The zenith angle distributions of upward stopping muons (upper right) and upward through-going muons (lower right). The red histograms show expectations without neutrino oscillations. The green histograms show the expected flux for the $\nu_\mu \leftrightarrow \nu_\tau$ oscillation with $\sin^2 2\theta = 1.0$ and $\Delta m^2 = 2.5 \times 10^{-3} \text{eV}^2$.

multi-ring events is also subdivided into e -like and μ -like events using the event pattern of the most energetic Cherenkov ring in each event. Fig. 3 shows the zenith angle distribution of multi-ring events and they also agree well with the expectations from neutrino oscillations.

Energetic atmospheric ν_μ 's passing through the Earth interact with rock surrounding the detector and produce muons via charged current interactions. These neutrino events are observed as upward going muons. Upward going muons are classified into two types. One is ‘‘upward through-going muons’’ which have passed through the detector, and the other is ‘‘upward stopping muons’’ which come into and stop inside the detector. The mean neutrino energies of upward through-going muons and upward stopping muons are ~ 100 GeV and ~ 10 GeV, respectively. SK-I observed 1856 upward through-going muons and 458 upward stopping muons during 1646 days’ live time and SK-II observed 889 and 228 events during 828 days, respectively. Fig. 3 shows the zenith-angle distributions of those upward muons. They agree with the expectations assuming neutrino oscillations.

We carried out a neutrino oscillation analysis using the entire SK-I and II atmospheric neutrino data. Fig. 4 shows the allowed neutrino oscillation parameter regions for $\nu_\mu \leftrightarrow \nu_\tau$ oscillations. The best fit oscillation parameters are $\sin^2 2\theta = 1.0$ and $\Delta m^2 = 2.5 \times 10^{-3} \text{eV}^2$. The allowed oscillation parameter range is obtained to be $\sin^2 2\theta > 0.93$ and $\Delta m^2 = (1.9 - 3.1) \times 10^{-3} \text{eV}^2$ at 90% C.L.

The atmospheric neutrino data is well described by the neutrino oscillations shown above. In this case, the survival probability of ν_μ is given by a sinusoidal function of L/E , where L is the travel distance, E is the neutrino energy. How-

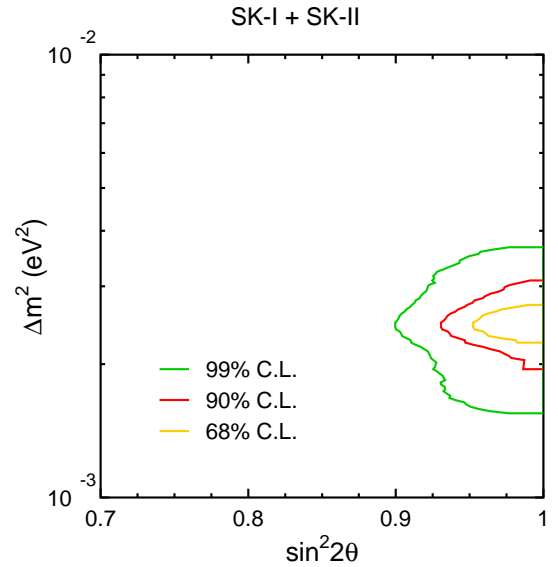


Fig. 4. Allowed region of $\nu_\mu \rightarrow \nu_\tau$ neutrino oscillation parameters obtained by SK by using contained atmospheric neutrino events and the upward-going muon events.

ever, the sinusoidal L/E dependence of the survival probability of ν_μ has not yet been directly observed. We used a selected sample of these atmospheric neutrino events, those with good resolution in L/E , to search for an oscillation maximum in the L/E distribution.

The neutrino energy, E , was estimated from the total energy of charged particles observed in the inner detector. The flight length of neutrinos, L , which ranges from approximately 15 km to 13,000 km depending on the zenith angle, was estimated from the reconstructed neutrino direction. The neutrino direction was taken to be along the total momentum vector from all observed particles. Since the correlation between neutrino directions and the directions of observed particles are taken into account in Monte Carlo simulations, we applied same analysis both for real events and Monte Carlo events. We applied a cut to reject low energy or horizontal-going events since they have either large scattering angles or large $dL/d\Theta_{\text{zenith}}$.

Fig. 5 shows the observed L/E distribution after taking ratio to the Monte Carlo events without neutrino oscillations. In the figure, a dip, which should correspond to the first oscillation maximum, is observed around $L/E = 500 \text{km/GeV}$. The distribution was fit assuming $\nu_\mu \leftrightarrow \nu_\tau$ oscillations. The best-fit expectation shown in the figure corresponds to $(\sin^2 2\theta, \Delta m^2) = (1.00, 2.3 \times 10^{-3} \text{eV}^2)$. Fig. 6 shows the contour plot of the allowed oscillation parameter regions. The result is consistent with that of the oscillation analysis using zenith angle distributions. The observed L/E distribution gives the first direct evidence that the neutrino survival probability obeys the sinusoidal functions as predicted by neutrino flavor oscillations.

Another interest is an observation of ν_τ in the atmospheric neutrinos since there has not been apparent evidence for the appearance of ν_τ charged current interactions due to $\nu_\mu \leftrightarrow \nu_\tau$ oscillations. We have performed a search for the ν_τ appear-

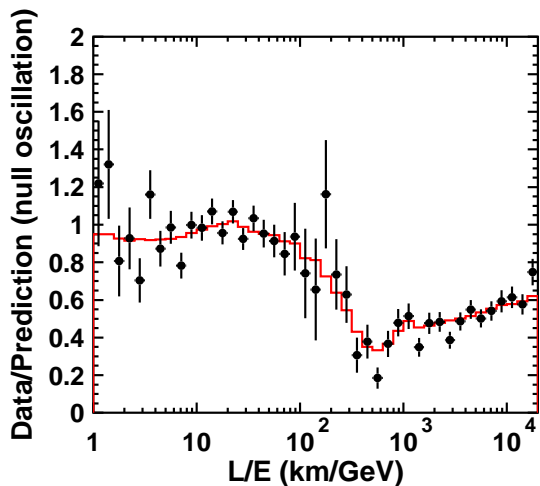


Fig. 5. Ratio of the data to the MC events without neutrino oscillation (points) as a function of the reconstructed L/E together with the best-fit expectation for 2-flavor $\nu_\mu \leftrightarrow \nu_\tau$ oscillation (red line). The error bars are statistical only.

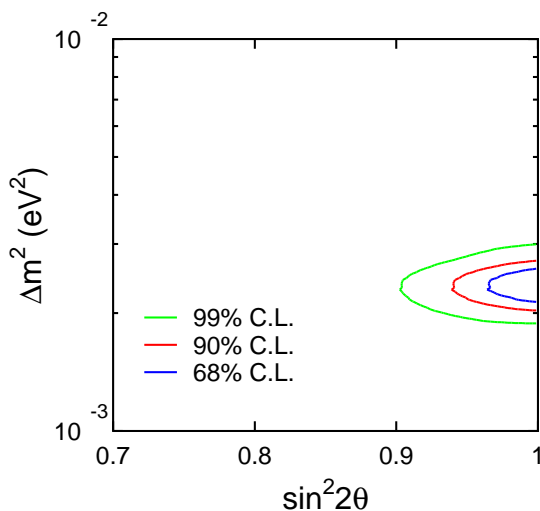


Fig. 6. 68, 90 and 99% C.L. allowed oscillation parameter regions for 2-flavor $\nu_\mu \leftrightarrow \nu_\tau$ oscillations obtained in the L/E analysis.

ance by using the SK-I atmospheric neutrino data [1]. The analysis is based on two statistical methods: a likelihood analysis and a neural network. Since τ 's produced in the Super-K detector would immediately decay into many hadrons, the event pattern would be similar to that of high-energy multi-ring ν_e events. Using the statistical difference in τ -like and background events, we have derived the variables to select an enriched sample of ν_τ charged current events in the atmospheric neutrino data. The differences appear in the energy spectrum, the number of charged pions in the final state, the fraction of lepton energy with respect to neutrino energy and so on. We optimized a combination of the variables and defined a likelihood function so that the signal to noise ratio becomes the maximum. We also use the neural network for the analysis. Before these analyses, we applied a pre-selection: (1) fiducial events, (2) multi-GeV, and (3) the most energetic ring is e -like.

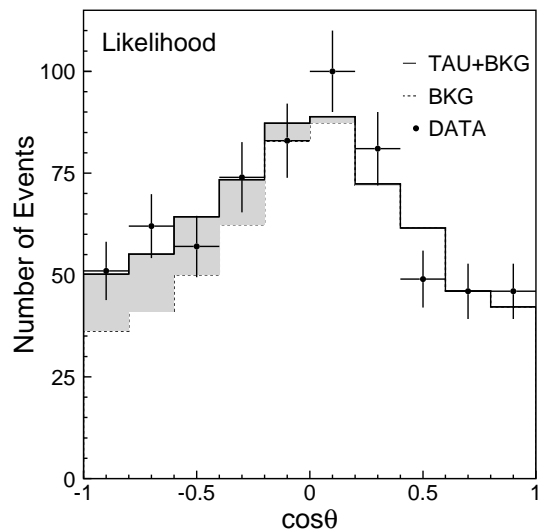


Fig. 7. The zenith angle distribution for tau candidate events in the likelihood analysis. The dashed histogram (background neutrinos) and the solid line (excess by ν_τ) show the best fit for the data.

After the pre-selection and cuts based on the likelihood and neural network, we fit the zenith angle distribution of a ν_τ enriched sample to a combination of the expected ν_τ and the atmospheric neutrinos (ν_μ and ν_e) including oscillations with the oscillation parameter, $\sin^2 2\theta = 1.0$ and $\Delta m^2 = 2.1 \times 10^{-3} \text{eV}^2$. Fig. 7 shows the fitted zenith angle distribution. Using τ selection efficiencies estimated by Monte Carlo study, we concluded the number of tau events with SK-I exposure is $138 \pm 48^{+14.8}_{-31.6}$ for the likelihood analysis and $134 \pm 48^{+16.0}_{-27.2}$ for the neural network while 78.4 ± 26 and 8.4 ± 27 are expected for each analysis. Thus the fitted results are found to be consistent with pure $\nu_\mu \leftrightarrow \nu_\tau$ oscillations and ν_τ appearance.

The two flavor neutrino oscillations successfully described the SK atmospheric neutrino data. However, any contributions by electron neutrinos have not been observed yet. We extended our neutrino oscillation analysis in order to treat three neutrino flavors. For the analysis, $\Delta m_{23}^2 \sim \Delta m_{13}^2 \equiv \Delta m^2 \gg \Delta m_{12}^2$ was assumed. If the parameter θ_{13} in the mixing matrix of lepton sector (MNS matrix) is finite, neutrino oscillations among $\nu_\mu \leftrightarrow \nu_e$ may be observed. Moreover, the mixing parameter is affected by potentials caused by matter and oscillations are expected to have a resonance around 5 GeV. Therefore, we can expect an increase at upward-going Multi-GeV e -like samples. Fig. 8 shows the result of the three-flavor neutrino oscillation analysis. Though there was no significant excess of electrons, we set an upper limit on θ_{13} . More statistics is needed to have better sensitivity [5].

A search for Q-balls has been carried out in Super-Kamiokande-II with 541.7 days of live time. A neutral Q-ball passing through the detector can interact with nuclei to produce pions, generating a signal of successive contained pion events along a track. No evidence for successive contained event groups has been found in Super-Kamiokande-II. New upper limits at 90% C.L. for neutral Q-ball flux are obtained in Fig. 9. These limits are the most stringent bounds on Q-ball

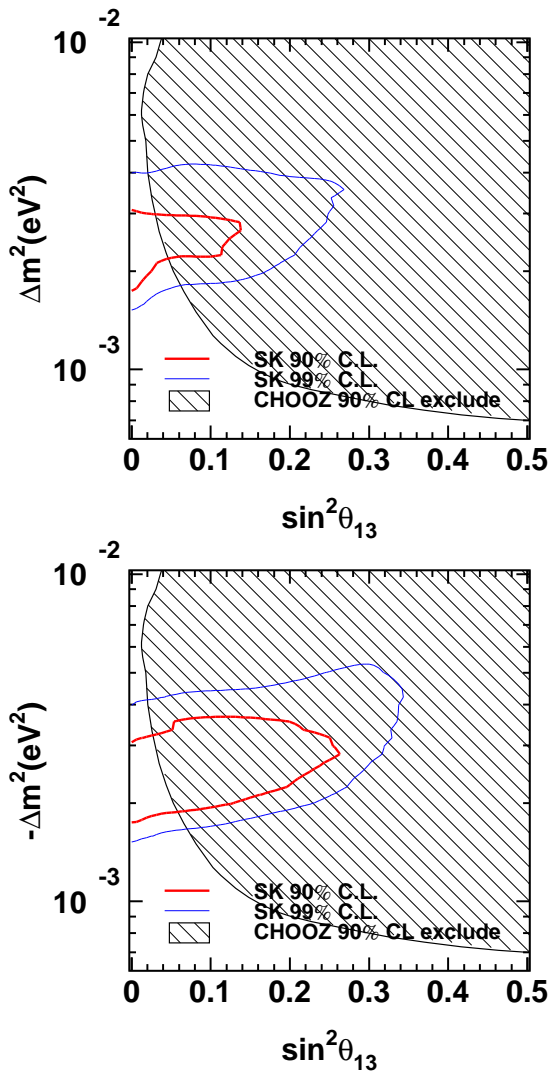


Fig. 8. The allowed region for $(\Delta m^2, \sin^2 \theta_{13})$ in case of normal (upper figure) and inverted (lower figure) hierarchy. We assumed positive Δm^2 . The red and blue contours correspond to allowed regions obtained by this analysis. The hatched region corresponds to 90% C.L. excluded area by CHOOZ experiment.

flux for Q-ball cross section below 200mb [6].

We perform several studies used to search for astrophysical sources of high energy neutrinos using the Super-Kamiokande-I neutrino induced upward-going muon data. The data set consists of 2359 events with minimum energy 1.6GeV, of which 1892 are through-going and 467 stop within the detector. No statistically significant evidence for point sources or any diffuse flux from the plane of the galaxy is found. The 90% C.L. upper limits on upward-going muon flux from astronomical sources which are located in the southern hemisphere and always under the horizon for Super-Kamiokande are $(1 \sim 4) \times 10^{-15} \text{cm}^{-2} \text{s}^{-1}$ [2] [3].

Solar neutrinos

SK detects solar neutrinos through neutrino-electron scattering, $\nu + e \rightarrow \nu + e$, with which the energy, direction and time of the recoil electron are measured. Due to its large fidu-

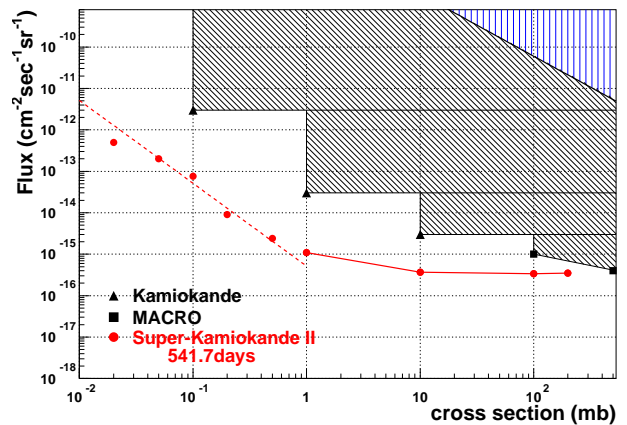


Fig. 9. 90% C.L. upper flux limits on the neutral Q-ball flux as a function of the Q-ball-nucleon interaction cross section. The circles show the results of this analysis and the dashed line in the region below 1mb cross section is obtained assuming that the flux limits should be in inverse proportion to the square of cross section.

cial mass of 22.5 kilotons, SK gives the most precise measurement of the solar neutrinos' flux with accurate information of the energy spectrum and time variations. For this precision experiment precise calibrations are performed for the energy scale, energy resolution, angular resolution and the vertex position resolution using a LINAC and ^{16}N radioisotope generated by a DT neutron generator.

The SK-I measurement from May 1996 until July 2001 yielded 22,400 solar neutrino events with the 5 MeV energy threshold. This corresponds to the ^8B solar ν flux of 2.35 ± 0.02 (stat.) ± 0.08 (sys.) $\times 10^6 \text{cm}^{-2} \text{s}^{-1}$ assuming the events purely due to $\nu_e e$ elastic scattering and the undistorted ^8B beta decay spectrum. We have published the full paper[4] in this year.

In this year, we have summarized the final results of the SK-II solar neutrino analysis. The live-time is 791 day between 2002 Dec. 24 and 2006 Oct. 5. The analysis energy threshold for the flux measurement set at 7.0 MeV. The obtained number of signal events is $7212.8^{+152.9}_{-150.9}$ (stat.). The corresponding ^8B solar neutrino flux is 2.38 ± 0.05 (stat.) $^{+0.16}_{-0.15}$ (syst.) $\times 10^6 \text{cm}^{-2} \text{s}^{-1}$. This is consistent with the SK-I result.

The day- and night-time fluxes in 7.5 MeV – 20MeV energy region are 2.29 ± 0.07 (stat.) $\times 10^6 \text{cm}^{-2} \text{s}^{-1}$ and 2.47 ± 0.07 (stat.) $\times 10^6 \text{cm}^{-2} \text{s}^{-1}$, respectively, means day-night asymmetry of -6.3 ± 4.2 (stat.) ± 2.3 (syst.)%.

The energy spectrum of the solar neutrino signals in SK-II is also obtained. Figure 10 shows the energy spectrum in SK-II. The energy spectrum of SK-II is consistent with that of SK-I. We are preparing a paper to report the final results from SK-II.

The SK-III solar neutrino observation with the 5 MeV energy threshold was started from Jan. 24, 2007. The energy spectrum at each reduction step looks consistent with SK-I. We are going to report the first look of the SK-III solar neutrino data in 2007.

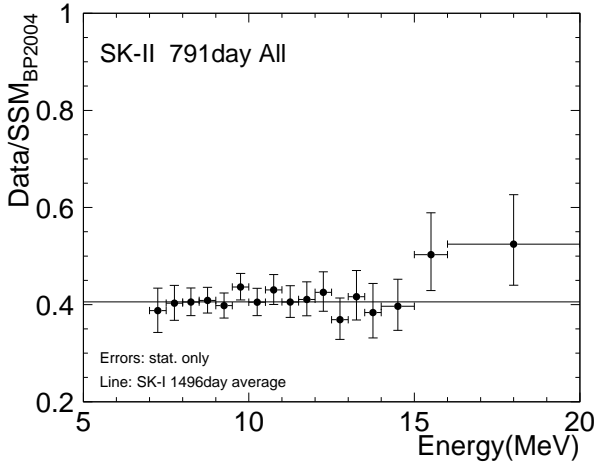


Fig. 10. Energy spectrum of the solar neutrino signal in SK-II. The horizontal axis is the total energy of the recoil electrons. The vertical axis is the ratio of the event rates between the observation and the BP04 SSM prediction. The horizontal line shows the SK-I flux value.

Search for nucleon decay

Proton decays and bound neutron decays (nucleon decays in general) is a most dramatic prediction of Grand Unified Theories in which three fundamental forces of elementary particles are unified into a single force. Super-Kamiokande (SK) is the world largest detector to search for nucleon decays and it has accumulated data of 91.6 kt-yrs (SK-I) and 49.3 kt-yrs (SK-II) resulting in 140.9 kt-yrs data in total. Various nucleon decay modes have been looked for in the SK but we found no significant signal excess so far.

A proton decay into one positron and one neutral pion ($p \rightarrow e^+\pi^0$) is one of most popular decay mode. This decay mode is mediated by super-heavy gauge bosons and discovery of the signal would give us the information of the mass of the gauge mesons. To discriminate the signal from atmospheric neutrino background, we reconstruct the number of particles (Cherenkov rings) and reconstruct the total visible energy corresponding to parent proton mass and total momentum corresponding to proton's Fermi momentum. Even the photo-coverage area is about half (19%) in SK-II, we achieved high detection efficiency of signals as 43.6% and low background levels as 0.04 events in 49.3 kt-yrs of SK-II. Because there are no candidate events in SK-I + SK-II data, we obtained lower limit on the partial lifetime of the proton, $\tau/B_{p \rightarrow e^+\pi^0} > 8.4 \times 10^{33}$ years at a 90% confidence level.

Moreover, we looked for SUSY favored decay modes which include K mesons in final state; $p \rightarrow \bar{\nu}K^+$, $n \rightarrow \bar{\nu}K^0$, $p \rightarrow \mu^+K^0$, and $p \rightarrow e^+K^0$. In $p \rightarrow \bar{\nu}K^+$ search, we looked for 236 MeV/c monochromatic muons from the decay of K^+ . Figure 11 shows the comparison between data and fitting results of muon momentum distribution for single-ring μ -like events. We observed no excess of signal. In any other modes, there are no significant signal excess. Therefore we conclude that there is no evidence of nucleon decays and we calculated partial lifetime limits taking into account systematic uncertainties. Obtained limits are 2.3×10^{33} , 1.3×10^{32} , 1.3×10^{33} ,

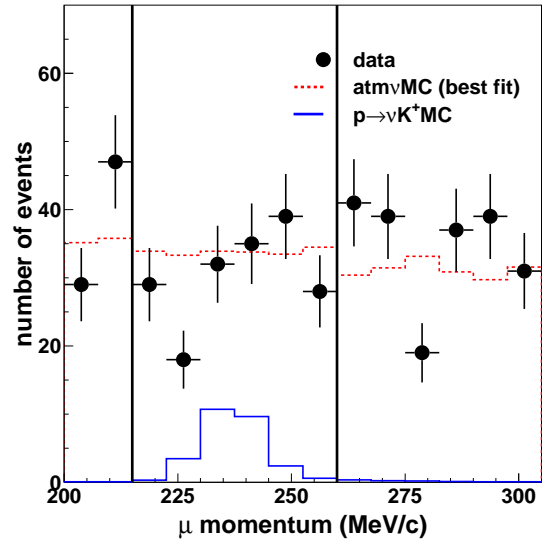


Fig. 11. The comparison between data and fitting results of muon momentum distribution for single-ring μ -like events. The filled circles show data with statistical errors. The solid line shows $p \rightarrow \bar{\nu}K^+$ MC. The dashed line shows the best fitted atmospheric neutrino MC with free normalization.

1.0×10^{33} , years at 90% confidence level for $p \rightarrow \bar{\nu}K^+$, $n \rightarrow \bar{\nu}K^0$, $p \rightarrow \mu^+K^0$, and $p \rightarrow e^+K^0$ modes, respectively [3].

Supernova neutrinos

Kamiokande and IMB observed neutrino burst from supernova 1987a. Those observations confirmed that the energy release by neutrinos is about several $\times 10^{53}$ erg. Super-Kamiokande is able to detect several thousand neutrino events if it happens near the center of our galaxy. Until now, no clear neutrino burst from a supernova was observed in Super-Kamiokande.

In this year, we have summarized the results of the neutrino burst searches in SK-I and SK-II. We have performed 3 searches; distant supernova search, burst search with low-energy threshold, and neutronization burst search. The livetime for the analyses in SK-I and SK-II were 1703.9 days and 885.3 days, respectively. Figure 12 shows a summary of the livetime in SK.

The purpose of the distant supernova search is to search for neutrinos from supernovae in nearby galaxies. For this search, we set our criteria as a long time-window and low multiplicity threshold with a high energy threshold, such as ≥ 2 events / 20 seconds with 17 MeV threshold. We couldn't find any candidate cluster.

In the burst search with low-energy threshold, we have applied 3 short time-windows of ≥ 3 events / 0.5 seconds, ≥ 4 events / 2 seconds, and ≥ 8 events / 10 seconds with low energy thresholds of 6.5 MeV for SK-I and 7.0 MeV for SK-II. No candidate cluster remained in this analysis.

Prior to the core explosion, many ν_e 's are emitted via the neutronization reaction $e^- + p \rightarrow \nu_e + n$. The duration of the neutronization burst is expected less than 10 milliseconds. In the neutronization burst search, we have applied the following short time-windows: ≥ 2 events / 1 msec, ≥ 2 events / 10 msec,

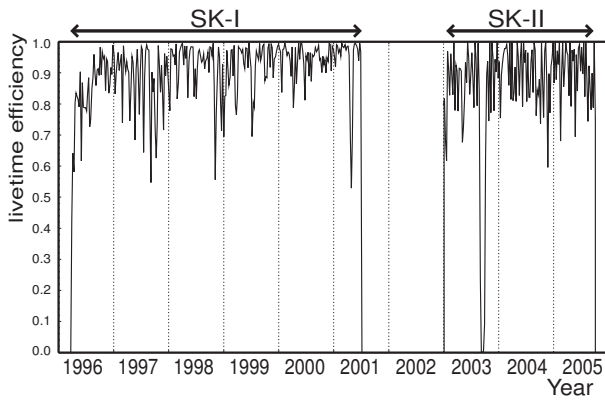


Fig. 12. SK livetime efficiency as a function of time. Most of the big dips in efficiency were due to planned calibration runs such as LINAC energy calibration.

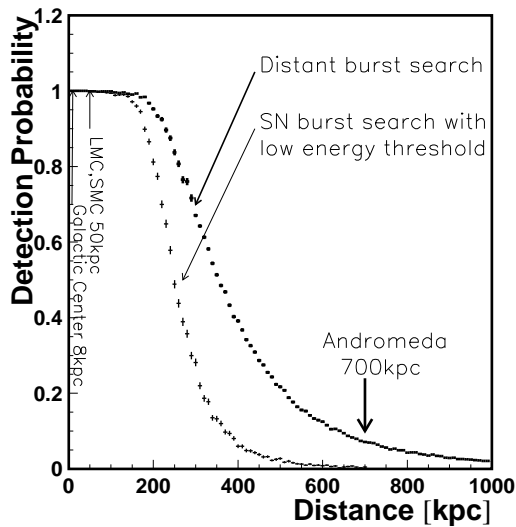


Fig. 13. The probability of detecting supernovae assuming a specific supernova model at SK. Full (100%) detection probability is retained out to around 100 kpc.

and ≥ 2 events / 100msec. The observed number of clusters were consistent with the expected background.

Figure 13 shows the probability of detecting supernovae assuming a specific supernova model at SK. The full detection probability is maintained out to around 100 kpc. Therefore, the upper limit at 90% C.L. for the supernova explosion rate out to 100 kpc is determined to be 0.32 per year by combining the results from SK-I and SK-II. While the probability for the burst search with lower energy thresholds goes down rapidly to almost 0.0 at 700 kpc — the distance to the Andromeda Galaxy — the probability of the distant supernova search is still 0.075 at this distance, which demonstrates the benefit of conducting a long time-window search in addition to the usual burst search. We are preparing a paper to report these results.

Bibliography

- [1] K. Abe *et al.* (Super-Kamiokande Collaboration), “A measurement of atmospheric neutrino flux consistent with tau neutrino appearance”, *Phys. Rev. Lett.* 97 (2006) 1711801.
- [2] K. Abe *et al.* (Super-Kamiokande Collaboration), “High energy neutrino astronomy using upward-going muons in Super-Kamiokande-I” *Astrophys. J.* 652, (2006) 198.
- [3] M. E. C. Swanson *et al.* (Super-Kamiokande Collaboration), “Search for Diffuse Astrophysical Neutrino Flux Using Ultrahigh Energy Upward-going Muons in Super-Kamiokande-I.” *Astrophys. J.* 652, (2006) 206.
- [4] Super-Kamiokande Collaboration, “Solar Neutrino Measurements in Super-Kamiokande-I”, *Phys. Rev. D* 73, (2006) 112001.
- [5] J. Hosaka *et al.* (Super-Kamiokande Collaboration), “Three flavor neutrino oscillation analysis of atmospheric neutrinos in Super-Kamiokande”, *Phys. Rev. D* 74 (2006) 032002.
- [6] Y. Takenaga *et al.* (Super-Kamiokande Collaboration), “Search for neutral Q-balls in Super-Kamiokande-II.”, *Phys. Lett.* B647, (2007) 18-22.

K2K Experiment

[Spokesperson : K. Nishikawa]

High Energy Accelerator Research Organization, Japan, Tsukuba 305-0801

In collaboration with the members of:

ICRR, University of Tokyo, Japan; Kyoto University, Japan; KEK, High Energy Accelerator Research Organization, Japan; Kobe University, Japan; Osaka University, Japan; Hiroshima University, Japan; Okayama University, Japan; Niigata University, Japan; Tokyo University of Science, Japan; Tohoku University, Japan; Miyagi Edu. University, Japan; Nagoya University, Japan; Chonnam University, Korea; Seoul National University, Korea; Dongshin University, Korea; Korea University, Korea; University of California at Irvine, USA; State University of New York at Stony Brook, USA; Boston University, USA; University of Washington at Seattle, USA; Louisiana State University, USA; Massachusetts Institute of Technology, USA; University of Hawaii at Manoa, USA; Duke University, USA; TRIUMF, Canada; University of British Columbia, Canada; University of Barcelona, Spain; University of Valencia, Spain; INRM, Russia; CEA Saclay, France; University of Rome, Italy; University of Geneva, Swiss; University of Warsaw, Poland; A. Soltan Institute for Nuclear Studies, Poland; Institute for Nuclear Research, Russia;

The discovery of the neutrino oscillation by Super-Kamiokande in 1998 has led to the conclusion that neutrino has a finite mass. The discovery implies the existence of new physics beyond the standard model of the elementary particles at a huge energy scale. Since the observed neutrino mass difference of $\Delta m^2 \sim 3 \times 10^{-3} \text{eV}^2$ suggests the oscillation length

is about a few hundred km for one GeV neutrinos, this phenomena can be experimentally tested by using the artificially created neutrino beam with the detector placed at a few hundred km away from the neutrino production point.

The K2K experiment was planned to detect such oscillation effect and to determine the oscillation parameters precisely. The neutrino beam created at KEK has a mean energy of 1.3 GeV and was sent to the Super-Kamiokande detector, 250 km west of KEK, every 2.2 seconds with the duration of 1.1μ second. In the site of KEK, at the distance of 300 m from the target, we have prepared 1 kt water Cherenkov detector and fine grained detector system (FGD) as near neutrino detectors. The fine grained detector system consists of a scintillation fiber tracking detector (SciFi), a lead glass calorimeter, and the muon ranger in the first phase (K2K-I). The arrangement of the near neutrino detectors in K2K-I is shown in Fig. 1. Later, we have replaced the lead glass calorimeter with a fully active scintillator tracking detector (SciBar) as phase 2(K2K-II). We started the physics run in June 1999 and the experiment was completed in November 2004. Now we have analyzed all the data, which corresponds to 9.2×10^{19} protons on target (POT). The near detector data from this period include 2.3×10^{19} POT without the lead glass (K2K-IIa), and then 2.2×10^{19} POT with a fully-active scintillator detector (SciBar) in its place (K2K-IIb and K2K-IIc).

Several primary and secondary beam monitors, such as proton profile monitors, the muon monitor and the pion monitor are placed along the neutrino beam line. Because the length of the pion decay region is long compared to the distance from the production target to near neutrino detectors, the neutrino beam at the near detector hall and SK is not scaled exactly by $1/r^2$ law. Therefore, the flux ratio of the near to the far detector was estimated by the beam Monte Carlo simulation in which the spread and emittance of the beam at the target, the production of the pions, the focusing effect by electromagnetic horns and the decay of pions to neutrinos are taken into account. Also, we employ the results from the pion production experiment, HARP experiment, as an input of the simulation. The beam simulation results were validated by the pion monitor which measured the produced pion directions

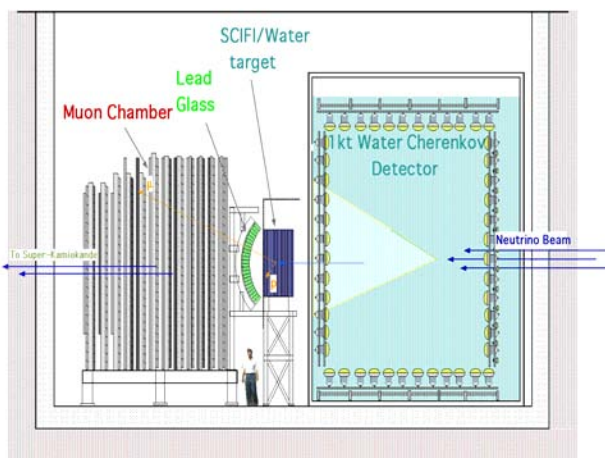


Fig. 1. The arrangement of the near detectors.

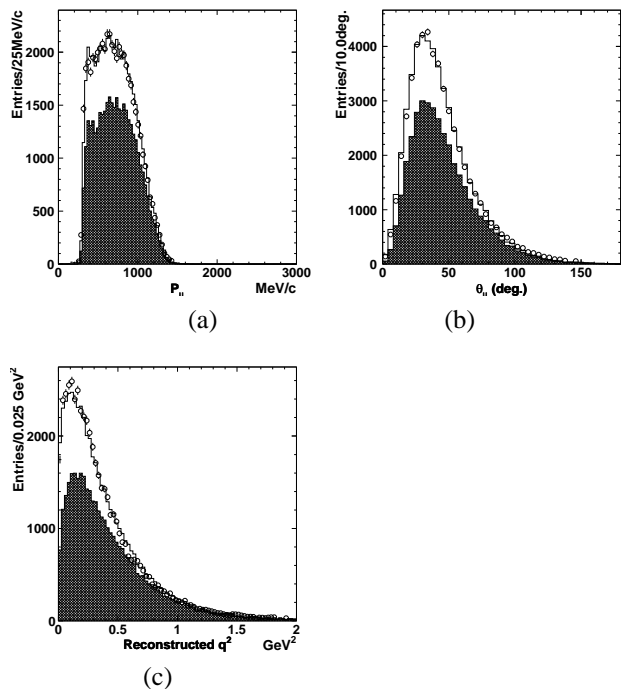


Fig. 2. Muon momentum (p_μ), direction (θ_μ) and reconstructed q^2 distributions: (a) the p_μ distribution of 1KT fully contained 1-ring μ -like sample, (b) 1KT θ_μ for the same sample, (c) 1KT reconstructed q^2 for the same sample. Open circles represent data, while histograms are MC predictions using the best fit systematic uncertainties.

and momentum in-situ.

The beam flux and the spectrum were measured by the front detectors. ICRR group has a responsibility of providing the Super-Kamiokande data and the construction of the 1 kt front detector and the analysis of the data from those detector components. The coverage of PMT in the 1 kt front detector is same as the Super-Kamiokande detector with the 40% of the total inner detector surface. The 1kt detector provides information of the absolute neutrino flux and the spectrum of the neutrino beam. In figure 2, the muon momentum spectrum (a), the muon direction (b), and the reconstructed q^2 (c) by using the single ring fully contained events at 1 kt detector are shown. The observed spectrum is well reproduced by the Monte Carlo simulation program in which the beam energy spectrum and neutrino interactions in water are taken into account. Combining the 1 kt data and the FGD data together with constraints of results from the HARP experiment and measurements of pion monitor, the expected neutrino energy spectrum for the far detector was obtained. All the systematic errors due to detector biases or uncertainty of neutrino interactions were taken into account.

The neutrino beam induced event was selected by using the beam timing measured at the KEK 12 GeV Proton Synchrotron. We had two sets of GPS receivers in both KEK and SK sites for the event selection. Figure 3 shows the timing distribution of the fully contained events observed at Super-Kamiokande with respect to the proton beam injection timing. The time of flight of neutrinos from KEK to Super-Kamiokande ($\sim 830 \mu$ sec) is corrected in the figure.

Neutrino events were clearly observed near $\Delta T=0$ and the

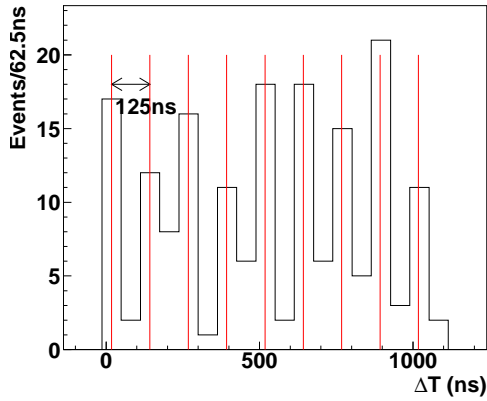


Fig. 3. The timing distribution of fully contained event observed at Super-Kamiokande with respect to the beam injection timing. Periodical structure coming from proton beam bunches is seen in the Super-Kamiokande, 250 km away from the accelerator.

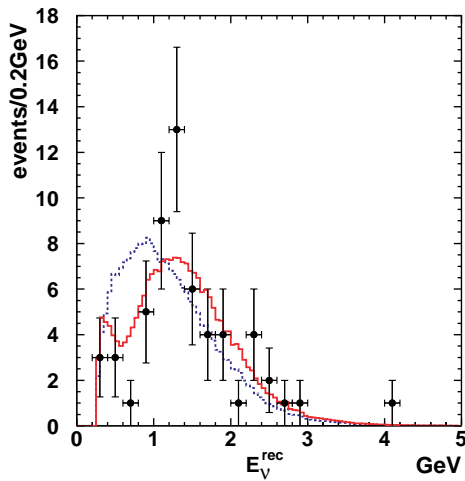


Fig. 4. The reconstructed E_V distribution from single ring fully contained events at SK. Points with error bars are data. The solid line is the best fit spectrum. The dashed line shows the expected spectrum without oscillation. Both histograms are normalized by the number of events observed(58).

spread in the timing was consistent with the duration of beam injection at KEK 12 GeV PS. In total, 112 events were identified as K2K beam induced events at Super-Kamiokande. Using the large number of observed neutrino events at front detectors, expected number of neutrino events at Super-Kamiokande was estimated to be $158.1^{+9.2}_{-8.6}(\text{syst})$ assuming no-oscillation.

58 μ -like single ring events were observed and the neutrino energy spectrum obtained from the energy and scattering angle of the observed muons is shown in Fig. 4. From the deficit of observed number of events together with the shape distortion of neutrino energy spectrum, we have concluded that probability of null oscillation is 0.0015% (4.3σ). The allowed region of Δm_{23}^2 and $\sin^2 2\theta_{23}$ is shown in Fig. 5. The obtained result for neutrino oscillation parameters are consistent with those from atmospheric neutrino oscillations.

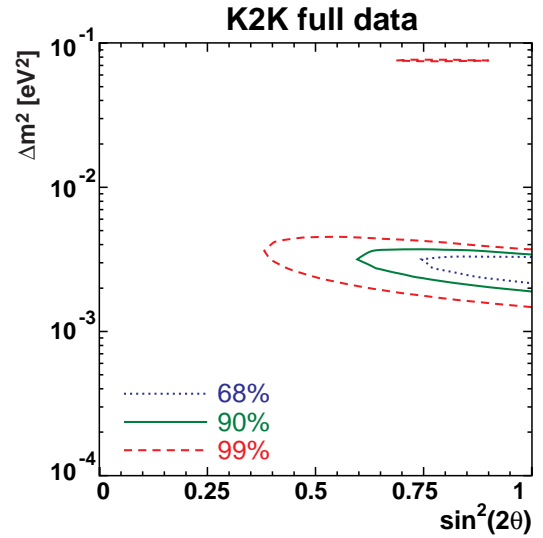


Fig. 5. Allowed regions of ν_μ - ν_τ oscillation parameters. Dashed, solid and dot lines are 68.4%, 90% and 99% C.L. contours, respectively.

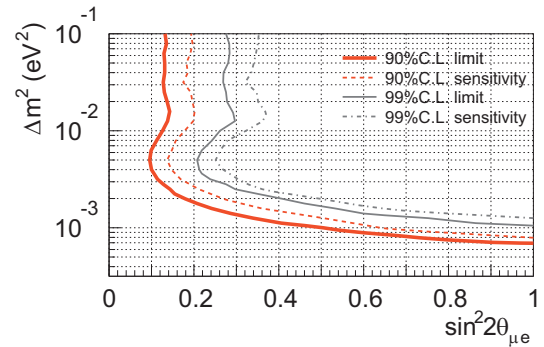


Fig. 6. The upper bound on ν_μ to ν_e oscillation parameters at 90% and 99% C.L. The sensitivities of the K2K experiment for each C.L. are also indicated with dashed lines.

We have also searched for the ν_e appearance in a beam of ν_μ , which is the signature of finite value of the unknown mixing parameter θ_{13} . As a result, no evidence for a ν_e appearance signal was found. Therefore, we set bounds on the oscillation parameters. Figure 6 shows the upper bound on the oscillation parameters for two flavor mixing, at the 90% and 99% confidence level (C.L.). At $\Delta m^2 = 2.8 \times 10^{-3} \text{eV}^2$, we set an upper limit of $\sin^2 2\theta_{13} = 0.26$ at 90% confidence level, assuming $\sin^2 2\theta_{\mu e} = \frac{1}{2} \sin^2 2\theta_{13}$ and $\Delta m_{\mu e}^2 \sim \Delta m_{13}^2$.

The accumulated data collected with the K2K near detector system are also used to study neutrino interactions. The axial vector coupling parameter for the quasi-elastic scattering was extracted from the data taken with the SciFi detector. It is found to be larger than the previous experimental results. The same analysis is still on-going by using the data from the SciBar detector. Also, there is no indication of the charged current coherent pion scattering in this energy range. These information are used to update the neutrino interaction simulation program, which is used in the analysis of the atmospheric neutrino oscillation and the study of the T2K experiment.

Bibliography

- [1] K2K collaboration, Detection of accelerator produced neutrinos at a distance of 250 km, *Phys. Lett. B*, 511, 178–184, 2001.
- [2] K2K collaboration, Indication of neutrino oscillation in a 250 km long baseline experiment, *Phys. Rev. Lett.*, 90, 041801, 2003.
- [3] K2K collaboration, Search for Electron Neutrino Appearance in a 250 km Long-baseline Experiment, *Phys. Rev. Lett.*, 93, 051801, 2004.
- [4] K2K collaboration, Measurement of single π^0 production in neutral current neutrino interactions with water by a 1.3 GeV wide band muon neutrino beam, *Phys. Lett. B*, 619, 255, 2005.
- [5] K2K collaboration, Evidence for muon neutrino oscillation in an accelerator-based experiment *Phys. Rev. Lett.*, 94, 081802, 2005.
- [6] K2K Collaboration, Search for coherent charged pion production in neutrino carbon interactions, *Phys. Rev. Lett.*, 95, 252301 2005.
- [7] K2K Collaboration, An improved search for $\nu/\mu \rightarrow \nu/e$ oscillation in a long-baseline accelerator experiment, *Phys. Rev. Lett.*, 96, 181801, 2006.
- [8] K2K Collaboration, Measurement of the quasi-elastic axial vector mass in neutrino oxygen interactions, *Phys. Rev. D*, 74, 052002, 2006.
- [9] K2K Collaboration, Measurement of neutrino oscillation by the K2K experiment, *Phys. Rev. D*, 74, 072003, 2006.

T2K Experiment (under construction)

[Spokesperson : K. Nishikawa]

High Energy Accelerator Research Organization, Japan, Tsukuba 305-0801

In collaboration with the members of:

ICRR, University of Tokyo, Japan; Hiroshima University, Japan; KEK, Japan; Kobe University, Japan; Kyoto University, Japan; Miyagi University of Education, Japan; Osaka City University, Japan; University of Tokyo, Japan; Triumf, Canada; University of Alberta, Canada; University of British Columbia, Canada; University of Regina, Canada; University of Toronto, Canada; University of Victoria, Canada; York University, Canada; CEA/DAPNIA Saclay, France; IPN Lyon (IN2P3), France; LLR Ecole polytechnique (IN2P3), France; LPNHE-Paris, France; RWTH Aachen University, Germany; INFN Sezione di Roma, Italy; Napoli University and INFN, Italy; Rome University and INFN, Italy; Chonnam National University, Korea; Dongshin University, Korea; Gyeongsang National University, Korea; Kyungpook National University, Korea; Sejong University, Korea; Seoul National University, Korea; Sungkyunkwan University, Korea; A Soltan Institute for Nuclear Studies, Poland; Technical University, Poland; University of Silesia, Poland; Warsaw University, Poland; Wroclaw University, Poland; INR, Russia;

IFIC, Valencia; Universitat Autònoma de Barcelona/IFAE, Spain; Bern, Switzerland; ETHZ, Switzerland; University of Geneva, Switzerland; Imperial College London, UK; Lancaster University, UK; University of London Queen Mary, UK; Sheffield University, UK; SFTC/Rutherford Appleton Laboratory/Daresbury Laboratory, UK; The University of Liverpool, UK; University of Warwick, UK; Boston University, USA; Brookhaven National Laboratory, USA; Colorado State University, USA; Duke University, USA; Louisiana State University, USA; Stony Brook University, USA; University of California, Irvine, USA; University of Colorado, USA; University of Pittsburgh, USA; University of Rochester, USA; University of Washington, USA

The K2K experiment successfully confirmed the neutrino oscillation phenomena and established the method of the accelerator based long baseline neutrino oscillation experiment. Meanwhile, precise measurements of accelerator, atmospheric, solar and reactor neutrinos have been done and 2 out of 3 neutrino mixing angles and 2 mass differences have been measured. However, only the upper limit of the remaining mixing angle, θ_{13} has been obtained until now. Because the K2K has limited with statistics to measure θ_{13} but the measurement will be possible with much intense neutrino beam. Furthermore, if θ_{13} is large enough, there is a possibility to search for the CP violation in the lepton sector and to measure the CP phase, δ , which is the last parameter of the neutrino oscillation. Therefore, several next generation experiments, which utilize much intense beam for the further investigation of the neutrino oscillation, have been proposed. Among of them, the Tokai to Kamioka long baseline neutrino oscillation experiment (T2K) was accepted in Japan. The T2K experiment uses the intense neutrino beam produced by a new high intensity proton synchrotron accelerator being constructed at the J-PARC site in Tokai village. T2K utilize Super-Kamiokande as a far detector, located at 295 km from the beam production point. This experiment is expected to start in the Spring 2009.

The T2K neutrino beam is about 50 times more intense compared to K2K. The neutrino beam line of T2K utilize the so-called off-axis technique¹ to have a tunability of the peak energy and a narrow energy spread of the neutrino beam. The peak position of the neutrino beam energy will be adjusted to ~ 650 MeV by setting the off-axis angle to $\sim 2.5^\circ$. With this configuration, it is possible to maximize the neutrino oscillation effects at a distance of 295 km when the mass squared difference is about $\Delta m^2 = 2.8 \times 10^{-3} \text{eV}^2$. The beam primarily consists of ν_μ with a contamination of $\sim X.X\%$ ν_e at the flux peak.

As described, one of the motivations of this experiment is to measure the neutrino oscillation parameter θ_{13} , which is only known to be small ($\sin^2 \theta_{13} < 0.04$) by reactor experiments. It is of great interest to know the value of a nonzero θ_{13} or how close to zero θ_{13} is; a new underlying symmetry may be required to explain this. In the case of nonzero θ_{13} , T2K may observe the appearance of electron neutrinos for the first time. Also, there is a possibility to be the first time in

^{*1} Long Baseline Neutrino Oscillation Experiment BNL E889 proposal, (1995).

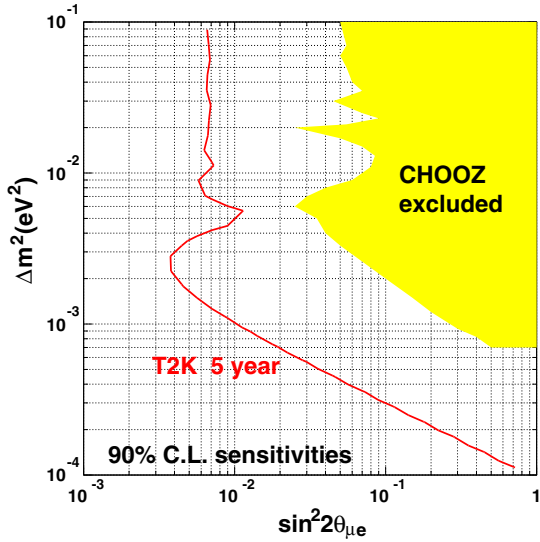


Fig. 1. Expected sensitivity on $\theta_{\mu e}$ by T2K as a function of Δm_{23}^2 compared with current best limit by CHOOZ reactor experiment. Note that $\sin^2(2\theta_{\mu e}) = \frac{1}{2} \sin^2 2\theta_{13}$.

observing the neutrino oscillation signature by the appearing experiment.

Figure 1 shows T2K's expected sensitivity to $\theta_{\mu e}$ as a function of Δm_{23}^2 . Note that $\sin^2(2\theta_{\mu e}) = \frac{1}{2} \sin^2 2\theta_{13}$.

If the measured θ_{13} is large enough, there will be a way to investigate the CP violation in the lepton sector with further extensions of this experiment.

The other purpose is precise measurements of θ_{23} and Δm_{23}^2 . Owing to the high statistics, these parameters will be measured almost one order of magnitude precisely. Figure 2 shows the expected accuracy of the measurement of $\sin^2 2\theta_{23}$ and Δm_{23}^2 [1]. So far, θ_{23} mixing is known to be very large and consistent with unity from the Super-Kamiokande, K2K and the MINOS experiments. If $\sin^2 2\theta_{23}$ is exactly one, it may suggest an underlying new symmetry.

To achieve these precise measurements, the Super-Kamiokande detector has several to-do items in the near future: (1) detector upgrade, (2) precise detector calibration, and (3) software upgrade. Details of these items are described below.

Detector Upgrade

The reconstruction work of Super-Kamiokande has been completed in 2006 and all the PMTs were installed as SK-I era. It will help the T2K experiment in a search for electron neutrino appearance, to distinguish single π^0 production backgrounds from the ν_e signal more effectively.

In 2008, electronics and the DAQ system, including newly developed ADC/TDC modules called QBEE, are planned to be replaced. The new QBEE board consists of custom analog ASIC chips and multi-hit TDC chips. The new system will allow us to observe T2K neutrino events with good stability and accuracy.

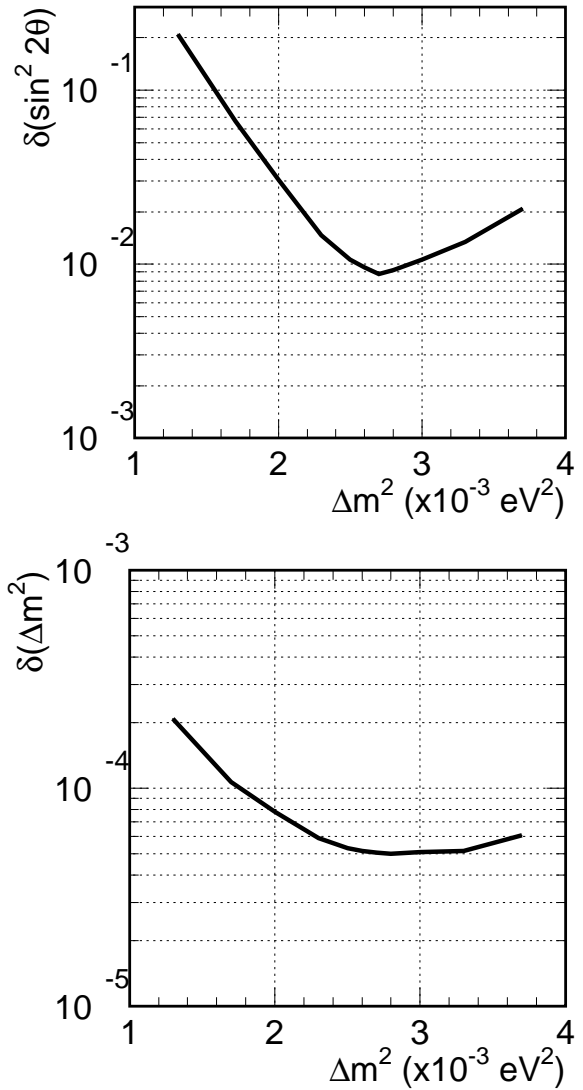


Fig. 2. T2K's expected accuracy of the measurement of $\sin^2 2\theta_{23}$ and Δm_{23}^2 as a function of Δm_{23}^2 [1].

Precise Detector Calibration

The response of the far detector must be well understood in order to maximize the sensitivities to oscillation parameters such as θ_{13} , θ_{23} , and Δm_{23}^2 . In the electron appearance search, single π^0 production backgrounds can fake single-ring electron signals when one of the two γ rings are not identified. Even small portion of muon events being mis-identified as electron could also be serious backgrounds. Therefore, we will study the ring identification and the particle identification capability of the detector very carefully. It will also be important to improve the current uncertainty in the absolute energy scale measurement (2.5%) in order to achieve a Δm_{23}^2 measurement with $\sim 1\%$ accuracy. Moreover, further calibration of fundamental properties such as charge/timing response of each PMT, light attenuation/scattering in water, and light reflection by detector materials are indispensable.

Software Upgrade

All measurement of physical quantities of an event, such as vertex position, the number of Cherenkov rings, momentum, particle type and the number of decay electrons, is auto-

matically performed by reconstruction algorithms. Improvements and re-tuning of many of the algorithms are now ongoing to achieve the physics goals of T2K.

Bibliography

- [1] Y. Itow *et al.*, The JHF-Kamioka neutrino project, (2001), hep-ex/0106019.

XMASS experiment

XMASS is a multi-purpose experiment using liquid xenon which aims at the detection of cold dark matter, search for neutrinoless double beta decay, and detection of low energy solar neutrinos. An R&D study for the liquid xenon detector is being performed at Kamioka observatory.

Astronomical observations suggest that there is dark matter (non-luminous particles with mass) in the universe. One of the most likely candidates for dark matter is a weakly interacting massive particle (WIMP), for example the lightest supersymmetric particle. A recoil of a xenon nucleus from an interaction with dark matter will produce scintillation light in liquid xenon.

The Super-Kamiokande experiment shows that neutrinos have mass. However, we do not yet know the absolute mass of neutrinos and whether the neutrinos are Majorana type or Dirac type. Xenon nuclei with mass number 136 is one of the double beta nuclei which is best suited for this research.

The energy spectrum of the solar neutrinos is measured only above 5 MeV by SK and SNO so far but that of low energy solar neutrinos (pp, ^7Be neutrinos, etc.) is not measured yet. With 10-ton liquid xenon, it will be able to detect pp neutrinos and ^7Be neutrinos by $\nu+e$ scattering with a rate of 10 events/day and 5 events/day, respectively.

For all these purposes, background caused by gamma rays which comes outside liquid xenon is needed to be suppressed. The key idea to reduce background is that gamma rays can be absorbed by liquid xenon itself (self-shielding). A sphere of liquid xenon absorbs low energy gamma rays from the outside within 10-20 cm thickness and realizes a low background at the central volume. WIMPs and neutrinos, however, interact throughout the detector. Therefore, if the vertices of the events can be reconstructed, WIMPs and neutrinos can be observed in a low background environment by extracting only events which observed deep inside the detector. The event reconstruction can be accomplished by observing photons with the many photo multipliers mounted outside the fiducial volume. Liquid xenon has the following advantages to realize this idea:

- With the high atomic number of xenon ($Z = 54$) and the high density of liquid xenon ($\sim 3 \text{ g/cm}^3$), external gamma-rays can be absorbed in a short distance from the detector wall (self-shielding).
- A large light yield of 42,000 photons/MeV, which is as good as NaI(Tl) scintillator, enables good event reconstruction as well as detection of small energy signals like dark matter recoil.
- 175 nm scintillation light of liquid xenon can be read out by typical PMTs of bi-alkaline photocathode with a quartz window.



Fig. 1. 3 kg fiducial volume liquid xenon detector constructed for R&D study

- Purification is easier than other materials (e.g. distillation is possible).
- Isotope separation is possible. It is possible to enrich ^{136}Xe for double beta decay or deplete ^{136}Xe for solar neutrino measurements.

We have been studying liquid xenon detectors since the year 2000. A 3 kg fiducial volume liquid xenon detector has been developed for R&D study and test data have been taken for the last three years. The event reconstruction, self-shielding and low internal activity have been confirmed as shown in the next section. As a next step, we are planning to build an 800 kg liquid xenon detector (100 kg fiducial volume) for dark matter search. The third step of the XMASS project is to construct a 10-ton class liquid xenon detector which aims at the detection low energy solar neutrinos. Different detector designs to search for neutrinoless double beta decay are under study.

R&D study with a 3 kg fiducial volume detector

Figure 1 shows the 30 liter liquid xenon detector developed for R&D study. It is a 30 cm cubic detector viewed by 54 2-inch PMTs which were developed for low background purposes. The detector is placed in a low background setup which consists of 5 cm-thick pure copper, 15 cm-thick lead, 10 cm-thick boric acid, and 15 cm-thick polyethylene for reducing gamma rays, neutron and radon backgrounds.

Test data were taken in December 2003 and August 2004. Figure 2 shows the background distributions for the latest measurement. A large reduction of backgrounds in a smaller detector volume is observed at several hundred keV which demonstrates the self-shielding of the detector. The reduction of backgrounds is as expected by Monte Carlo simulations. The background of most inner 10 cm cube at the energy range where dark matter signals are expected ($< 100 \text{ keV}$) is $10^{-2} \text{ day}^{-1} \text{ kg}^{-1} \text{ keV}^{-1}$. This value is comparable with that of a dark matter experiment, the CDMSII experiment, ($0(10^{-3}) \text{ day}^{-1} \text{ kg}^{-1} \text{ keV}^{-1}$).

As for the internal source of backgrounds, ^{85}Kr in xenon is one potential source. In order to purify xenon, a test distillation system was constructed which is able to process 0.6 kg Xe/hour and achieve better than 1/1000 reduction in krypton concentration. In March 2004, it produced pure xenon with

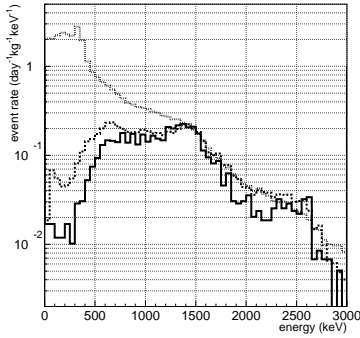


Fig. 2. Background spectrum measured by the 3 kg fiducial volume detector. The dashed, dotted and solid histograms show the rate of the events which were observed in the full volume, 20 cm and 10 cm cube at the center of the detector, respectively.

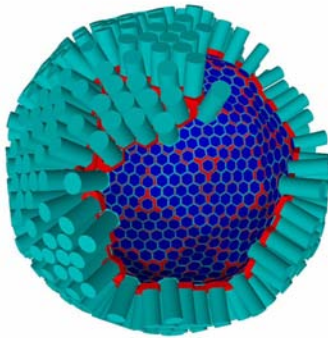


Fig. 3. Schematic view of the proposed 800kg liquid xenon detector aiming at dark matter search. The detector has a sensitivity of $10^{-45} \sim 10^{-44} \text{cm}^2$ in cross section which is more than two orders of magnitude better than the current best limits in the world.

only 3.3 ± 1.1 ppt mol/mol of krypton concentration which gives background at a level of $7 \times 10^{-4} \text{day}^{-1} \text{kg}^{-1} \text{keV}^{-1}$.

The internal contamination of ^{238}U and ^{232}Th daughters are also found to be small. By observing the Bi-Po chain and assuming radioactive equilibrium, ^{238}U is $33 \pm 7 \times 10^{-14} \text{g/g}$ and ^{232}Th is less than $63 \times 10^{-14} \text{g/g}$. These radioactive contaminants are of a similar level required by the next 800 kg detector.

800 kg detector

We plan to make the 800 kg detector (Figure. 3) aiming to search for dark matter down to $10^{-45} \sim 10^{-44} \text{cm}^2$ in cross section which is more than two orders of magnitude better than the current best limits in the world. The validity of the Monte Carlo simulation which is used for estimating background and sensitivity of this detector is confirmed by the previous experimental results. The advantages of our detector design are:

1. It is easy to extend the detector because the target substance is liquid.
2. The energy threshold is as low as 5 keV since the photo electron yield is high.
3. It is easy to purify the target substance because xenon is naturally in a gas phase.

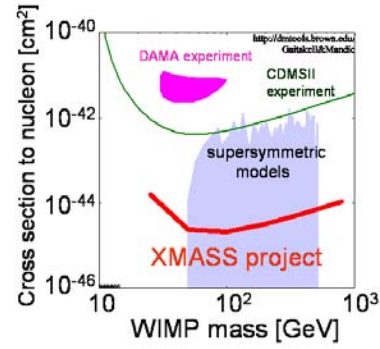


Fig. 4. Expected sensitivity of the proposed 800kg liquid xenon detector. See <http://dmtools.berkeley.edu/>

4. A pulse shape analysis is possible to select nuclear recoil events.

The expected sensitivity for particle dark matter is better than the current experimental limits by two orders of magnitude. Figure 4 shows the expected sensitivity of the 800 kg detector.

References

1. Y. Suzuki et al., “Low energy solar neutrino detection by using liquid xenon”, Aug. 2000, hep-ph/0008296.
2. S. Moriyama, “XMASS EXPERIMENT I”, proceedings of the International Workshop on Technique and Application of Xenon Detectors, Kashiwa, Japan, 3-4 Dec. 2001.
3. A. Takeda, “XMASS experiment”, proceedings of the 6th International Workshop on The Identification of Dark Matter (IDM2006), Rhodes Island, Greece, 11-16 Sep. 2006.
4. Y.D. Kim, “Status and Background Considerations for XMASS experiment”, proceedings of the 2nd Topical Workshop in Low Radioactivity Techniques (LRT2006), Aussois, France, 1-4 Oct. 2006.
5. K. Abe, “XMASS, status of 800kg detector design”, presentation in the the Joint Meeting of Pacific Region Particle Physics Communities (DPF2006), Honolulu, Hawaii, USA, 29 Oct. - 3 Nov. 2006.

HIGH ENERGY COSMIC RAY DIVISION

Overview

Three major research activities of the High Energy Cosmic Ray division are the study of very high energy gamma-rays by the CANGAROO group, extremely high energy cosmic rays by the Telescope Array (TA) group, and very high energy cosmic rays and gamma-rays by the Tibet AS γ Collaboration. Other activities, such as experiments utilizing the Akeno observatory, the Norikura observatory, the Mt. Chacaltaya observatory (jointly operated with Bolivia), and the emulsion-pouring facilities are closely related to inter-university joint research programs. Also an all-sky high resolution air-shower detector (Ashra) has been developed and is under installation on the Hawaii island.

The CANGAROO project (Collaboration of Australia and Nippon for a GAMMA-Ray Observatory in the Outback) is a set of large imaging Cherenkov telescopes to make a precise observation of high-energy air showers originated by TeV gamma-rays. It started as a single telescope with a relatively small mirror (3.8 m in diameter) in 1992. In 1999 a new telescope with a 7-m reflector has been built, and now it has a 10-m reflector with a fine pixel camera. The main purpose of this project is to explore the violent, non-thermal universe and to reveal the origin of cosmic-rays. An array of four 10-m telescopes has been completed in March 2004 so that more sensitive observation of gamma-rays is realized with its stereoscopic imaging capability of Cherenkov light. Several gamma-ray sources have been detected in the southern sky and detailed study of these sources are now ongoing.

At the Akeno observatory, a series of air shower arrays of increasing geometrical sizes were constructed and operated to observe extremely high energy cosmic rays (EHECRs). The Akeno Giant Air Shower Array (AGASA) was operated from 1991 to January 2004 and covered the ground area of 100 km² as the world largest air shower array. In 13 years of operation, AGASA observed a handful of cosmic rays exceeding the theoretical energy end point of the extra-galactic cosmic rays (GZK cutoff) at 10²⁰ eV. The Telescope Array (TA), a large plastic scintillator array with air fluorescence telescopes has just been constructed in Utah, USA, which will succeed AGASA and measure the EHECRs with an order of magnitude larger aperture than that of AGASA to unveil the origin of super-GZK cosmic rays discovered by AGASA. It is now under tuning and will soon start taking data.

An air shower experiment aiming to search for celestial gamma-ray point sources started in 1990 with Chinese physicists at Yangbajing (Tibet, 4,300 m a.s.l.) and has been successful. This international collaboration is called the Tibet AS γ Collaboration. An extension of the air shower array was completed in 1995 and an emulsion chamber has been combined with this air shower array since 1996 to study the primary cosmic rays around the knee energy region. After successive extensions carried out in 1999, 2002 and 2003, the total area of the air shower array amounts to 37,000 m². The

sun's shadow in cosmic rays affected by the solar magnetic was observed for the first time in 1992, utilizing its good angular resolution at multi-TeV energy region. From this experiment with better statistics, we expect new information to be obtained on the large-scale structure of the solar and interplanetary magnetic field and its time variation due to the 11-year-period solar activities.

A new type of detector, called Ashra (all-sky survey high resolution air-shower detector), has been developed and the first-phase stations have been installed near the Mauna Loa summit in the Hawaii Island. It will monitor optical and particle radiation from high-energy transient objects with a wide field-of-view. The system is under tuning and real observation will start soon.

CANGAROO-III Project

[Spokespersons : R.W. Clay, M. Mori, and T. Tanimori]

In collaboration with the members of:

Institute for Cosmic Ray Research, University of Tokyo, Chiba, Japan; School of Chemistry and Physics, University of Adelaide, Australia; Mt Stromlo and Siding Spring Observatories, Australian National University, Australia; Dept. of Radiological Sciences, Ibaraki Prefectural University of Health Sciences, Ibaraki, Japan; Faculty of Science, Ibaraki University, Ibaraki, Japan; Institute of Space and Astronautical Science, Japan Aerospace Exploration Agency, Kanagawa, Japan; School of Allied Health Sciences, Kitasato University, Kanagawa, Japan; Department of Physics, Konan University, Hyogo, Japan; Department of Physics, Kyoto University, Kyoto, Japan; Solar-Terrestrial Environment Laboratory, Nagoya University, Aichi, Japan; National Astronomical Observatory of Japan, National Institutes of Natural Sciences, Tokyo, Japan; Faculty of Engineering, Shinshu University, Nagano, Japan; Department of Physics, Tokai University, Kanagawa, Japan; Department of Physics, Yamagata University, Yamagata, Japan; Faculty of Management Information, Yamanashi Gakuin University, Yamanashi, Japan [1].

Status of the Project

CANGAROO is an acronym for the Collaboration of Australia and Nippon (Japan) for a GAMMA Ray Observatory in the Outback. As its third-generation experimental setup, the CANGAROO-III stereoscopic Cherenkov telescope system has been in operation since March 2004 with four imaging Cherenkov telescopes of 10 m diameter in the desert area near Woomera, South Australia (136°47'E, 31°06'S, 160m a.s.l.). Stereoscopic observations of atmospheric Cherenkov light images produced by particle showers caused by high-energy particles bombarding the earth allow effective discrimination of gamma-rays from charged cosmic-rays which are the overwhelming backgrounds. Three of the four telescopes (called

T2, T3 and T4 in the order of construction) are currently used in observations as the first telescope, completed in 2000 and having been used as CANGAROO-II, has degraded and is equipped a different electronics system from the others. A stereoscopic triggering system was installed at the beginning of 2005 and has been working properly, rejecting most single muon events, which are the major background component at low energies. We are continuing observations of various candidates of celestial gamma-ray emitters on moonless, clear nights.

CANGAROO-III results

SNR RX J0852.0-4622 [2]

We reported a discovery of a gamma-ray signal from this SNR using observations by CANGAROO-II (single 10 m telescope) in 2001 and 2002 [3]. This discovery was confirmed by the H.E.S.S. experiment [4]. In January and February 2005, we observed this SNR with CANGAROO-III using T2, T3 and T4 in the “wobble” mode, in which the pointing position of each telescope was shifted in declination between ± 0.5 degree from the center of the remnant. After the coarse selections, 1,129 minutes (ON) and 1,081 minutes (OFF) data were available. We applied the Fisher discriminant method to extract a gamma-ray signal from background cosmic-ray events using image moments calculated for each event. The excess count map is shown in Figure 1. The smoothing was carried out using the average of the center and neighboring eight pixels where the pixel size was $0.2^\circ \times 0.2^\circ$. The strong gamma-ray emission from the NW rim is obviously seen, which was first reported by CANGAROO-II [3]. The emission profile shows shell-like structure like that seen in X-rays. The differential energy spectra for the whole remnant is reasonably in agreement with that of H.E.S.S. [4]. The energy spectrum around the NW-rim was measured to be consistent with that of the whole remnant, i.e., flatter than that reported from the previous CANGAROO-II data. The difference can be partially explained by the deterioration of the hardware of the CANGAROO-II telescope.

Galaxy NGC 253

We reported the observation of diffuse gamma-ray emission from NGC253 based on data taken in 2000 and 2001 by CANGAROO-II, indicating a gamma-ray signal at 11σ level [5, 6]. H.E.S.S., however, claimed no detection from that direction [7]. We observed this source with three telescopes in 2004 using the wobble mode in which the pointing position of each telescope was shifted in declination between ± 0.5 degree from the center of the galaxy. Analysis with 1,179 and 753 min. for ON and OFF observations, respectively, showed no significant excess from NGC 253, and we obtained upper limits for this source (Fig. 2) [8]. We suspect there was a problem in the treatment of ‘hot’ channels in the imaging camera which led an apparent excess in the CANGAROO-II data (see [8] for details).

Radio galaxy Cen A/globular cluster ω Cen [9]

We observed a nearby ($z = 0.002$) radio galaxy, Cen A, and a globular cluster, ω Cen, region in March–April 2004

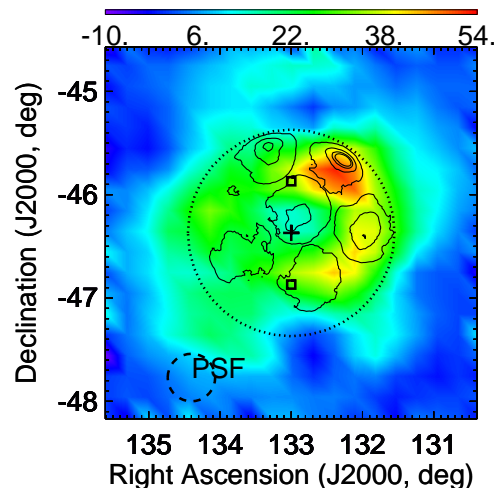


Fig. 1. Excess event map around the SNR RX J0852.0-4622 obtained from the CANGAROO-III stereo observations in 2005 above 1 TeV [2]. The vertical scale (number of events per pixel, $0.2^\circ \times 0.2^\circ$) is indicated in the top bar. The cross indicates the average pointing position, i.e., the center of the remnant and the squares the “wobble” pointing positions. The dashed circle of 0.23° shows the (1σ) point spread function. The dotted circle of 1 degree from the supernova center is also shown. Overlaid contours show X-ray intensity observed by ASCA GIS.

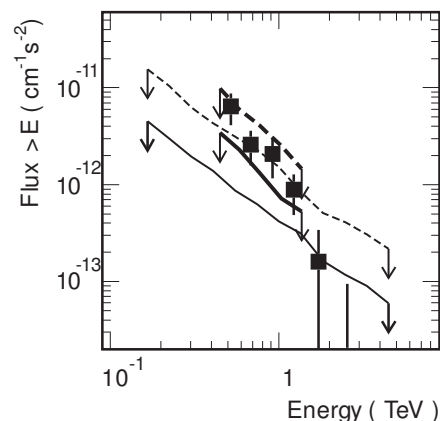


Fig. 2. Upper limits on the gamma-ray flux from NGC 253 [8]. The points with error bars are the CANGAROO-II fluxes [5, 6]. The thin solid line is 99% upper limit (UL) by H.E.S.S. for point source assumption, and the thin dashed is that for 0.5 degree diffuse source [7]. The thick solid line is 2σ upper limit for this observation for point source assumption and the thick dashed line for 0.5 degree diffuse.

with CANGAROO-III. The total observation times were 640 min for Cen A and 600 min for ω Cen. The analysis was carried out inside a one-degree (radius) circle from the average pointing position, but there found no indication of a gamma-ray signal. We derived flux upper limits for regions containing the jet and inner lobes, the middle lobe, and portions of the outer lobes of Cen A, and center of ω Cen above about 400 GeV, depending on the positions. The Cen A upper limits are an order of magnitude lower than previous measurements. The derived upper limits were also used set constraint to the density of cold dark matter. Around the TeV region, we obtained upper limits of its density of $2M_\odot \text{ pc}^{-3}$ for Cen A and

$100M_{\odot} \text{ pc}^{-3}$ for ω Cen (Fig. 3). Note that the limit for Cen ω is smaller than its gravitational mass.

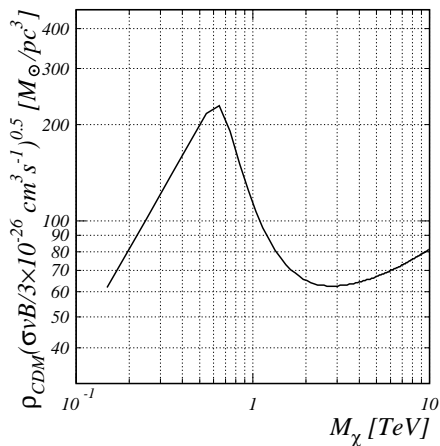


Fig. 3. Upper limits of the cold dark matter density versus particle mass assumption for ω Cen [9]. The abscissa is the dark matter mass, and the ordinate is the dark matter density, assuming the annihilation cross section (σ) multiplied by the relative velocity (v) and the branching fraction (B) is $3 \times 10^{-26} \text{ cm}^{-3} \text{ s}^{-1}$.

Blazar PKS 2155-304

In 2006 July/August, H.E.S.S. reported a large flare of this nearby ($z = 0.117$) blazar [10], and we observed this source as a Target-of-Opportunity observation. With 15 hours of data taken between July 28 and August 2, 2006, we detected a gamma-ray signal at 6.8σ level above 620 GeV [11]. Follow-up observations between August 17 and 25 indicate the source activity had decreased. Fig. 4 shows the daily average flux observed by CANGAROO-III. Note that CANGAROO-III observations are offset in time by about eight hours from contemporaneous H.E.S.S. observations, so that two experiments are complementary in monitoring the flaring activity at TeV energies.

Summary

We have been carrying out stereo observations of sub-TeV gamma-rays with CANGAROO-III since March 2004. There has been a significant progress in the analysis of the stereoscopic observations. On the supernova remnant RX J0852.0-4622, our new results are consistent with the recent H.E.S.S. results. We could not confirm our detection of NGC 253 by the CANGAROO-II observations. Upper limits were given for the nearby radio galaxy, Cen A, and the globular cluster, ω Cen. For the flaring activity of PKS 2155-304 in July/August 2006, we detected time-varying gamma-ray flux from this source. Observations and analyses of other sources are in progress and results will be reported soon.

Bibliography

- [1] Collaboration website:
<http://icrhp9.icrr.u-tokyo.ac.jp>.

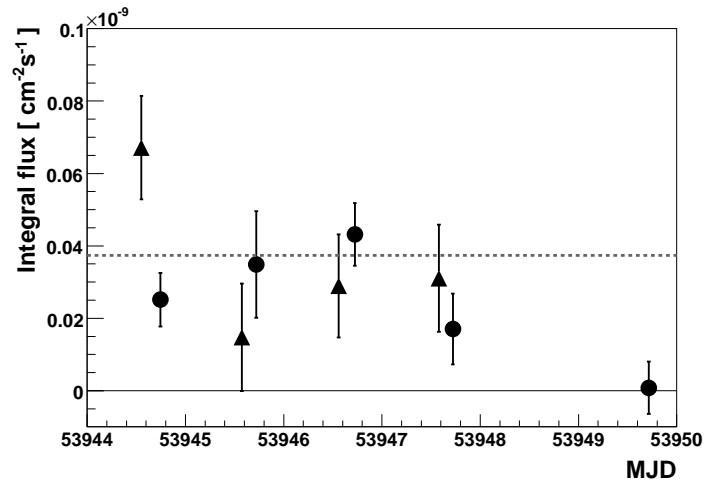


Fig. 4. Daily average integral flux of PKS 2155-304 above 620 GeV between 2006 July 28 and August 2 [11]. Only data taken at zenith angles smaller than 30° are used. Two data points for each night are obtained from two-telescope coincidence before culmination (closed triangles) and three-telescope coincidence after culmination (closed circles), respectively. The data for August 2 is plotted only for after culmination. Dashed line indicates 100 % Crab flux level above 620 GeV.

- [2] R. Enomoto et al., *Astrophys. J.*, **652**, 1268–1276 (2006).
 [3] H. Katagiri et al., *Astrophys. J.* **619**, L163–L165 (2005).
 [4] F. Aharonian et al., *Astron. Astrophys.* **437**, L7–10 (2005).
 [5] C. Itoh et al., *Astron. Astrophys.* **396**, L1–L4 (2002)
 [6] C. Itoh et al., *Astron. Astrophys.*, **402**, 443–455 (2003)
 [7] F.A. Aharonian et al., *Astron. Astrophys.* **442**, 177–183 (2005).
 [8] C. Itoh et al., *Astron. Astrophys.*, **462**, 67–71 (2007).
 [9] Kabuki S et al., *Astrophys. J.*, in press (October 2007).
 [10] W. Benbow et al., *Astronomer's Telegram #867*, July 27, 2006.
 [11] Y. Sakamoto et al., submitted for publication (2007).

TA: Telescope Array Experiment

Spokespersons:

M. Fukushima / ICRR, University of Tokyo
 P. Sokolsky / Dept. of Physics, University of Utah
 Collaborating Institutions:

Chiba Univ., Chiba, Japan; Chonnam National Univ., Gwangju, Korea; Ehime Univ., Matsuyama, Japan; Ewha W. Univ., Seoul, Korea; Hiroshima City Univ., Hiroshima, Japan; ICRR, Univ. of Tokyo, Kashiwa, Japan; Kanagawa Univ., Yokohama, Japan; KEK/IPNS, Tsukuba, Japan; Kinki Univ.,

Higashi-Osaka, Japan; Los Alamos Nat. Lab., Los Alamos, NM, USA; Max-Planck-Inst. for Physics, Muenchen, Germany; Musashi Inst. of Tech., Tokyo, Japan; Nat. Inst. of Rad. Sci., Chiba, Japan; Osaka City Univ., Osaka, Japan; Rutgers Univ., Piscataway, NJ, USA; Saitama Univ., Saitama, Japan; Shibaura Inst. of Tech., Saitama, Japan; Tokyo Inst. of Tech., Tokyo, Japan; Tokyo Univ. of Science, Noda, Japan; Univ. of Denver, Denver, CO, USA; Univ. of Montana, Missoula, MT, USA; Univ. of New Mexico, Albuquerque, NM, USA; Univ. of Utah, Salt Lake City, UT, USA; Utah State Univ., Logan, UT, USA; Yamanashi Univ., Kofu, Japan; Yonsei Univ., Seoul, Korea

Super-GZK Cosmic Rays

The AGASA air shower array observed 11 extremely-high energy cosmic rays (EHECRs) exceeding the energy of 10^{20} eV in 13 years of operation. with a continued spectrum with a power law of $E^{-2.7}$ and the expected GZK-cutoff structure due to the interaction of EHE protons with the cosmic microwave background [1] was not observed. The Fly's Eye air fluorescence telescope also reported an event with 3×10^{20} eV in 1994 [2]. High energy astronomical objects such as the active galactic nuclei and radio galaxies were searched as a possible origin of such EHECRs, but none were found in the arrival direction of these events within 100 Mpc of our galaxy [3]. More distant origins may be considered, but only if a special mechanism to allow a longer propagation of EHECRs to take place, for example the violation of special relativity [4] or the EHE neutrinos as the carrier of such energy [5]. It was therefore conceived that super-GZK ($E > 10^{20}$ eV) cosmic rays may be generated by the decay of super-heavy particles in the nearby universe. Energies beyond 10^{20} eV are easily attained if the mass of the particle is at the Grand Unification scale. A concentration of the particles in the galactic halo makes the non-observation of GZK-cutoff viable. Such super-heavy particles may be surviving as a relic particle of the Big Bang or presently generated by the decay of topological defects [6]. An abundant generation of EHE gamma rays and neutrinos, in place of protons and nuclei, is expected in the decay of such particles.

Overview of TA

The Telescope Array (TA) project was proposed in 2000 [7] to investigate the origin of super-GZK cosmic rays by employing a large array of fluorescence telescopes with ~ 100 times larger acceptance than AGASA. The HiRes experiment, however, presented an energy spectrum indicating the GZK-cutoff in the 27th ICRC in Hamburg and the result was later published in 2003 [8]. It was a monocular spectrum obtained by the single telescope. A preliminary version of the stereo spectrum using two telescopes was presented in 2005 at the 29th ICRC in Pune [9]. It exhibits a clear cutoff structure although the E^3 multiplied flux below $10^{19.5}$ eV seems larger than the monocular flux by a factor of ~ 1.5 . With contradictory results on the existence of GZK cutoff appearing, it became urgent to understand the experimental bias in the energy and the acceptance determination of super-GZK cosmic rays. The construction of full TA is thus deferred, and we initiated constructing a composite detector with AGASA-like

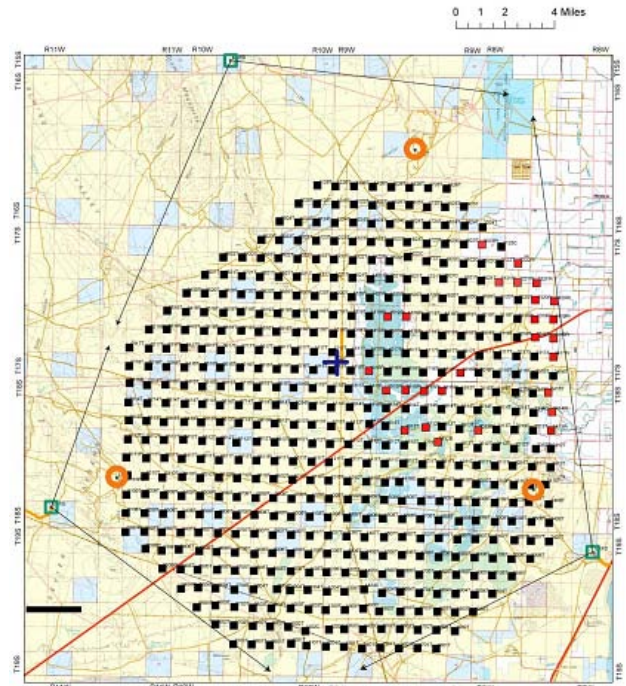


Fig. 1. Detector Arrangement of ph-1 TA. The surface detector locations are indicated by filled black boxes for the deployed ones and filled red boxes for the undeployed ones. The fluorescence telescope stations are marked by green square boxes.

ground array and TA fluorescence telescopes [10] instead. We call it as phase-1 TA (ph-1 TA). We expect simultaneous measurement of the same EHECRs by two detectors will sort out the systematics of two methods. It will guide us to a reliable determination of the primary energy and the acceptance of EHECRs. The phase-1 TA consists of a large plastic scintillator array and three stations of air fluorescence telescopes overlooking the array from periphery as shown in Fig.1. The ground array will give an aperture of ~ 1200 km² sr, which is approximately an order of magnitude larger than that of AGASA. The fluorescence telescope will have a stereoscopic aperture of ~ 300 km² sr with 10% duty factor at 10^{20} eV. The telescope will also supply information on the primary particle species by measuring the longitudinal shower profile. It is being built in the West Desert of Utah, 140 miles south of Salt Lake City (lat. 39.3°N, long. 112.9°W, alt. ~ 1400 m), and the construction is nearly completed.

Ground Array of ph-1 TA

The ground detector consists of 512 plastic scintillators deployed in a grid of 1.2 km spacing. It covers the ground area of ~ 700 km². Approximately 80% of them will be on the Federal land, $\sim 10\%$ on the state trust land and the rest on privately owned land. The detection (trigger) efficiency is $\sim 100\%$ for cosmic rays with energies more than 10^{19} eV with zenith angle less than 45° . The counter is composed of two layers of plastic scintillator overlaid on top of each other. The scintillator (CIMS-G2; CI Kogyo Ltd.) is 1.2 cm thick, 3 m² large and is read out by 104 wave length shifter fibers installed in grooves on the surface (see Fig.2). The fiber (Y-11(200)M; Kuraray Co., Ltd.) has a diameter of 1 mm and a length of



Fig. 2. Scintillation Detector of TA.



Fig. 3. Deployed Surface Detector.

5 m. Both ends of the fiber are optically connected to the photomultiplier (9124SA; Electron Tubes Ltd.). A passage of cosmic ray muon gives ~ 25 photo-electrons in average. Two layers are used for the coincidence measurement, for the muon calibration trigger and for extending the dynamic range by setting different PMT gains for two counters. The signal from each PMT is continuously digitized with a 12-bit flash ADC with 50 MHz sampling. When both of the PMTs record more than $1/3$ of the muon signal, wave forms of $\sim 4 \mu\text{s}$ duration are stored with a time stamp supplied by the GPS (M12+ Timing Oncore Receiver; Motorola, Inc.). This rate of local buffering is less than 1 kHz. The relative timing between remotely separated counters will be better than ± 20 ns by the GPS, which is sufficient to supply good resolution for the determination of the arrival direction. When one of the PMT signals exceeds a trigger threshold of three muons, the timing is recorded in a local trigger list. The content of the list is transmitted to a branch DAQ board by the wireless LAN at 1 Hz. The list may contain less than 100 events for normal counters. The branch DAQ board is installed on a communication tower built at the periphery of the array. In September 2006 three main towers about 12 m high were built for the communication up to ~ 20 km. An air shower event is identified by the branch DAQ firmware by requiring clustered hits with a good coincidence timing. The air shower event rate will be less than 1 Hz when at least three adjacent counters are required in coincidence.

When an air shower trigger is generated in a branch DAQ board, a command is sent to all counters, and relevant coun-



Fig. 4. Deployment of surface detectors by helicopter.

ters storing the event with good coincidence timing respond by transmitting the wave form data to the branch DAQ board. The data are then transmitted to a central DAQ system via tower to tower wireless communication and stored in a mass storage. We employ a commercially produced wireless transmitter with the maximum speed of 11 Mbps using 2.4 GHz spread spectrum technology. The dead-time-less DAQ operation is aimed with the high transmission speed together with a large buffering memory at each counter. One of the counters test-deployed to the field in December 2004 is shown in Fig.3. The total electrical power consumed by the PMT, ADC, GPS and LAN is approximately 7 W and is locally generated by the solar panel of ~ 120 W capacity (KC-120J; Kyocera Co., see Fig.3). Behind the panel is a heat-insulated enclosure containing the backup battery (DCS100-L; 12V, ~ 100 Ah and deep cycle) and all the electronics. A communication antenna is fixed to a mast 3.3 m tall. The total weight of the counter is about half tons, such that it can be easily deployed by helicopter without disturbing the wilderness environment. We started the assembly of scintillator detectors in ICRR in the spring of 2005 and completed the assembly in the autumn of 2006. We exported them to the Cosmic Ray Center in Delta of Utah, USA, where we finally assembled scintillator detectors on the platforms together with other components. We started major deployment of the counters in October 2006. The assembled surface detectors were carried by trucks with trailers to the staging areas by the existing roads in the TA site. Each surface detector was transported by helicopter from the staging area to the position to be deployed (see Fig.4). We deployed 485 counters by the end of February, 2007 before the



Fig. 5. Fluorescence Station at Black Rock Mesa.

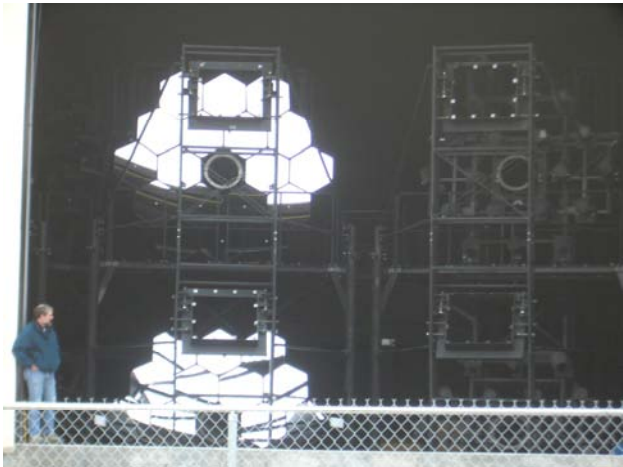


Fig. 6. Fluorescence Telescopes of TA.

period for the protection of active raptor nests between March and August in regards to Bureau of Land Management. At first we will tune the detectors among about 1/3 of the surface array and check on DAQ using these detectors from each branch. After this debugging, we will tune the remaining detectors and deploy remaining 27 counters in the autumn of 2007 and the surface array will be fully operational.

Fluorescence Telescope

The ph-1 TA has three fluorescence stations. The fluorescence station in the southeast is called the Black Rock Mesa (BRM) site. The southwestern station is called Long Ridge (LR) site and the station in the north is called Middle Drum (MD) site. Twelve reflecting telescopes are installed at each of the BRM and LR stations (see Fig.5) and cover the sky of 3° – 34° in elevation and 108° in azimuth looking toward the center of the ground array. The field of view of each telescope (see Fig.6) is 18.0° in azimuth and 15.5° in elevation. A spherical dish of 6.8 m^2 is composed of 18 hexagonal mirrors with a radius of curvature of 6067 mm. The direction of each mirror is individually adjustable and a spot size of less than 20 mm in diameter is realized at the focal plane (2960 mm). The mirror is made by 10.5 mm thick high thermal resistivity glass (Schott Borofloat) and is aluminum coated by vacuum deposition. The surface of the aluminum is protected by producing a $\sim 50 \text{ nm}$ thick anodization layer. The air shower image is detected by a mosaic PMT camera on the focal plane



Fig. 7. Prototype of TA Camera.

(see Fig.7). A set of 16×16 PMTs (Hamamatsu 6234) with a hexagonal window is used for one camera. Each PMT covers $1.1^{\circ} \times 1.0^{\circ}$ patch of the sky. A UV transmitting glass filter (Schott BG3, 4 mm thick) is attached in front of each PMT for blocking the night sky background in the visible light range. The whole camera is assembled in a chassis with a window made by a UV transparent plexiglass. Negative high voltage is applied to the PMT by a bleeder circuit using zener diodes to ensure a stable operation under high night sky background. The high voltage is individually adjustable for all PMTs. With a PMT gain of $\sim 10^5$, a linearity of up to 32 k photoelectrons in 100 ns was achieved. A signal from the PMT is amplified by a factor of 50 by the pre-amplifier and is sent to a Signal Digitizer and Finder (SDF) with a twisted pair cable 25 m long. The SDF module receives the signal with a shaping filter and digitizes it with a 12-bit, 40 MHz FADC. Consecutive four samplings are added by the following FPGA. A trace of fluorescence signal is searched in pipeline at the FPGA employing a sliding sum algorithm for every $25.6 \mu\text{s}$ of the time window. The dc component from the night sky background is estimated every 1 ms and is subtracted. The SDF is a 9U VME module and 16 channels are mounted in one module. The result of the “hit” search by the SDF is reported to a Track Finder (TF) in the same VME crate and an air shower track is searched in one camera. A track is found when five or more adjacent PMTs are fired. A looser track definition is applied to a camera-crossing event. The results of all TF modules are concentrated to a Central Trigger Decision (CTD) module and the decision of data acquisition is made. The wave form data stored in the SDF memory are read out to “a camera PC” in parallel and a complete event is subsequently built from the camera PCs by Ethernet. Sample PMT wave forms triggered and collected in Utah by the prototype electronics is shown in Fig.8. The calibration of the telescope sensitivity is important for the measurement of energy. Characterizing parameters of each component such as the mirror reflectivity, filter transmission, PMT quantum efficiency and the electronics gain will be

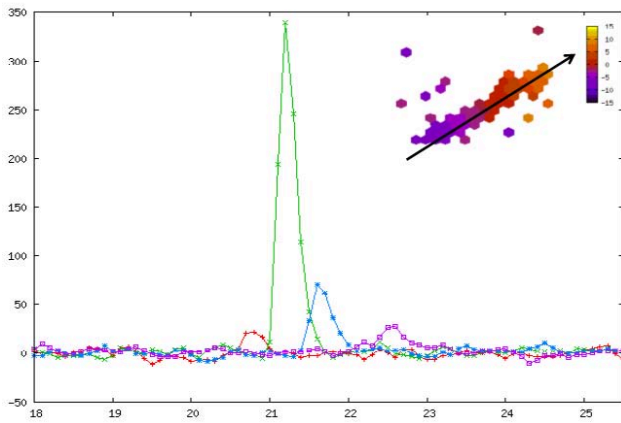


Fig. 8. One of the first fluorescence signals of TA. Wave forms of several PMTs in the track are overlaid in order to show the time evolution of the signal.

measured piece by piece at the production. The relative gain of all PMTs will be adjusted in situ by the Xenon Flasher installed at the center of the mirror. The light from the flasher is diffused and filtered by BG3. The Xenon Flasher supplies a light pulse of good uniformity ($< 3\%$) to all PMTs in a camera. There are three “standard” PMTs installed in a camera. The efficiency and the gain of the standard PMT are calibrated before installing to a camera and their values are transmitted to other PMTs by the Xenon Flasher calibration. A tiny YAP (YAlO₃:Ce) scintillator with 50 Bq ²⁴¹Am source is embedded in the BG3 filter of the standard PMT. The YAP generates a short light pulse of ~ 3000 photons around 370 nm and has an excellent temperature stability. The calibration of the standard PMT will be maintained by the YAP pulser. For the calibration of the standard PMT, we developed a light source using a Rayleigh scattering of nitrogen laser (337 nm) in the nitrogen atmosphere. The power of laser is measured pulse by pulse to an accuracy of 5% and the known cross section of Rayleigh scattering is applied to calculate the intensity of the scattered light. The UV fluorescence light generated by the air shower is scattered and lost along the path of transmission to the telescope. The responsible processes are Rayleigh scattering by the air molecule and Mie scattering by the aerosol. The Rayleigh scattering can be calculated with an accuracy of $\sim 5\%$ from the known density and temperature distribution of the atmosphere. The amount of Mie scattering differs from place to place and changes with time reflecting the aerosol distribution in the air. It has to be continuously monitored on site. A lidar system located at each station will be used for the atmospheric monitoring. It consists of a pulsed Nd:YAG laser (the third harmonic, 355 nm) and a telescope attached to an alto-azimuth mount and sharing the same optical axis as shown in Fig.9. The laser can be shot to any direction and the back-scattered light is received by the telescope to analyze the extinction coefficient along the path of the laser. We had shown in Akeno that the change of the three-dimensional distribution of extinction coefficient can be monitored within 10 km from each station [11]. We are also building a laser shooting facility in the middle of the array. The site is chosen such that a vertical shot of the laser from this station is equidistant to all fluorescence stations. The intensity of the laser shot



Fig. 9. TA Lidar at Black Rock Mesa.

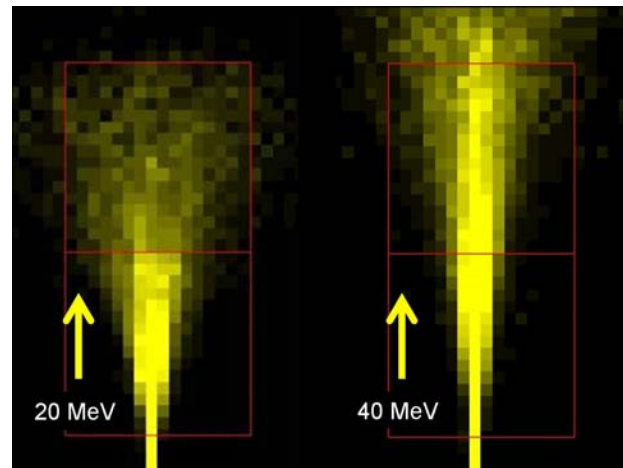


Fig. 10. Electron Linac Beam seen by the Fluorescencetelescopes (simulation by GEANT).

is monitored to 5% accuracy and the Rayleigh scattering at high altitude can be considered as a “standard candle” observable at all stations. The comparison of the received light will give a reliable information for the difference and the change of atmospheric conditions. For monitoring the cloud in the night sky, we will install an infra-red CCD camera at each station. In order to confirm the absolute energy scale of the fluorescence detector in situ, we are planning to deploy a compact accelerator ~ 100 m away from the fluorescence station and inject an electron beam vertically up into the atmosphere. The simulation of observed fluorescence signal by 20 and 40 MeV electron beams is shown in Fig.10. A beam of 10^9 electrons with a duration of $1 \mu\text{s}$ well simulates a shower energy deposition of $\sim 4 \times 10^{16}$ eV, which corresponds to a shower of $\sim 4 \times 10^{20}$ eV 10 km away. The calibration is obtained by comparing the observed fluorescence signal with the expected energy deposition calculated by the GEANT simulation. The accelerator was designed with a collaboration of KEK accelerator physicists and are being assembled in KEK. We will test the basic performance of the accelerator in KEK in 2007.

In the autumn of 2006, we measured the focal length of the remaining hexagonal mirrors and assembled 16 cameras in the Akeno Observatory. In March 2007, the telescope system at the BRM station is nearly completed. Fig. 11 shows an event of a laser shot from the lidar taken with multiple cameras by

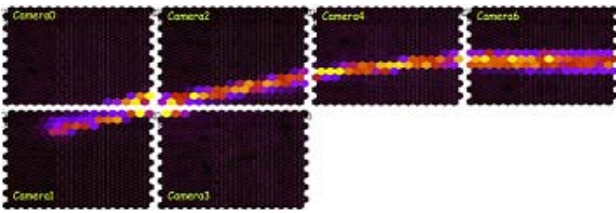


Fig. 11. The views taken by the cameras of the six fluorescence telescopes for a laser shot from the lidar.



Fig. 12. The Middle Drum Observatory Building.

the shower event trigger. We installed the telescope structures, adjusted hexagonal mirrors, and partially attached the cameras at the LR telescope station in February and March of 2007.

The HiRes observatory was shut down in April 2006. The Middle Drum fluorescence station has been constructed using refurbished equipment from the old HiRes-I observatory at Dugway in Utah. The equipment has been modified somewhat and has been relocated to a new building. A picture of the Middle Drum Observatory is shown in Fig. 12. The building, which houses 14 telescopes, consists of seven bays each about the size of a two car garage. HiRes mirrors are 20% smaller in area than the mirrors in the BRM and LR stations. The MD fluorescence detector will also observe at elevation angles from 3 to 31 degrees.

Three fluorescence stations will be fully operational in the autumn of 2007.

Prospects

The construction of the ph-1 TA is almost completed by the collaboration of Japanese, Korean, and American physicists. We plan to start taking data partially rather soon and complete the construction in the autumn of 2007 and the ph-1 TA will be fully operational. The group consists of physicists who have been working in AGASA, HiRes and other HEP experiments in US, Korea, and Japan. The Japanese fund for ph-1 TA was approved in 2003 by the Grants-in-Aid for Scientific Research (Kakenhi) of Priority Areas. The US group has submitted a matching proposal to NSF in 2005. The US proposal includes a construction of TALE, a Low Energy extension of TA down to 10^{17} eV, to investigate the modulation of CR composition and spectrum expected by the galactic to extra-galactic transition of CR origins. The infrastructure of

TA and TALE in Utah is also the responsibility of US group. The US fund is supported by the US National Science Foundation (NSF) through awards PHY-0307098 and PHY-0601915 (University of Utah) and PHY-0305516 (Rutgers University). The Pierre Auger group is constructing a large hybrid experiment in Argentina with 1600 water tank detectors. All the fluorescence telescopes are operational. The deployment of the surface detectors will be completed by the end of 2007. The group presented the first EHECR spectrum at the 29th ICRC in August 2005 using an exposure already larger than what AGASA had accumulated in 13 years of operation. There was no event exceeding 10^{20} eV. The group considers, however, premature to conclude the existence of GZK-cutoff because the present systematic error of energy determination is estimated to be at least 40%. The Auger group calibrated the ground array energy estimator $\rho(1000)$, the muon density 1000 m away from the shower center, by the measurement of shower energy from the fluorescence telescope. The extrapolation of the calibration from the lower energy, where most of the hybrid events were collected, caused the major part of the systematic error. The construction of ph-1 TA will be finished a few months after the Pierre Auger is completed in Argentina. The acceptance of Auger ground array is ~ 4.5 times larger than that of ph-1 TA assuming the same zenithal acceptance. The scintillator of TA counts the number of penetrating charged particles and it is dominated by the electrons which outnumber the muons by an order of magnitude. The water tank of Auger on the other hand is more sensitive to the penetrating high energy muons rather than the soft electrons which stop near the surface of the water tank and do not generate as many Cherenkov photons. The energy measurement of ph-1 TA therefore is less sensitive to the unknown composition of the primary cosmic rays and the details of hadronic interactions at EHE, whereas its sensitivity to the composition determination using the muon content is severely limited particularly for the EHE gamma rays and neutrinos. It is our belief that the characteristic features of ph-1 TA, the sampling of electromagnetic shower energy, the unique calibration of fluorescence generation and the measurement in the Northern Hemisphere, will make an essential contribution to the understanding of the intricate problem of GZK cutoff.

Bibliography

- [1] K.Greisen, Phys. Rev. Lett. **16**, 748 (1966); T.Zatsepin and V.A.Kuzmin, JETP Lett. **4**, 178 (1966).
- [2] D.J.Bird et al., Astrophys. J., **424**, 491 (1994).
- [3] Y.Uchihori et al., Astropart. Phys. **13**, 151 (2000); G.Sigl et al., Phys. Rev. **D63**, 081302 (2001).
- [4] H.Sato and T.Tati, Prog. Theo. Phys. **47**, 1788 (1972); S.Coleman and S.L.Glashow, Phys.Rev. **D59**, 116008 (1999).
- [5] T.J.Weiler, Astropart.Phys. **3**, 303 (1999).
- [6] V.Kuzmin and I.Tkachev, JETP Lett. **68**, 271 (1998); V.Berezinsky, P.Blasi and A.Vilenkin, Phys.Rev. **D58**, 103515 (1998); K.Hamaguchi, I.Izawa, Y.Nomura

and T.Yanagida , Phys.Rev. **D60**, 125009 (1999);
V.Berezinsky, Nucl. Phys. Proc. Suppl. **81**, 311 (2001).

[7] The Telescope Array Project: Design Report, July, 2000.

[8] T.Abu-Zayyad et al., Phys. Rev. Lett. **92**, 151101 (2004);
T.Abu-Zayyad et al., Astropart. Phys. **23**, 157 (2005).

[9] Proc. of 29th ICRC, Pune (2005) to be published.

[10] M.Fukushima et al., Proc. of 28th ICRC, Tsukuba, **2**,
1025 (2003); S.Kawakami et al., Proc. of 28th ICRC,
Tsukuba, **2**, 1033 (2003); F.Kakimoto et al., Proc. of 28th
ICRC, Tsukuba, **2**, 1029 (2003); M.Fukushima, Proc. of
APPI2003 workshop, KEK Proceedings 2003-6.

[11] T.Yamamoto et al., Nucl. Instr. and Methods **A488**, 191
(2002).

Tibet AS γ Project

[Spokesperson : Masato Takita]

ICRR, Univ. of Tokyo, Kashiwa, Chiba 277-8582

In collaboration with the members of:

Hirosaki Univ., Hirosaki, Japan; Saitama Univ., Urawa, Japan;
Yokohama National Univ., Yokohama, Japan; IHEP, Bei-
jing, China; Tibet Univ., Lhasa, China; Shandong Univ., Jin-
nan, China; South West Jiaotong Univ. Chengdu, China;
Yunnan Univ., Kunming, China; Kanagawa Univ., Yoko-
hama, Japan; Utsunomiya Univ., Utsunomiya, Japan; ICRR,
Univ. of Tokyo, Kashiwa, Japan; Konan Univ., Kobe, Japan;
Shibaura Inst. of Technology, Saitama, Japan; Shinshu Univ.,
Matsumoto, Japan; Center of Space Science and Applica-
tion Research, Beijing, China; AMNC, Utsunomiya Univ.,
Utsunomiya, Japan; NII, Tokyo, Japan; Tokyo Metropolitan
Coll. of Aeronautical Eng., Tokyo, Japan; Shonan Inst. of
Technology, Fujisawa, Japan; Waseda Univ., Tokyo, Japan;
RIKEN, Wako, Japan.

Experiment

The Tibet air shower experiment has been successfully op-
erated at Yangbajing (90°31' E, 30°06' N; 4300 m above sea
level) in Tibet, China since 1990. It has continuously made a
wide field-of-view (approximately 2 steradian) observation of
cosmic rays and gamma rays in the northern sky.

The Tibet I array was constructed in 1990 and it was grad-
ually upgraded to the Tibet II by 1994 which consisted of
185 fast-timing (FT) scintillation counters placed on a 15 m
square grid covering 36,900 m², and 36 density (D) counters
around the FT-counter array. Each counter has a plastic scin-
tillator plate of 0.5 m² in area and 3 cm in thickness. All the
FT counters are equipped with a fast-timing 2-inch-diameter
photomultiplier tube (FT-PMT), and 52 out of 185 FT coun-
ters are also equipped with a wide dynamic range 1.5-inch-
diameter PMT (D-PMT) by which we measure up to 500 par-
ticles which saturates FT-PMT output, and all the D-counters
have a D-PMT. A 0.5 cm thick lead plate is put on the top
of each counter in order to increase the counter sensitivity by

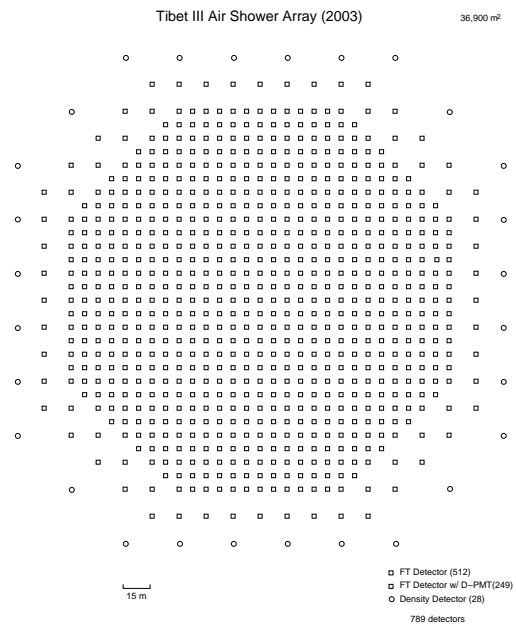


Fig. 1. Schematic view of the Tibet III array.

converting gamma rays into electron-positron pairs in an elec-
tromagnetic shower. The mode energy of the triggered events
in Tibet II is 10 TeV.

In 1996, we added 77 FT counters with a 7.5 m lattice in-
terval to a 5,200 m² area inside the northern part of the Tibet II
array. We called this high-density array Tibet HD. The mode
energy of the triggered events in Tibet HD is a few TeV.

In the late fall of 1999, the array was further upgraded by
adding 235 FT-counters so as to enlarge the high-density area
from 5,200 m² to 22,050 m², and we call this array and further
upgraded one Tibet III. In 2002, all of the 36,900 m² area was
covered by the high-density array by adding 200 FT-counters
more. Finally we set up 56 FT-counters around the 36,900 m²
high density array and equipped 8 D-counters with FT-PMT
in 2003. At present, the Tibet air shower array consists of 761
FT-counters (249 of which have a D-PMT) and 28 D-counters
as in Fig. 1.

The performance of the Tibet air shower array has been
well examined by observing the Moon's shadow (approximate-
ly 0.5 degree in diameter) in cosmic rays. The deficit map
of cosmic rays around the Moon demonstrates the angu-
lar resolution to be around 0.9° at a few TeV for the Tibet III
array. The pointing error is estimated to be better than ~0.01°,
as shown in Fig. 2(a), by displacement of the shadow's center
from the apparent center in the north-south direction, as the
east-west component of the geomagnetic field is very small at
the experimental site. On the other hand, the shadow center
displacement in the east-west direction due to the geomag-
netic field enables us to spectroscopically estimate the energy
scale uncertainty at ±15 % level, as shown in Fig. 2(b).

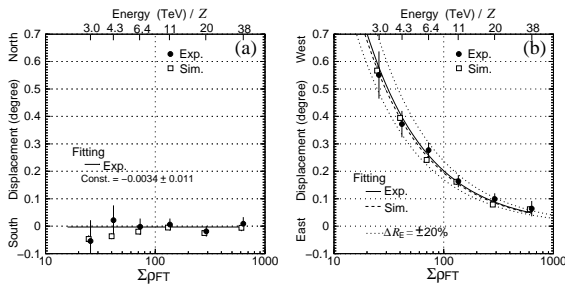


Fig. 2. The Moon's shadow center displacement from the apparent position as a function of energy for (a) in the north-south direction and (b) in the east-west direction, respectively, observed by Tibet III.

Thanks to high statistics, the Tibet air shower experiment introduces a new method for energy scale calibration other than the conventional estimation by the difference between the measured cosmic-ray flux by an air shower experiment and the higher-energy extrapolation of cosmic-ray flux measured by direct measurements by balloon-borne or satellite experiments.

Physics Results

We study:

- (1) TeV celestial gamma-ray point/diffuse sources,
- (2) Chemical composition and energy spectrum of primary cosmic rays in the knee energy region,
- (3) Cosmic-ray anisotropy in the multi-TeV region with high precision,
- (4) Global 3-dimensional structure of the solar and interplanetary magnetic fields by observing the Sun's shadow in cosmic rays.

(1) TeV celestial gamma-ray point/diffuse sources

Using this HD array, in 1999, we succeeded in observing multi-TeV gamma-ray signals from the Crab Nebula at 5.5σ confidence level [1]. This was the first detection of multi-TeV γ -ray signals by a conventional air shower array. Subsequently, we also detected multi-TeV γ rays successfully at 3.7σ level from Mrk501 which was in a highly flaring state between March 1997 and August 1997 [4]. Multi-TeV γ -ray signal was successfully detected at $\sim 5\sigma$ level from the Crab (the standard candle in γ -ray astronomy) by the Tibet-III array.

We also succeeded in observing multi-TeV gamma-ray flares at 5.1σ level from Markarian 421 [9] which was in a very active phase during the year 2000 and 2001. We observed a clear long-term positive correlation between X-ray data (Rossi X-ray Timing Explorer (RXTE) satellite) and our TeV γ -ray data from Mrk421 in the active period.

We also searched for multi-TeV diffuse γ -rays from the galactic plane [8]. As there was no significant signal, flux upper limits were obtained from the inner galaxy ($20^\circ < \ell < 55^\circ$, $-2^\circ < b < 2^\circ$) and the outer galaxy ($140^\circ < \ell < 225^\circ$, $-2^\circ < b < 2^\circ$), where ℓ and b are the galactic longitude and

latitude, respectively. For example, we set the most stringent upper limits at multi-TeV energies.

We searched for TeV steady point sources in the northern sky. No statistically significant point source is found except for well established Crab and Mrk421 [12]. The flux upper limits obtained is typically 0.3 to 0.6 in unit of Crab gamma-ray intensity at 90% confidence level.

Search for steady PeV gamma-ray emission from the Monogem ring region is done with the Tibet data taken from 1997 to 2004 [13]. No evidence for statistically significant gamma-ray signals is found in a region $111^\circ < \text{R.A.} < 114^\circ$, $12.5^\circ < \text{decl.} < 15.5^\circ$ in the Monogem ring where the MAKET-ANI experiment recently claimed a positive (approximately 6σ) detection of PeV high-energy cosmic radiation ², although our flux sensitivity is approximately 10 times better than MAKET-ANI's. We set the most stringent integral flux upper limit at 99% confidence level of $4.0 \times 10^{-12} \text{cm}^{-2} \text{s}^{-1} \text{sr}^{-1}$ above 1 PeV on diffuse γ rays extended in the $3^\circ \times 3^\circ$ region.

We are now accumulating Tibet III data to search for unknown constant/transient TeV gamma-ray sources. Possible hadron/gamma-ray separation is under extensive study.

(2) Chemical composition and energy spectrum of primary cosmic rays in the knee energy region

A hybrid experiment of emulsion chambers (EC) and air shower array started in 1996 to obtain the energy spectrum of the primary cosmic-ray proton flux around the knee energy region. The total area of EC, each having the size of $40 \text{ cm} \times 50 \text{ cm}$, is 80 m^2 and the total thickness of lead plates is 14 radiation length (r.l.) High-sensitivity X-ray films were interleaved between the 14 r.l. lead plates at every 2 r.l. to detect γ -ray families. Just below the emulsion chambers, the burst detectors (BD) with the same area as EC were set up to locate the air shower cores of the family events to be observed in EC. This detector complex was set up near the center of the Tibet-II array (AS) to get on the information on air showers accompanied with the family events. The first EC exposure was terminated in August of 1997 and X-ray films inserted in EC were developed for analysis. A high-energy family event of about 500 TeV was observed in this exposure and its primary energy is estimated to be about 10^{16} eV from the size of the accompanying AS data. This hybrid experiment continued until 1999. Using the BD + AS data, we obtained the energy spectrum of primary protons (820 proton-induced events during 690-day detector live time) with its primary energies 200–1000 TeV by a neural network method [6, 7]. As a proton tends to cause a young air shower penetrating deep into the atmosphere due to its longest mean free path among various nuclei and leaving a big energy deposit in BD, the ratio of energy deposit in BD to that in AS is the most important input to artificial neural network (ANN). The differential energy spectrum obtained in this energy range, as shown in Fig. 3, can be fit by a power law function with the spectral index of -2.97 ± 0.06 , which is steeper than that obtained by direct measurements at

^{*2} A. Chilingarian, H. Martirosian, and G. Gharagozyan, Ap. J. 597, L129 (2003).

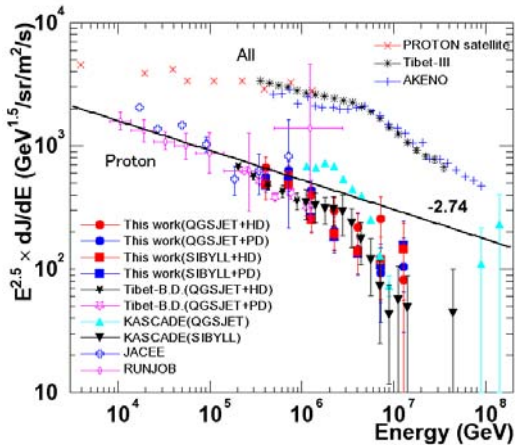


Fig. 3. Primary proton energy spectrum in the knee energy region, assuming the QGSJET and SIBYLL models. The upper 3 (lower 10) measurements correspond to all particles (protons).

lower energies. We also obtained the energy spectrum of helium nuclei. All of the features of BD events are wholly compatible with the heavy enriched composition in the knee region. In 2003, we finished the analysis of all the EC data by means of an automatic analysis program based on track information read out by image scanners. The primary proton spectrum around the knee region [14], being inaccessible by any direct observations, are obtained again by an ANN analysis of the 3-year EC + BD + AS data, as shown in Fig. 3. The proton spectrum can be expressed by a single power-law function with a differential index of -3.01 ± 0.11 and -3.05 ± 0.12 based on the QGSJET+HD and SIBYLL+HD models, respectively, which are steeper than that extrapolated from the direct observations of -2.74 ± 0.01 in the energy range below 10^{14} eV. The energy spectrum of helium nuclei is obtained as well. The absolute fluxes of protons and helium nuclei are estimated within 30% systematic errors depending on the hadronic interaction models used in our Monte Carlo simulation. This is the first measurement of the differential energy spectra of primary protons and heliums by selecting them event by event at the knee energy region.

We also obtained a preliminary result on the primary cosmic-ray all-particle energy spectrum by Tibet III, as shown in Fig. 3, which is consistent with the one obtained by the Tibet I experiment. The (all-particle - (proton+helium))/all-particle flux ratio is shown in Fig. 4, indicating that the knee is composed of nuclei heavier than helium. It should be noted that the flux ratio largely cancels out the systematic energy scale uncertainty in the air shower energy determination.

The Tibet hybrid experiment measures the electromagnetic component in an air shower which is weakly dependent on hadron interaction models, as it is a central-region phenomenon described by the Feynman scaling (or QCD). On the other hand, the KASCADE results³ which measures both air shower size (N_e) and muon size (N_μ) to deduce the energy spectrum of separate mass groups from the all-particle energy spectrum, strongly depend on the interaction models. The muon size contained in the air shower depends on the

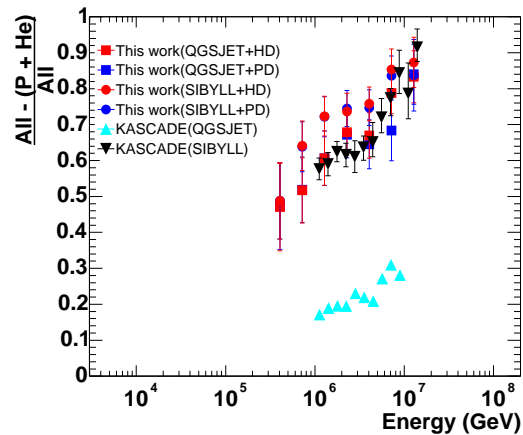


Fig. 4. Primay (all-particle - (proton+helium))/all-particle flux ratio in the knee energy region, assuming the QGSJET and SIBYLL models.

number of charged pions produced in the central and backward region (in the center of mass system) in the collisions of primary cosmic rays on air nuclei, which has a sizeable uncertainty experimentally as well as theoretically and is largely dependent on the interaction models. From this point of view, the size of low-energy muons N_μ may not be a suitable parameter for separating the air showers into different primary mass groups.

(3) Cosmic-ray anisotropy in the multi-TeV region with high precision

Based on the Tibet III data from 1999 and 2003, we succeeded in observation of the multi-TeV galactic cosmic-ray anisotropy (approximately 0.05 % level) at solar time frame due to the terrestrial orbital motion around the Sun, i.e. Compton-Getting (C-G) effect [10].

We observed a clear C-G anisotropy in the 6.2 and 12 TeV data samples, while the anisotropy observed in the 4 TeV data sample deviates from the expected C-G anisotropy. This suggests an additional anisotropy superposed at the multi-TeV energies, e.g., the solar modulation effect. This suggests an additional anisotropy superposed at multi-TeV energies, e.g., the solar modulation effect. This is the highest-precision measurement of the C-G anisotropy ever made and showed its energy dependence for the first time. In addition, the successful detection of the existent C-G anisotropy, the standard candle as a calibration source, ensures the reliability of an experiment which measures the sidereal cosmic-ray anisotropy (approximately 0.1 % level).

As the precision of the Tibet III array is back-checked by the observation of the C-G effect, we proceed to measure the multi-TeV cosmic-ray anisotropy in sidereal time frame with the world best statistics [11]. Both the amplitude and the phase of the first harmonic vector of the daily variation are remarkably independent of primary energy at least up to multi-TeV energies. This is the first result determining energy dependence of the full 24-hour profiles of the sidereal daily variation in the multi-TeV region with a single air shower ex-

*3 T. Antoni et al., *Astroparticle Phys.* 24, 1-25 (2005).

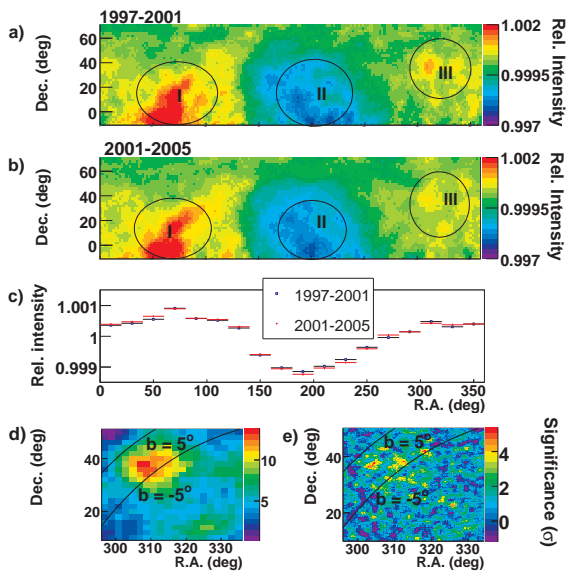


Fig. 5. 2-dimensional relative intensity map of multi-TeV cosmic-ray anisotropy at sidereal time frame obtained by Tibet III.

periment.

The 2-dimensional anisotropy in the equatorial coordinates are obtained for the first time [12] in the multi-TeV energy range, thanks to high statistics, as shown in Fig. 5. The “Tail-in” (hump) and “Loss-cone” (dip) structures are impressive. Furthermore, we discovered a very interesting excess in the Cygnus region, although we cannot judge currently whether it is caused by gamma rays and/or a local cosmic-ray anisotropy. The Milagro group capable of hadron/gamma-ray discrimination recently claimed detection of TeV diffuse gamma-ray signal in the Cygnus region along the galactic plane⁴. The estimated flux may be plotted under the Tibet-III sensitivity by a factor of 3 approximately. We also find that the observed anisotropy tends to be faint over 300 TeV region. This implies that cosmic rays corotate with our galaxy.

(4) Global 3-dimensional structure of the solar and interplanetary magnetic fields by observing the Sun’s shadow in cosmic rays

The Tibet air shower array is very powerful to get new information on the relation between time variation of the large-scale structure of the solar and interplanetary magnetic fields and the solar activities by the sun’s shadow in cosmic rays, since high-statistics data taken by the Tibet air shower array can follow up the movement of the Sun’s shadow at every one-two months. The depth and displacement of the center position in the Sun’s shadow are expected to have an anti-correlation with the 11-year-period solar activities which affect the solar and interplanetary magnetic fields, as the charged cosmic rays are bent by them.

The Sun’s shadow was observed in the direction significantly away from the optically observed Sun’s position during the period from 1990 through 1993. Note that this period corresponded to the near-maximum or at the decreasing phase in the solar Cycle 22. In 1996 and 1997, however, we found

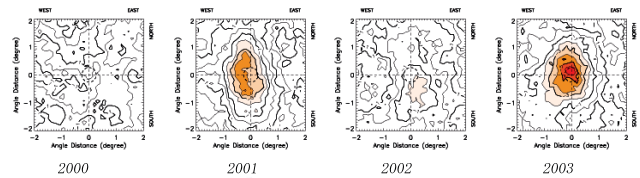


Fig. 6. Yearly variation of the Sun’s shadow observed by the Tibet air shower array from 2000 to 2003. Mode energies are 3 TeV. A contour map demonstrates the weights of deficit event densities around the Sun in the area of $4^\circ \times 4^\circ$ centered at the Sun. The contour curves are drawn from a level of no deficit, 0σ , with a step of 1σ .

that the Sun’s shadow was observed in the direction close to the optically observed Sun’s direction, since the solar cycle was in a quiet phase then [5]. Since 1998, the Sun’s shadow has been obscure, as the solar activities were back in an active phase in solar Cycle 23 went toward its maxima in the years of 2001 and 2002. The year 2001 inbetween corresponds to “Gnevyshev Gap” in sunspot numbers which is an empirical phenomenon supposed to have a relation with the reversal process of the solar dipole-magnetic field. Figure 6 shows an anti-correlation of the Sun’s shadow at 3-TeV mode energy with “Gnevyshev Gap”.

Although we have not observed a clear Sun’s shadow yet, we expect to see a darker Sun’s shadow around 2006 when the next solar minimum appears. As the existing measurements of the solar and interplanetary magnetic fields are limited near the Earth or near the Sun, the Sun’s shadow analysis may contribute considerably to the study of them. An extensive comparison between the solar and interplanetary magnetic field models and our data is under way.

Other Activities

This group has developed and completed several automatic measuring systems that are powerful for analyzing cosmic ray tracks or air shower spots, that is, automatic microdensitometers, precise coordinate-measuring systems and image scanners controlled by a computer. Enormous data recorded on nuclear emulsion plates or X-ray films are rapidly and precisely measured by the use of these measuring systems.

The emulsion-pouring facilities can meet the demands for making any kind of nuclear emulsion plates which are used for cosmic ray or accelerator experiments. The thermostatic emulsion-processing facilities are operated in order to develop nuclear emulsion plates or X-ray films. Using these facilities, it is also possible to make and develop emulsion pellicles in $600 \mu\text{m}$ thickness each. In this way, these facilities are open to all the qualified scientists who want to carry out joint research program successfully.

Future Plans

(1) Gamma-ray astronomy in the 100 TeV region

We have a plan to construct a large ($\sim 10,000 \text{ m}^2 \times 1.5 \text{ m}$ deep) underground ($\sim 2.5 \text{ m}$ soil+concrete overburden) wa-

*⁴ R. Atkins et al., Phys. Rev. Lett. 95, 251103 (2005)

ter Cherenkov muon detector array (Tibet MD) around an extended version (Tibet AS, $\sim 83,000 \text{ m}^2$) of Tibet III. By Tibet AS + MD, we aim at background-free detection of celestial point-source gamma rays in the 100 TeV region (10 TeV – 1000 TeV) with world-best sensitivity and at locating the origins of cosmic rays accelerated up to the knee energy region in the northern sky. The measurement of cut off energies in the energy spectra of such gamma rays in the 100 TeV region may contribute significantly to understanding of the cosmic-ray acceleration limit at SNRs. Search for extremely diffuse gamma-ray sources by Tibet AS + MD, for example, from the galactic plane or from the Cygnus region may be very intriguing as well. Above 100 TeV, the angular resolution of Tibet AS with 2-steradian wide field of view is 0.2° and the hadron rejection power of Tibet MD is 1/10000. The proposed Tibet AS + MD, demonstrated in Fig. 7, has the world-best sensitivity in the 100 TeV region, superior to HESS above 10-20 TeV and to CTA above 30-40 TeV.

Then, how many unknown/known sources do we expect to detect by Tibet AS + MD, assuming the energy spectra of the gamma-ray sources extend up to the 100 TeV region? Eleven of the HESS new 14 sources discovered by the galactic plane survey in the southern sky would be detected by Tibet AS + MD, if it were located at the HESS site. As no extensive search has been done by an apparatus with sensitivity comparable to HESS (1 % in unit of RX J1713.7-3946/50-hour observation) in the northern sky, we expect to discover some 10 new gamma-ray sources in the northern sky. In addition to unknown point-like sources, we expect to detect established sources in the 100 TeV region: TeV J2032+4130 (*sim1* Crab intensity), HESS J1837-069 (~ 0.4 Crab intensity), Crab, four new Milagro sources, Mrk421, Mrk501 are sufficiently detectable and Cas A, HESS J1834-087, LS I+63 303, IC443 and M87 are marginal.

Furthermore, our integral flux sensitivity to diffuse gamma rays will be the world-best as well. The diffuse gamma rays from the Cygnus region reported by the Milagro group and also diffuse gamma-rays from the galactic plane will be clearly detected. Diffuse gamma-rays of extragalactic origin may be an interesting target as well.

(2) Chemical composition of primary cosmic rays making the knee in the all-particle energy spectrum

We have measured the energy spectra of primary cosmic-ray protons, heliums, all particles around the knee energy region. The main component responsible for making the knee structure in the all particle energy spectrum is heavier nuclei than helium. The next step is to identify the chemical component making the knee in the all particle energy spectrum. We have a plan to install an air shower core detector array (approximately 1000 m^2 in area) around the center of Tibet III to distinguish the heavy component making the knee by measuring the difference in lateral distribution of energetic air shower cores. This will be the first experiment to selectively measure the energy spectrum of the heavy component in the knee energy region and will demonstrate that the knee of the all particle energy spectrum is really composed of heavy nuclei.

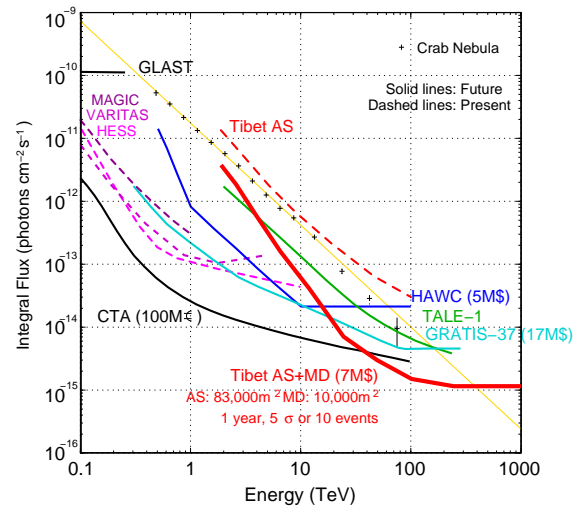


Fig. 7. Tibet AS + MD (red curve) integral flux sensitivity (5σ or 10 events/1yr) for a point source.

Bibliography

Papers in refereed journals

- [1] “Observation of Multi-TeV Gamma Rays from the Crab Nebula using the Tibet Air Shower Array”, M. Amenomori *et al.*, *ApJ*, **525**, L93-L96 (1999).
- [2] “Sun’s shadow by 10 TeV cosmic rays under the influence of solar activity”, M. Amenomori *et al.*, *Advances in Space Research*, **23**, 611-615 (1999).
- [3] “Sidereal daily variation of 10 TeV cosmic-ray intensity observed by the Tibet air shower array”, K. Munakata *et al.*, *Advances in Space Research*, **23**, 599-602 (1999).
- [4] “Detection of Multi-TeV Gamma Rays from Markarian 501 During an Unforeseen Flaring State in 1997 with the Tibet Air Shower Array”, M. Amenomori *et al.*, *ApJ*, **532**, 302-307 (2000).
- [5] “A Study of the Shadowing of Galactic Cosmic Rays by the Sun in a Quiet Phase of Solar Activity with the Tibet Air Shower Array”, M. Amenomori *et al.*, *ApJ*, **541**, 1051-1058 (2000).
- [6] “Measurement of air shower cores to study the cosmic ray composition in the knee energy region”, M. Amenomori *et al.*, *Phys. Rev. D*, **62**, 072007 (2000).
- [7] “Primary proton spectrum between 200 TeV and 1000 TeV observed with the Tibet burst detector and air shower array”, M. Amenomori *et al.*, *Phys. Rev. D*, **62**, 112002 (2000).
- [8] “OBSERVATION OF MULTI-TeV DIFFUSE GAMMA RAYS FROM THE GALACTIC PLANE WITH THE TIBET AIR SHOWER ARRAY”, M. Amenomori *et al.*, *ApJ*, **580**, 887-895 (2002).
- [9] “MULTI-TeV GAMMA-RAY FLARES FROM MARKARIAN 421 IN 2000 AND 2001 OBSERVED

WITH THE TIBET AIR SHOWER ARRAY”, M. Amenomori *et al.*, *ApJ*, **598**, 242-249 (2003).

- [10] “Observation by an Air-Shower Array in Tibet of the Multi-TeV Cosmic-Ray Anisotropy due to Terrestrial Orbital Motion Around the Sun”, M. Amenomori *et al.*, *Phys. Rev. Lett.*, **93**, 061101 (2004).
- [11] “Large-Scale Sidereal Anisotropy of Galactic Cosmic-Ray Intensity Observed by the Tibet Air Shower Array”, M. Amenomori *et al.*, *ApJ*, **626**, L29-L32 (2005).
- [12] “A Northern Sky Survey for Steady TeV Gamma-Ray Point Sources Using the Tibet Air Shower Array”, M. Amenomori *et al.*, *ApJ*, **633**, 1005-1012 (2005).
- [13] “Observation of PeV Gamma Rays from the Monogem Ring with the Tibet Air Shower Array”, M. Amenomori *et al.*, *ApJ*, **635**, L53-L56 (2005).
- [14] “Are protons still dominant at the knee of the cosmic-ray energy spectrum?”, M. Amenomori *et al.*, *Phys. Lett. B* **632** 58-64, (2006).
- [15] “Anisotropy and Corotation of Galactic Cosmic Rays”, M. Amenomori *et al.*, *Science* **314** 439-443, (2006).

Papers in conference proceedings

- [16] “Primary cosmic-ray energy spectrum around the knee energy region measured by the Tibet hybrid experiment”, Amenomori *et al.*, *Physics At The End Of The Galactic Cosmic Ray Spectrum*, (25-30 April 2005, Aspen, U.S.A.), *J.Phys.Conf.Ser.*47: 51-58,2006.

The Ashra Project

[Spokesperson: Makoto Sasaki]

ICRR, Univ. of Tokyo, Kashiwa, Chiba 277-8582

ICRR, Univ. of Tokyo, Japan; Chiba Univ., Japan; Ibaraki Univ., Japan; Nat. Astr. Obs. Japan; High Energy Accel. Res. Org. (KEK), Japan; Toho Univ., Japan; Tokyo Inst. Tech., Japan; Univ. Hawaii Manoa, USA; Univ. Hawaii Hilo, USA

Overview

Ashra (*All-sky Survey High Resolution Air-shower detector*) [1, 2, 3] is a project to build an unconventional optical telescope complex that images very wide field of view, covering 80% of the sky, yet with the angle resolution of a few arcmin, sensitive to the blue to UV light with the use of image intensifier and CMOS technology. The project primarily aims to observe Cherenkov and fluorescence lights from the lateral and longitudinal developments of very-high energy cosmic rays in the atmosphere. It can also be used to monitor optical transients in the wide field of sky. In 2004 we built prototype telescopes to verify and develop techniques on Haleakala in Hawaii, needed for the development of the full-scale telescopes under construction on Mauna Loa.

Project

The observatory will firstly consist of one main station having 12 detector units and two sub-stations having 8 and 4 detector units. One detector unit has a few light collecting systems with segmented mirrors. The features of the system were studied with a prototype detector unit located on Haleakala. The main station is being constructed on Mauna Loa (3,300 m).

The key technical feature of the Ashra detector rests on the use of electrostatic lenses to generate convergent beams rather than optical lens systems. This enables us to realize a high resolution over a wide field of view. This electron optics requires:

- *image pipeline*; the image transportation from imaging tube (image intensifier) to a trigger device and image sensors of fine pixels (CCD+CMOS), with high gain and resolution, and
- *parallel self-trigger*: the systems that trigger separately for atmospheric Cherenkov and fluorescence lights.

Observational Objectives

optical transients; Ashra will acquire optical image every 5 s after 4-s exposure. This enables us to explore optical transients, possibly associated with gamma ray bursts (GRBs), flares of soft gamma-ray repeaters (SGRs), supernovae explosion, and so on, in so far as they are brighter than $B \simeq 15$ mag, for which we expect 3- σ signals (Fig. 1). The unique advantage is the on-time detection of the events without resorting to usual satellite alerts. 10~20 events per year are expected in coincidence with the Swift gamma-ray events. The field of view that is wider than satellite instruments allows to detect more optical transients, including an interesting possibility for an optical flash, not visible with gamma-rays.

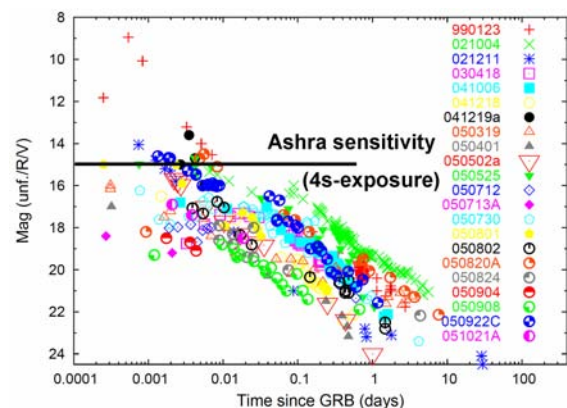


Fig. 1. Early light curves (unfiltered, R and V) for a set of GRBs with detections within minutes of the gamma-ray event. All the measurements shown have been taken from GCN circulars (Guidorzi et al. astro-ph/0511032). The limiting magnitude ($\simeq B$) expected with Ashra (4s-exposure) is shown as a horizontal line. There are no observations within 10 s after the GRB events.

TeV gamma rays; Atmospheric Cherenkov radiation will be imaged by Ashra. Requiring the signal-to-noise ratio (SNR) >5 , the system will allow to explore VHE gamma-ray sources

Opt. Transients	TeV- γ	Mountain- ν	Earth-skimming- ν	EeV-CR
B-UV $\lambda=300\sim 420\text{nm}$ 15 mag./4s @ 3σ 2 arcmin	Cherenkov 2 TeV 5% Crab/1yr@ 5σ 6 arcmin	Cherenkov 100 TeV 5 WB-limit/1yr unknown	Fluorescence 10 PeV 2 WB-limit/1yr 3 arcmin @ 100 PeV	Fluorescence 100 PeV 1600/1yr >10 EeV 1 arcmin @ 10 EeV

Table 1. Summary of performance with the full configuration (Ashra-2) of three Ashra sites. Detected light, energy threshold, sensitivity limit, and angular resolution are listed from top down for each objective. For EeV-CRs, trigger requirement is two or more stations. Waxman and Bahcall have calculated a neutrino flux upper limit from astrophysical transparent source, here referred to as the WB-limit. For the observation time for objectives other than optical transients, the realistic detection efficiency is taken into account.

with the energy threshold of 2 TeV at the limiting flux sensitivity of 5% Crab for 1-year observation.

EeV cosmic rays; For fluorescence lights from VHE cosmic rays the effective light gathering efficiency is comparable with that of the High Resolution Fly's Eye detector (HiRes). The arcmin pixel resolution of Ashra provides finer images of longitudinal development profiles of EeV cosmic ray (EeV-CR) air-showers. The resolution of arrival direction with the stereo reconstruction is thus significantly improved and it is better than one arcmin for the primary energy of EeV and higher [4]. This is useful to investigate events clustered around the galactic and/or extragalactic sources. This in turn would give us information as to the strength and coherence properties of the magnetic field

PeV-EeV neutrinos; Ashra may detect Cherenkov and/or fluorescence signals generated from tau-particle induced air-showers that is generated from interactions of tau neutrinos with the mountain and/or the earth. This is identified by peculiar geometry of the air-shower axis. The 1-year detection sensitivity with the full configuration of Ashra is 5 and 2 times larger than the Waxman-Bahcall limit for mountain-produced event (Cherenkov) and earth-skimming event (fluorescence), respectively. The most sensitive energy of around 100 PeV is suitable for the GZK neutrino detection.

The expected performance for each observational object is summarized in Table 1.

Test Observation

We have constructed a 2/3-scale prototype Ashra detector and a 3m-diameter altazimuth Cherenkov telescope on Haleakala to verify the optical and trigger performances. From October 2004 to August 2005 at the observatory, We made good observations for 844 hours out of 1,526 hours of the moonless night time. The efficiency is 55% of the moonless night time and 11% of entire time. This inefficiency is due primarily to bad weather.

The fine resolution (arc-minutes) in the ultra wide field of view (0.5 sr) has already been demonstrated using a 2/3-scale model. Fig. 2 shows an example of a 50-degree FOV image in which the constellations Taurus and Orion can be clearly identified with the 2/3-scale prototype. The inset, a two-degree square window, shows a close-up view of the Pleiades.

Our wide field observation covered the HETE-2 WXM error box at the time of GRB041211. 2,000 images were taken every 5 s with 4-s exposure from the time 1h7m before

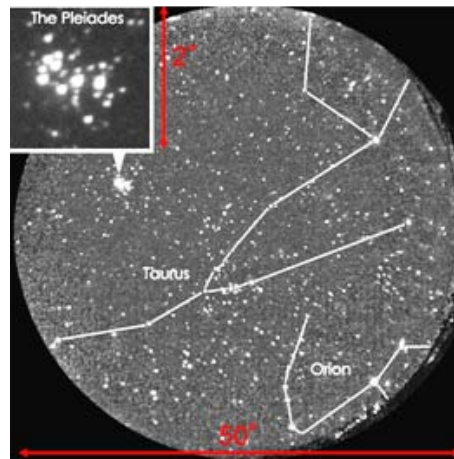


Fig. 2. Example of a 50-degree FOV image taken by the Ashra prototype. The solid lines are drawn to indicate the constellations Taurus and Orion. The inset, a two-degree square window, shows a close-up view of the Pleiades.

GRB041211 to 1h41m after GRB041211. We detected no objects showing time variation in the WXM error box. It indicates the 3-sigma limiting magnitudes of $B\sim 11.5$ magnitude [5]. This is compared with other observations in Fig. 3 [6] [7]. We also successfully performed two more observations coincident with Swift: GRB050502b [8] and GRB050504 [9].

A demonstration of air Cherenkov imaging of high-energy gamma/cosmic ray is shown in Fig. 4 which was taken during observing Mkr501. Separately, we have confirmed the alpha-parameter peak of TeV γ -rays from the Crab nebula to be greater than 5σ .

Current Status and Plan

After finishing the grading work for the area of 2,419 m² at the Mauna Loa site at the end of July 2005, installation of electrical power lines and transformers was performed until the beginning of September. We started the construction of the detector in October 2005 after receiving materials from Japan. Currently, (mid December 2005) a few shelters having motorized rolling doors, acrylic plate windows to maintain air-tightness, and heat-insulating walls and floors have been constructed and positioned on eight construction piers of concrete blocks at the Mauna Loa site. In the shelters, the optical elements of the light collectors have been already installed. The optical performance were checked and adjusted to be optimum with star light images from the pilot observation.

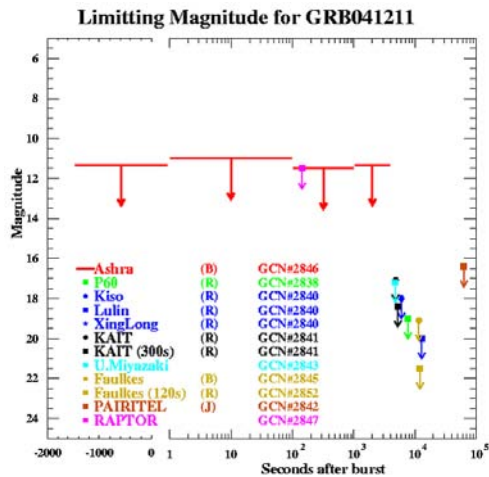


Fig. 3. 3-sigma limiting magnitudes of the test observation with the Ashra prototype and comparison with other observations for GRB041211 as a function of time after GRB. Note that the horizontal axis unavoidably stands for time (s) in logarithmic scale after the burst (positive) and in linear scale before the burst (negative).

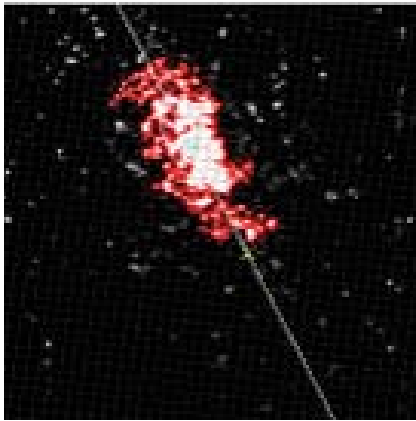


Fig. 4. Self-triggered Cherenkov image of air-shower detected by using the Ashra photoelectric image pipeline and a prototype trigger sensor system. This image was taken during tracking Mkr501.

In December 2005, we evaluated the night sky background flux on Mauna Loa using the Ashra light collector installed and aligned in a shelter. The result is fairly consistent with the background in La Palma and Namibia by the HESS group. From the star light observations, our understanding of the light correction efficiency to be accurate within 5% level.

The civil engineering construction of light collectors in shelters at the Mauna Loa site has been completed. Fig. 5 shows a picture of the constructed Mauna Loa stations. In this Ashra-1 experiment, we are performing device installation and specific observation in a step-by-step way to enhance the scientific impacts.

The full Ashra observatory (Ashra-2) will consist of three experimental sites separated by about 30 km on Mauna Loa (3,300 m), Camp Kilohana (2,014 m) on the side of Mauna Kea, and Hualalai (2,320 m) on the island of Hawaii. The full configuration emphasizes the stereoscopic observation



Fig. 5. The Ashra main and sub stations at the Mauna Loa sites.

Cherenkov and fluorescence lights from air-showers with two or three stations at separated sites as well as the effective detection area for air-showers. The parallax observation for optical transients with two or more stations is also useful for rejecting local background events.

Bibliography

- [1] <http://www.icrr.u-tokyo.ac.jp/~ashra>
- [2] Sasaki, M., "Very High Energy Particle Astronomy with All-sky Survey High Resolution Air-shower Detector (Ashra)", *Progress of Theoretical Physics Supplement*, vol. 151, pp. 192–200, 2003.
- [3] Sasaki, M., et al., 2005. "Status of Ashra project," Proc. 29th Int. Cosmic Ray Conf. Pune 8, 17-200.
- [4] Sasaki, M., et al., "Design of UHECR telescope with 1 arcmin resolution and 50° field of view", *Nucl. Instrum. Methods*, vol. A492, pp. 49–56, Oct. 2002.
- [5] Sasaki, M., et al., 2004. GCN Circ. 2846.
- [6] Sasaki, M., et al., 2005. Proc. 29th Int. Cosmic Ray Conf. Pune 8, 17-200.
- [7] Sasaki, M., et al., 2005. "Observation of Optical transients with the Ashra Prototype," Proc. 29th Int. Cosmic Ray Conf. Pune 5, 319-322.
- [8] Sasaki, M., et al., 2005. GCN Circ. 3499.
- [9] Sasaki, M., Manago, N., Noda, K., Asaoka, Y., 2005. "GRB050502b: Early Observation," GCN Circ. 3421.

ASTROPHYSICS and GRAVITY DIVISION

Overview

Astrophysics and Gravity Division consists of Gravitational Wave Group, The Sloan Digital Sky Survey Group and Theory Group. The Sloan Digital Sky Survey Group has accumulated data of images and spectroscopic observation of galaxies and is conducting their analysis in collaboration with worldwide researchers. Theory Group conducts both theoretical studies of the Universe and astroparticle physics. The Gravitational Wave Group conducts TAMA project jointly with researchers of gravitational wave experiment and theory in Japan. The Group also conducts a CLIO project that aims to practically test the cryogenic laser interferometer system underground in Kamioka as one of R&Ds for LCGT project to detect gravitational wave events.

TAMA Project

[Spokesperson : Kazuaki Kuroda] ICRR, Univ. of Tokyo, Kashiwa, Chiba 277-8582

In collaboration with the members of: TAMA collaboration NAOJ, Tokyo; KEK, Tsukuba; UEC, Tokyo; Osaka City Univ., Osaka; Kyoto Univ., Kyoto; Osaka Univ., Osaka; Niigata Univ., Niigata

Overview

A gravitational wave is a physical entity in space-time predicted by Einstein's theory of general relativity. Its existence was proven by the observation of PSR1913+16 by Taylor and Hulse⁵, who won the Nobel prize in 1993. However, nobody has succeeded to directly detect gravitational waves. The theory of gravitation can be tested by the detection of gravitational waves. A gravitational wave detector is the last eye of mankind to inspect the universe. In order to directly observe gravitational waves, we have been developing a sensitive interferometric gravitational wave detector, called TAMA, which is a 300 m baseline laser interferometer at the Mitaka campus of the National Astronomical Observatory of Japan (NAOJ) and several observations have been conducted, so far. TAMA project started in April, 1995, as a five-year project and it was extended by two years after 1999. TAMA is organized by researchers belonging to universities and national laboratories. We regard the TAMA interferometer as a step toward the final scale interferometer in the sense of technology and construction budget. We achieved nine data-taking runs that span from two to eight weeks (Table 1). In the former half runs, its sensitivity improvement was the first priority. Nonetheless, both the stability and reliability had to be improved to check the sensitivity, itself. In the latter half runs, the operation became easier after installing an automatic control system.

Table 1. TAMA data-taking runs including long-term observations

Run	Term	Year	Live Time (Hour)
DT1	6-Aug → 7-Aug	1999	7
DT2	17-Sept → 20-Sept	1999	31
DT3	20-Apr → 23-Apr	2000	13
DT4	21-Aug → 4-Sept	2000	161
DT5	2-Mar → 8-Mar	2001	111
DT6	15-Aug → 20-Sept	2001	1038
DT7	31-Aug → 2-Sept	2002	25
DT8	14-Feb → 14-Apr	2003	1158
DT9	28-Nov → 10-Jan	2004	558

Status of TAMA Project

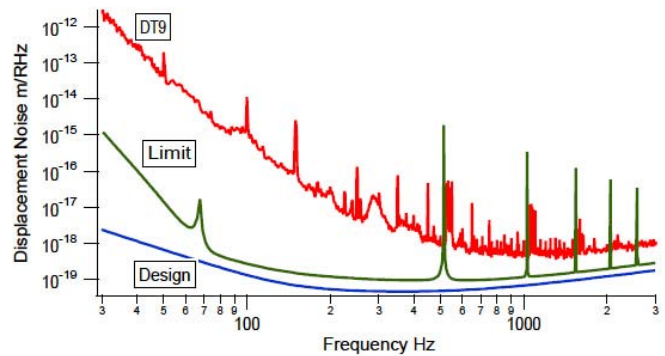


Fig. 1. Achieved sensitivity of TAMA at the time of data-taking run 9 (shown as DT9). The design sensitivity (Design) had several flaws arising from non-established theory to estimate thermal noise. The limit sensitivity (Limit) is a practically attainable one. The sensitivity (DT9) was physically limited by the photon shot noise at frequencies of more than 800 Hz. Since seismic noise at frequencies lower than 30 Hz disturbed the stable operation of the interferometer, a tighter feedback gain of the mirror alignment control loop was adopted, which resulted in an actuator force noise in a frequency range from 30 Hz to 300 Hz. We have not yet identified the noise source governing the range from 300 Hz to 800 Hz.

The achieved sensitivity of TAMA is shown as that of DT9 in Fig. 1. Since the design sensitivity had several flaws arising from non-established theory to estimate thermal noise of mirrors, we revised it as shown by "LIMIT". We recognize that there is still large gap between the achieved sensitivity and the practically attainable one, especially at low frequencies. However, we could demonstrate that the basic techniques for the interferometer operation was acquired by the fulfillment of the objective noise curve at frequencies more than 800 Hz, where the optical system properly worked and the control system was appropriate. The noise spectrum at frequencies lower than 30 Hz was disturbed by non-stationary ground motion and the spectrum in a frequency range from 30 Hz to 300 Hz was determined by the actuator noise to stabilize

*⁵ J. H. Taylor and J. M. Weisberg, *Astrophysical J.*, **345** (1989) 434.

the mirror alignment mainly due to relatively larger seismic noise at Mitaka campus. In order to identify the noise source governing the spectrum in a frequency range from 300 Hz to 800 Hz, we have installed SAS (Seismic Attenuation System) for four main mirrors and obtained preliminary noise spectrum as shown in Fig 2.

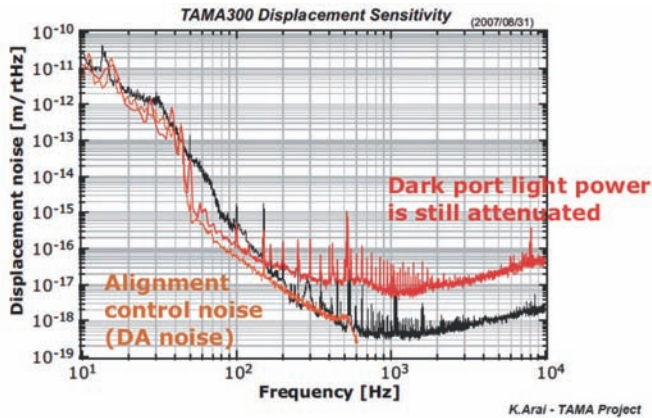


Fig. 2. Preliminary noise spectrum by newly installed SAS anti-vibration system in order to identify the noise source governing the spectrum in a frequency range from 300 Hz to 800 Hz.

In regard with the output signal including the former observation runs, the output was contaminated by extensive rate of non-stationary fake events. However, its rate has been gradually reduced during the course of repeating observation runs as shown in the next section of data analysis.

Analysis of inspiraling chirp waves

The main target of interferometric detectors is the event from coalescence of binary neutron stars. Orbiting binary star system is approximated by two point masses orbiting each other with losing kinematic energy and momentum by gravitational radiation. Until the coalescence, the radiated gravitational wave is a kind of sinusoidal wave with their frequencies going up and also with their amplitude increasing, which is called ‘chirp wave’. If we have an exact wave form of this chirp wave, we can apply filtering technique to extract signal from noisy data since the gravitational waves at the detector are so faint that they are usually covered with noise. The detector output, $s(t)$, is represented by

$$s(t) = Ah(t - t_c) + n(t)$$

where $h(t)$ is the template of known gravitational wave form, t_c is the coalescence time, A is the amplitude and $n(t)$ is the noise. The matched filtering is performed by calculation of ρ in a parameter space of masses, coalescence time, amplitude, and signal phase (α) as follows:

$$\rho(t_c, m_1, m_2, A, \alpha) = 2 \int \frac{\tilde{s}(f)\tilde{h}^*(f)}{S_n(f)} df,$$

where $\tilde{s}(f)$ and $\tilde{h}(f)$ are the Fourier transforms of $s(t)$ and $h(t)$, respectively, and $S_n(f)$ is one sided noise power spectrum density. The signal phase α reflects the polarization and

the angular configuration between the source and the interferometer direction. The asterisk denotes the complex conjugation. If $s(t)$ contains gravitational wave signal, ρ takes a large value. However, the output of the practical interferometer is contaminated by non-Gaussian noise, the origin of which has not been well identified, yet. Owing to this noise, matched filtering produces extensive fake events. To reduce fake events, we adopted a measure of the deviation of events from real signal, which is a χ^2 time-frequency test, since non-stationary noise does not have the time-frequency behavior of inspiral chirp.⁶ The frequency band (dc to Nyquist) is divided into n subintervals, chosen so that, for a chirp superposed on Gaussian noise with the observed power spectrum, the expected contribution to ρ is equal for each subinterval. χ^2 is calculated by summing the square of the deviation of each value of ρ from the expected value. This quantity must satisfy the χ^2 statistic with $2n - 2$ degrees of freedom as long as the data consist of Gaussian noise plus chirp signals only. Figure 3 shows the distribution of events obtained by the data of DT4[1], where χ^2 is renormalized as $\chi^2/(2n - 2)$ and signal-to-noise ratio, ζ , is calculated by $\rho/\sqrt{2}$. In this Fig. 3, the number of events are plotted for $\chi^2 < 2.5$, $\chi^2 < 1.5$, and $\chi^2 < 1.0$ as a function of ζ^2 , and an analytic fitting is also shown to $\chi^2 < 1.5$. The fitting was determined between $\zeta^2=35$ and 50. This fitting gives the number of events larger than $\zeta=7.2$ and $\chi^2 < 1.5$ as 2.5. The $\chi^2 < 2.5$, $\chi^2 < 1.5$, and $\chi^2 < 1.0$ corresponds to $10^{-3}\%$, 3.8%, and 46% false dismissal rates in Gaussian noise, respectively. By this analysis, we have recognized that non-stationary Gaussian noise produced fake events with high ζ but these fakes were statistically eliminated by introducing χ^2 threshold evaluating signal-noise behavior, which resulted in setting an appropriate threshold of ζ for reliable detection of gravitational wave events. This is the reason why we set $\zeta=10$ in the design sensitivity of LCGT.

After DT4, the sensitivity of TAMA was improved every observation run along with its stability as shown in Fig. 4. The analyzed data of DT6[2] was reanalyzed with those of DT8 and DT9 by applying a revised cut of fake events, which is $\rho/\sqrt{\chi^2}(\equiv \zeta)$. Table 2 summarizes the result [3]. Since the sensitivity was better in DT9 than in DT8, DT9’s detection probability would have been much larger. However, since the first half of DT9 was contaminated by abnormal seismic noise due to building constructions at the campus, fake events exceeding the threshold degraded the detection probability of DT9.

Analysis of burst waves

The second target of gravitational wave (GW) detectors is a burst GW from stellar-core collapse (core-collapse supernova explosion). Since it is difficult to predict its waveform analytically due to the complex time evolution of the mass densities in the explosion process, the process and GW radiation have been investigated by numerical simulations. Among these simulations, Dimmelmeier *et al.* have presented rather systematic surveys on GWs from stellar-core collapses⁷. We

*⁶ Firstly applied to CALTECH 40 m prototype interferometer appeared in Phys. Rev. Lett. **83**(1999)1498.

*⁷ H. Dimmelmeier *et al.*, *Astrophys.* **393** (2002) 523.

Table 2. Upper limit to the Galactic inspiral events. The unit of mass range is the solar mass and the threshold is set as the false alarm rate is once a year. The upper limit is given in a unit of event/yr for the Galaxy events with C.L.=90%

	mass range	detection probability	threshold of ζ	upper limit
DT6	1-3	$0.18^{+0.05}_{-0.05}$	21.8	130^{50}_{-30}
DT8	1-3	$0.60^{+0.07}_{-0.08}$	13.7	30^5_{-3}
DT9	1-3	$0.69^{+0.05}_{-0.07}$	17.7	60^{+7}_{-4}

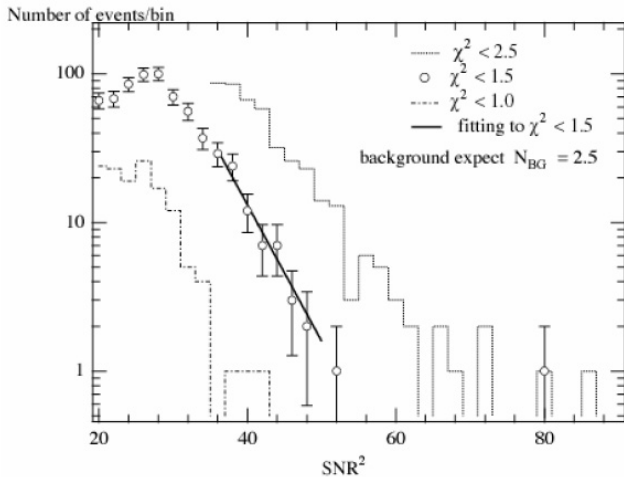


Fig. 3. Distribution of events obtained by the data of DT4[1]. The number of events are plotted for $\chi^2 < 2.5$, $\chi^2 < 1.5$, and $\chi^2 < 1.0$ as a function of ζ^2 , and an analytic fitting is also shown to $\chi^2 < 1.5$. The fitting was determined between $\zeta^2=35$ and 50. This fitting gives the number of events larger than $\zeta=7.2$ and $\chi^2 < 1.5$ as 2.5. The $\chi^2 < 2.5$, $\chi^2 < 1.5$, and $\chi^2 < 1.0$ corresponds to $10^{-3}\%$, 3.8%, and 46% false dismissal rates in Gaussian noise, respectively.

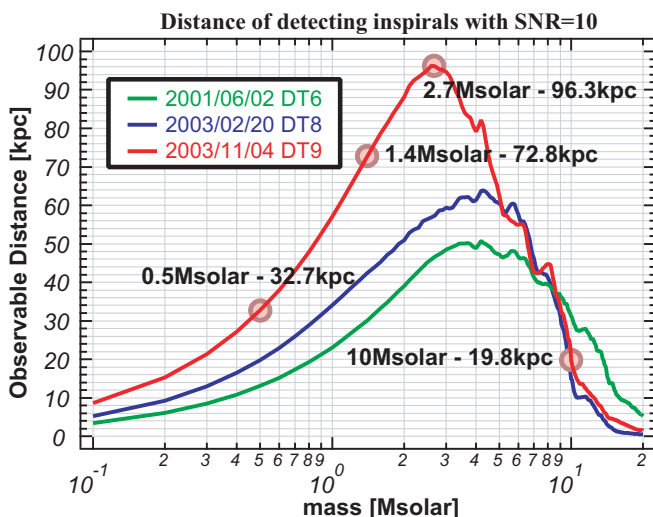


Fig. 4. Detectable range in DT6, DT8, and DT9 for each mass of a neutron star binary system by a signal-to-noise (SN) ratio of 10. The coalescence of the nominal binary system ($1.4 M_{\odot}$ of each mass) can be detected up to 33 kpc for DT6, 42 kpc for DT8 and 73 kpc for DT9.

adopted 26 waveforms from Dimmelmeier *et al.* to analyze TAMA data. According to the waveforms, the averaged amplitude of GWs radiated by supernovae at the Galactic center (8.5 kpc distance from the detector) is $\langle h_{\text{peak}} \rangle = 1.5 \times 10^{-20}$ in a peak strain amplitude, or $\langle h_{\text{rss}} \rangle = 4 \times 10^{-22} [\text{Hz}^{-1/2}]$ in root-sum-square (RSS) amplitude. Here a RSS amplitude is defined by

$$h_{\text{rss}} = \left[\int_{-\infty}^{\infty} |h(t)|^2 dt \right]^{1/2},$$

where $h(t)$ is the strain amplitude of the GW. As for the adopted waveforms, the central frequencies of the waves, which are calculated from the weighting average of the power spectra, range from 90 Hz to 1.2 kHz, which is around the observation band of TAMA[4]. Also, it is estimated that a total energy radiated as GWs in one event is $\langle E_{\text{tot}} \rangle = 8 \times 10^{-8} M_{\odot} c^2$ on average.

Extraction of signals is performed using an excess-power filter.⁸ The evaluation parameter is the total noise power in a given time-frequency region. Event triggers are generated by the following steps: (i) A spectrogram (time-domain change in noise spectrum) is calculated for each $\Delta t=12.8$ msec data segment from the output data of the detector. (ii) In each spectrum, power in a preselected frequency band, $\Delta f=2270$ [Hz] from 230 Hz to 2.5 kHz are averaged so as to obtain a time series of averaged power, P_n . Since each spectrum is normalized by the typical noise spectrum within 30 min before a calculation of the average in the frequency components, P_n represents the signal-to-noise ratio (ζ): the ratio of the averaged signal power to the typical noise power in the region. (iii) Event triggers are extracted if the averaged power is larger than a given threshold, $P_n \geq P_{\text{th}}$. The parameters of the filter, length of the time chunk (Δt) for each FFT and analysis frequency band (Δf) were selected to be effective for the adopted Dimmelmeier waveforms.

We applied two veto methods to reject fake events caused by detector instabilities. One is a veto method using auxiliary signals for the detector monitor. We had noticed that there is some correlation between the non-Gaussian noise in the output and the laser power intensity. We can set a threshold carefully by estimating a false-dismissal rate. However, it is not sufficient to reject all fake events coming from various origins. Therefore, we added another veto method utilizing the waveform behavior; the time scale of the signal. In the burst-wave analysis, the waveforms by numerical simulations suggest that GWs from stellar-core collapse have a short duration, typically less than 100 msec. We know that some of the detector instabilities last longer than a few seconds from experience. Thus, some of the fakes caused by these slow instabilities are

⁸ W. G. Anderson *et al.*, Phys. Rev. D **63** (2001) 042003.

rejected by evaluating the time scale of the event triggers. Table 3 lists the data analysis result obtained from TAMA data applying the above veto methods.

Figure 5 shows the event-trigger rates plotted as a function of h_{rss} amplitude. The detector was gradually improved during the intervals of these data-taking runs. The event trigger rates were reduced from DT6 to DT9 by about a few orders for a given GW amplitude and by about an order for given trigger rate (last column in Table 3).

The above analysis is applied to set upper limit for stellar-core collapse events in our Galaxy using Monte-Carlo simulations with a source distribution model of our Galaxy and with adopted waveforms. Considering detection efficiency of TAMA, we obtained an upper limit for the Galactic-event rate to be 5.0×10^3 events/sec, which is considerably larger than the theoretical expectation of about 10^{-9} events/sec. This large discrepancy will be improved in future both by higher sensitivity and reduction of non-stationary detector noise.

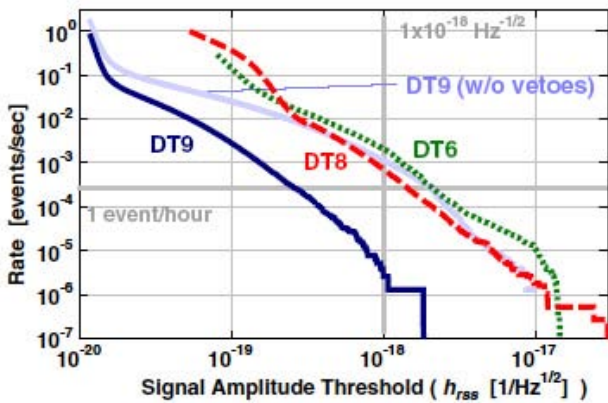


Fig. 5. GW amplitude and corresponding trigger rate: the event rate with larger amplitude than a given h_{rss} is plotted. The thin curve of DT9 represents the rate analyzed without any vetoes.

Other data analysis

Apart from the above data analysis, many other analysis results have been reported using TAMA data in several conferences [5, 6, 7]. Since DT8 was performed in keeping pace with a data-taking run of LIGO (second science run, S2), the result was analyzed for burst wave [8] and the result for inspiral wave was published [9].

After DT9, we stopped the observational operation of TAMA and entered a work phase of noise-hunting to attain the final sensitivity.

LCGT Project

[Spokesperson : Kazuaki Kuroda] ICRR, Univ. of Tokyo, Kashiwa, Chiba 277-8582

In collaboration with the members of:

LCGT collaboration; National Astronomical Observatory (Japan), KEK, Physics Department (Univ. of Tokyo), Department of Advanced Material Science (Univ. of Tokyo), Earthquake Research Institute (Univ. of Tokyo), Department of

Earth Science and Astronomy (Univ. of Tokyo), Institute for Laser Science (Univ. of Electro-Communications), Department of Physics (Osaka City Univ.), Department of Physics (Osaka Univ.), Physics Department (Kyoto Univ.), Yukawa Institute (Kyoto Univ.), Advanced Research Institute for Sciences and Humanities (Nihon Univ.), Agency of Industrial Science and Technology, National Institute of Information and Communications Technology, Department of Astronomy (Beijing Normal Univ.), Center for Astrophysics (Univ. of Science and Technology, China), Institute for High Energy Physics (Chinese Academy of Science), Inter University Centre for Astronomy & Astrophysics (IUCAA), Physics Department of Physics (University of Western Australia), Laboratory of Laser Interferometry (Sternberg State Astronomical Institute, Moscow Univ.).

Overview

After the discovery of the highly relativistic binary neutron star system⁹, a new young binary pulsar has been detected¹⁰. The former discovery had increased the coalescence rate from 10^{-6} to 10^{-5} a year in a galaxy as big as our Galaxy¹¹ and the latter pushes up by another factor of six. Although it is a good news for the detection of gravitational waves, we still need to wait for long time to detect by the presently existing detectors. This is the reason why we have planned LCGT (Large-scale Cryogenic Gravitational wave Telescope) [10]. There are many other possible gravitational wave sources in the universe other than the coalescence of binary neutron stars. However, the coalescence of binary neutron stars differs completely from other sources in the sense that its wave form is precisely predicted, and its existence has certainly been confirmed.

Status of LCGT Project

The target sensitivity of LCGT is to observe binary neutron star coalescence events occurring at 257 Mpc with $S/N=10$ in its optimum configuration. This is ten-times more sensitive than that of the LIGO (I), and by two orders more than that of TAMA at their most sensitive frequencies. This will be attained by dual interferometers located underground, using a three-kilometer length baseline, cooling mirrors at cryogenic temperature, and a high-power laser source employing 150 W output. The optical configuration is a power recycled Fabry-Perot-Michelson interferometer with the resonant-sideband-extraction (RSE) scheme (in Fig. 6). The detailed design of the control system is being tested for the resonant sideband extraction scheme.[11] Table 4 lists the important parameters of LCGT, which were revised two times from the original design. The ultimate sensitivity of a laser interferometer is determined by seismic noise at low frequencies (10-30 Hz) (which is reduced by improving the vibration isolation system), and it is limited by photon shot noise at higher frequencies (more than 300 Hz), which can be improved only

⁹ M. Burgay, *et al.*, Nature, **426** (2003) 531.

¹⁰ D.R. Lorimer, *et al.*, Astrophysical J. **640**(2006) 428.

¹¹ C. Kim, V. Kalogera and D. R. Lorimer, Astrophysical J. **584** (2003) 985.

Table 3. Summary of data-analysis results. The noise-equivalent GW RSS-amplitudes ($h_{\text{rss,noise}}$), the dead times by the vetoes (T_{rej}), the total effective observation times (T_{obs}), the trigger rates for $h_{\text{rss}} \geq 1 \times 10^{-18} [\text{Hz}^{-1/2}]$, and the GW RSS-amplitudes above which the trigger rates are one event per hour are described.

	$h_{\text{rss,noise}}$ [$\text{Hz}^{-1/2}$]	T_{rej} [hours]	T_{obs} [hours]	Rate [sec^{-1}]	1-hour $^{-1}$ amp. [$\text{Hz}^{-1/2}$]
DT6	4.5×10^{-20}	11.8	937.8	2.1×10^{-3}	2.1×10^{-18}
DT8	3.0×10^{-20}	18.0	1064.2	7.0×10^{-4}	1.4×10^{-18}
DT9	1.1×10^{-20}	0.8	194.6	2.5×10^{-6}	2.5×10^{-19}

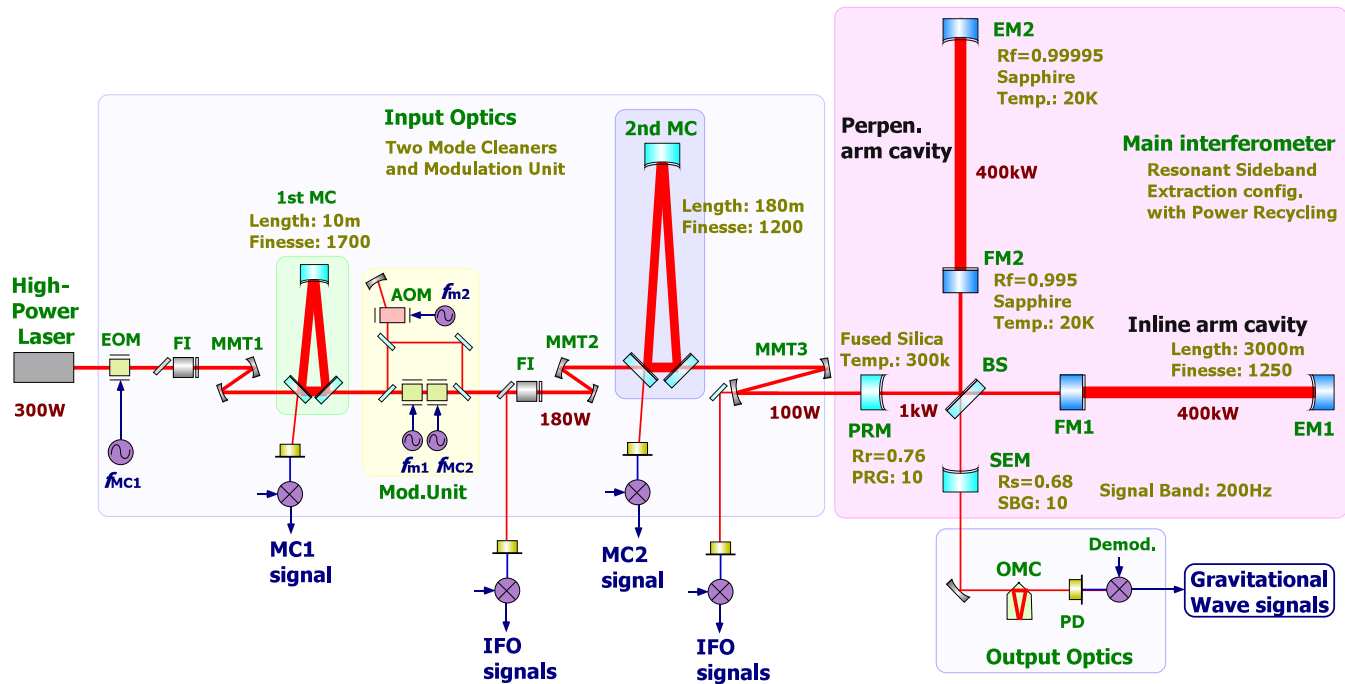


Fig. 6. Optical design of LCGT. The optical configuration is a power recycled Fabry-Perot-Michelson interferometer with the resonant-sideband-extraction (RSE) scheme.

by increasing the light power in the main cavities. The sensitivity of middle frequencies (30-300 Hz) is limited by the photon recoil force noise. This requires that thermal noise is reduced both by decreasing the temperature and by decreasing the internal mechanical loss (*i.e.*, increasing the mechanical Q of vibration modes). The source of thermal noise comes from both mirror internal vibration, mechanical loss of the optical coating and swing noise of the pendulum suspending the mirror. The reduction of thermal noise is attained by cooling both the mirror, itself, and the suspension system that suspends the mirror.

Figure 7 compares the sensitivity spectrum of LCGT with those of CLIO (a 100m prototype cryogenic interferometer placed underground of Kmioka mine) and the design of TAMA. The sensitivity in low frequencies of LCGT is attained by SAS, which will be proven by the current SAS in TAMA. That of higher frequencies is attained by higher laser power, which has been basically shown by TAMA. The mid-frequency region is improved by cryogenic mirror and suspension system, which will be proven by the on-going project of CLIO. Although the improvement, especially two orders of

magnitude at low frequencies, is adventurous, it is not impossible until the construction period of LCGT that needs four years after the beginning.

The main effort on the research and development for LCGT has been placed on cryogenic mirrors for the past years. The implementation of cryogenic mirrors is one of the most straight-forward solutions to improve the sensitivity.

The design of the cryogenic mirror system is shown in Fig. 8. The mirror is suspended by two loops of sapphire fibers connected to an auxiliary mirror that is a part of suspension point interferometer. This mirror is also suspended from an alignment control platform that is suspended with an insulator rod connected through the center holes of the radiation shields to an isolation table suspended by a low-frequency vibration isolator, which is placed at room temperature. The auxiliary mirror has a heat link to the platform and another heat link connects the platform and a heat anchor point (4 K) inside the vacuum located just above the platform.

Both the cryogenic system and the vibration isolator are put inside a common high-vacuum chamber.

To realize this concept, the following research subjects were considered:

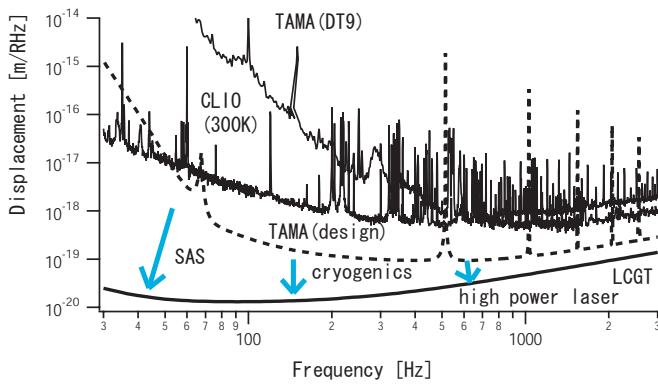


Fig. 7. LCGT sensitivity compared with those of CLIO (a 100m prototype cryogenic interferometer placed underground of Kmioka mine) and the design of TAMA. The horizontal axis is frequency [Hz] and the vertical axis represents square root of power spectrum of displacement [m/√Hz].

Table 4. LCGT design parameters to detect binary neutron-star coalescence events in 257 Mpc.

Item	Parameter
Baseline Length	3 km
Interferometers	Two set
Optical Power	Power recycled Fabry-Perot-Michelson with RSE
	Laser: 150 W; Finesse: 1550
	Input power at BS: 825 W Cavity power 780 kW
Beam radius at End	3 cm
Main Mirror	Sapphire 30 kg, 20 K
	Diameter 25 cm
	Mechanical Q: 10^8
Suspension pendulum	Frequency: 1 Hz; Q: 1×10^8
	10 K
Vacuum	$\leq 10^{-7}$ Pa

1. Removal of heat produced by high-power laser illumination.
2. Holding the high Qs of the mirror internal modes and suspension pendulum.
3. Reducing the contamination of mirror surfaces.
4. Estimating heat production by optical loss in the mirror.
5. Alignment control of mirrors in a cryogenic environment
6. Low mechanical loss of the optical coating.

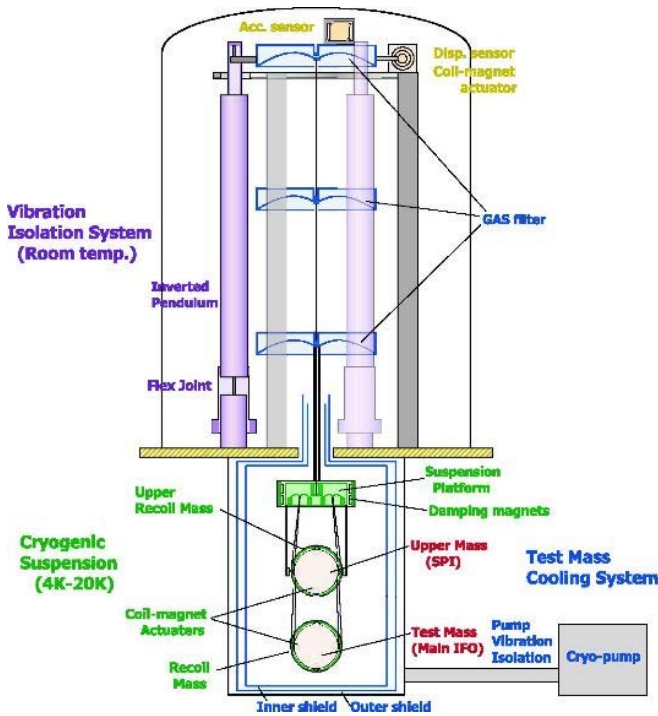


Fig. 8. Schematic design of the cryogenic suspension system. The mirror is suspended by sapphire fibers connected to an auxiliary mirror, which is suspended by metal wires from a platform that has a heat link to a 4 K heat anchor inside the vacuum. The platform is also suspended with an insulator rod connected through the holes of radiation shields to an isolation table suspended by a seismic attenuation system placed at room temperature in the common high vacuum.

We had already reported on experimental results of the first two items in the annual report (1997–1998) [12]. In regard to the third and fourth items, the results were reported in the annual report (2000–2001) and published in papers [13]. As for item 5, we confirmed that a superconducting film could be used for the receptor of the magnetic force in place of permanent bar magnets that are normally used in the existing detectors. The film can be easily sputtered on the mirror surface without harmfully degrading the mechanical Q of the mirror. The basic behavior of this method was reported in a paper [14]. With respect to the last item, we reported on a measurement of the bulk substrate of the mirror at cryogenic temperature in the annual report (2003–2004). We can now correctly estimate the thermal vibration noise of the optical coating while considering the inhomogeneous loss that had been neglected at an early stage of interferometer development. The substrate of the cryogenic mirror is sapphire, which has a large thermo-elastic thermal noise at room temperature. However, since the thermal-expansion ratio of sapphire at cryogenic temperature goes down to nearly 0 and the heat conductivity becomes greater, the thermo-elastic noise drastically reduces at the cryogenic temperature. Thermal noise estimated from the Q of the coating was well below the design sensitivity of LCGT, which means that this coating noise does not limit the sensitivity, whereas, the sensitivity of a room-temperature

mirror is limited by this effect. This is the significant merit of the cryogenic mirror system [15]. Recent problem arising from large power density of Fabry-Perot cavity is a parametric instability, which is caused by the coupling between optical cavity modes with elastic vibration modes of the mirror substrate.¹² Since the sapphire has larger elastic wave velocity, the number density of elastic modes is fewer than that of fused silica mirror, which is the case of advanced LIGO. And also the coupling constant between optics and mechanics is smaller in LCGT than in advanced LIGO, because the beam size on the mirror is smaller in LCGT. This merit comes from the adoption of cryogenics of LCGT[16]. All of the above R&D confirmed the feasibility of reducing the thermal noise of the interferometer in the middle-frequency region. This research underlines the basis of LCGT. However, for a practical cryogenic detector, many practical R&Ds are needed for the installation of cryogenic mirrors. One of the earliest R&D activities was the Kashiwa cryogenic interferometer system reported in the annual report (2000–2001; 2002–2003; 2003–2004). By this Kashiwa cryogenic interferometer, we learned the necessity of several practical R&D items and began to construct the CLIO interferometer in Kamioka to establish techniques for the cryogenic interferometer. Some of these practical studies were reported in the annual report (2004–2006).

Practical R&Ds: Measurement of the optical qualities of sapphire

The substrate of the main mirrors in the cryogenic interferometer (LCGT) is sapphire, because it has ultra-low mechanical loss and high heat conductivity at cryogenic temperature. Only fluorite is a possible substitute of sapphire, with some difficulties that should be removed if we have to utilize fluorite in place of sapphire. However, sapphire has birefringence, which is not a defect if the laser beam axis is aligned along its c-axis, which is the so-called optical axis. Also, sapphire has a rather high optical scattering loss compared with that of fused silica. A measurement of the birefringence of sapphire was scheduled both for inspecting the crystal quality of sapphire substrates that were purchased from companies producing sapphire, and for estimating the optical quality of each substrate. The measurement principle is shown in Fig. 9. Suppose that there is some imperfection of the crystal that causes an optical phase retardance between two orthogonal polarizations. Through a half-wave plate we introduce linearly polarized light that coincides with one of principle refractive axes. The retardance caused at traveling inside the sapphire substrate is compensated by a compensator (CMP), the condition of which is measured by knowing an angle position of a polarizer to extinguish the output light. Without the substrate the angle of this polarizer is orthogonally set with the input polarization angle. The fluctuation of the magnitude of the retardance is represented as the indices of the magnitude of the crystal imperfections. In this measurement, for a typical point of the substrate, the angle of the polarizer and the compensated angle were recorded. Practically, the polarizer angle was determined by knowing the optimum point.

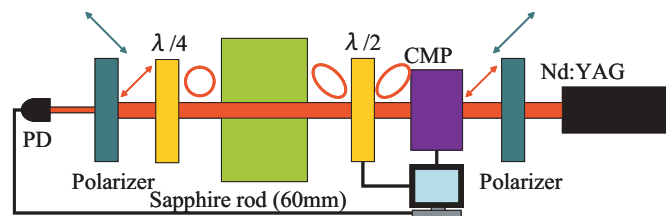


Fig. 9. Optical phase retardance caused by some imperfection is compensated by the Babinet-Soleil compensator (CMP), which is measured by determining two independent angles.

The example of the measured birefringence fluctuation shown in the previous annual report (Figure 9 one page 39, 2005) turned out to be contaminated by false interference light fringes and we reduced this contamination by slightly tilting the surface of the sample against the normal of the incident laser beam. The origin of the contamination is something like the Newton ring fringes as is usually observed by measuring flatness.

The measurement of the optical scattering loss of those sample rods was reported in the previous annual report (2005) under a collaboration with both the University of Western Australia and LMA (Laboratoire des Matériaux Avancés - Université Claude Bernard Lyon 1 - IN2P3 / CNRS)[17]. We have already obtained the knowledge that although we could not recognize any apparent correlation among the birefringence, optical scattering and optical loss, the magnitude of the fluctuation resembles each other.

We are preparing to apply our measuring system to a large sapphire piece, 250 mm in diameter and 100 mm in thickness, which is lent by the LIGO project.

Apart from the above R&D issues, a high power laser system that produces more than 100 W has been developed by a group in Advanced Material Science, School of New Frontier Science, University of Tokyo. Also, researchers at KEK tested the mechanical strength of bonded pieces made of sapphire, besides quiet refrigerators. We steadily advance towards the realization of LCGT by these R&D activities. The next step in R&D for cryogenic mirrors is to show a reduction of the noise amplitude, itself, which needs a more realistic interferometer other than the prototype with a shorter baseline. We expect that the CLIO interferometer at Kamioka will show its performance for LCGT, soon.

Bibliography

- [1] H. Tagoshi *et al.*, Phys. Rev. D **63**(2001)062001-1-5.
- [2] H. Takahashi *et al.*, Phys. Rev. D **70**(2004)042003-1-17.
- [3] H. Tagoshi, GWDATA 10 UTB, Dec. 14-17, 2005.
- [4] M. Ando *et al.*, Phys. Rev. D **71** (2005) 082002.
- [5] K. Soida *et al.*, Class. Quantum Grav. **20**(2003)S645-S654.

*¹² Braginskii, *et al.*, Physics Lett. A **305** (2002)111.

- [6] T. Akutsu *et al.*, in *Proceedings of the 6th Edoardo Amaldi Conference on Gravitational Waves*, Okinawa, 2005.
- [7] Y. Tsunesada *et al.*, *Phys. Rev. D* **71** (2005) 103005.
- [8] B. Abbott *et al.*, *Phys. Rev. D* **72** (2005) 122004.
- [9] B. Abbott *et al.*, gr-qc/0512078 (2005).
- [10] K. Kuroda, *et al.*, *Int. J. Mod. Phys. D* **8** (1999) 557; K. Kuroda, *et al.*, *Class. Quantum Grav.* **19** (2002) 1237; T. Uchiyama, *et al.*, *Class. Quantum Grav.* **21** (2004) S1161.
- [11] F. Kawazoe *et al.*, presented at Amaldi 7 meeting, Sydney, July 8-14, 2007.
- [12] T. Uchiyama, *et al.*, *Phys. Lett. A* **242** (1998) 211; T. Uchiyama, *et al.*, *Phys. Lett. A* **273** (2000) 310.
- [13] S. Miyoki, *et al.*, *Cryogenics* **40** (2000) 61; S. Miyoki, *et al.*, *Cryogenics* **41** (2001) 415; T. Tomaru, *et al.*, *Phys. Lett. A* **283** (2001) 80.
- [14] N. Sato, *et al.*, *Cryogenics* **43** (2003) 425.
- [15] K. Yamamoto, *et al.*, *Class. Quantum Grav.* **21** (2004) S1075.
- [16] K. Yamamoto, *et al.*, presented at Amaldi 7 meeting, Sydney, July 8-14, 2007.
- [17] Z. Yan, *et al.*, *Applied Optics* **40**(2006) 1.

Status of CLIO at Kamioka

[Spokesperson : Masatake Ohashi]

ICRR, Univ. of Tokyo, Kashiwa, Chiba 277-8582

In collaboration with members of: KEK, Tsukuba; Kyoto-U, Kyoto; ERI of UT, Tokyo

CLIO (Cryogenic Laser Interferometer Observatory) is a 100 m-baseline underground cryogenic interferometer at the Kamioka Mine. CLIO forms a bridge connecting the CLIK (7 m prototype cryogenic interferometer at Kashiwa campus) and the planned LCGT (3 km cryogenic interferometer at Kamioka). The site of CLIO, near the Super-Kamiokande neutrino detector, is shown in Fig. 1. The tunnel was dug in 2002, and a strain meter for geophysics was installed in 2003 [3]. The construction of CLIO began in late 2003, and installation of the mode cleaner vacuum system was reported in the annual report (2003–2004). Four sets of cryostats and whole vacuum system were installed (annual report 2004–2005). We started the operation of CLIO in 2006.

One of the aims of CLIO is to demonstrate the thermal noise suppression by cooling the mirrors. The main mirrors are cooled at 20 K by refrigerators. The lowest noise level of CLIO is designed to be $10^{-19} \text{m}/\sqrt{\text{Hz}}$ around 100 Hz, which would be $10^{-18} \text{m}/\sqrt{\text{Hz}}$ if cryogenics is not applied [1]. The current best sensitivity at the room temperature was obtained in the end of 2006. The displacement sensitivity around 300Hz reached at $6 \times 10^{-19} \text{m}/\sqrt{\text{Hz}}$. Of special note is

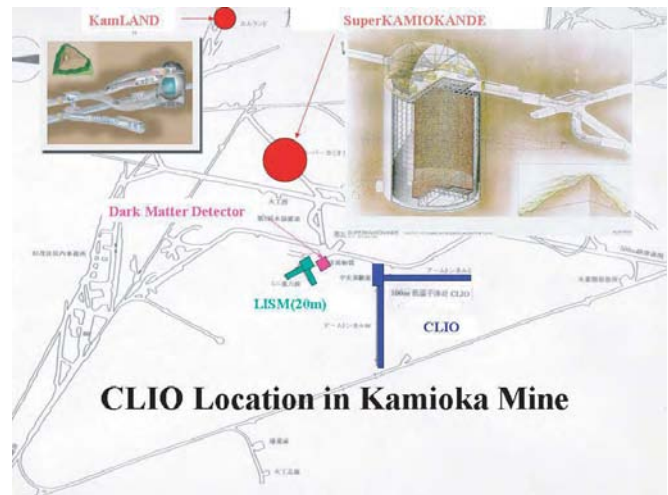


Fig. 1. Location of the CLIO interferometer.



Fig. 2. Overview of the CLIO interferometer.

its high strain sensitivity below 20Hz. It is comparable with LIGO sensitivity in spite of much shorter baseline. Now we are reducing the excess noise to realize the thermal noise limited sensitivity.

Once the objective is attained, the CLIO interferometer is used to observe gravitational wave events in parallel with the TAMA interferometer until completion of the construction of LCGT. The merits of the underground site are lower seismic noise and temperature stability. The former characteristic makes interferometer locking easily controlled, and the latter assures long-term stable operation (LISM) [2].

Bibliography

- [1] M. Ohashi, *et al.*, *Class. Quantum Grav.* **20** (2003) S599.
- [2] S. Sato, *et al.*, *Phys. Rev. D* **69** (2004) 102005.
- [3] S. Takemoto, *et al.*, *Journal of Geodynamics* **41** (2006) 23.
- [4] S. Miyoki, *et al.*, *Class. Quantum Grav.* **23** (2006) S231.
- [5] T. Uchiyama, *et al.*, *Journal of Physics* **32** (2006) 259.



Fig. 3. a sapphire mirror and cryogenic suspension system.

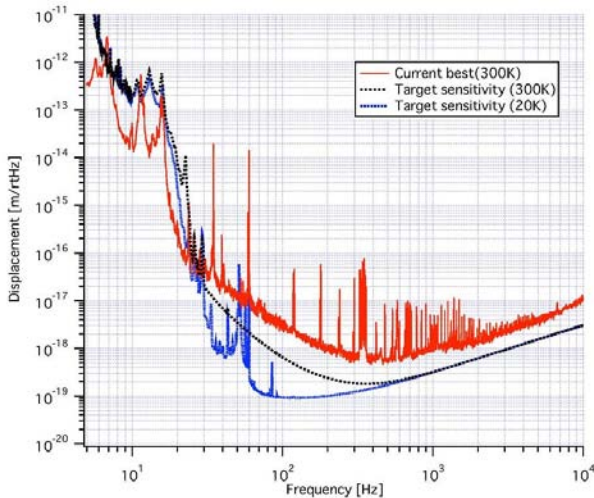


Fig. 4. CLIO displacement noise spectrum: The red curve is the current best sensitivity. The dotted line is the target sensitivity at room temperature.

Sloan Digital Sky Survey

[Spokesperson : Masataka Fukugita]

ICRR, University of Tokyo, Kashiwa, Chiba 277-8582

In collaboration with the members of:

University of Tokyo, 7-3-1 Hongo, Bunkyo-ku, Tokyo 113-0033, Japan; Nagoya University, Chikusa, Nagoya 464-8602, Japan; National Astronomical Observatory of Japan, 2-21-

1 Osawa, Mitaka, Tokyo 181-8588, Japan; Tohoku University, Aramaki, Aoba, Sendai 980-8578, Japan; Japan Women's University, 2-8-1, Mejirodai, Bunkyo-ku, Tokyo, 112-8681, Japan; The University of Chicago, 5640, South Ellis Ave., Chicago, IL 60637, USA; Fermi National Accelerator Laboratory, P.O. Box 500, Batavia, IL 60510, USA; Institute for Advanced Study, Einstein Drive, Princeton, NJ 08540, USA; Johns Hopkins University, Baltimore, MD 21218, USA; Los Alamos National Laboratory, Los Alamos, NM 87545, USA; Max-Planck-Institute for Astronomy, Königstuhl 17, D-69117 Heidelberg, Germany; Max-Planck-Institute for Astrophysics, Karl Schwarzschildstrasse 1, D-85748 Garching, Germany; New Mexico State University, P.O. Box 30001, Dept 4500, Las Cruces, NM 88003, USA; University of Pittsburgh, 3941 O'Hara St., Pittsburgh, PA 15260, USA; Princeton University, Princeton, NJ 08544, USA; United States Naval Observatory, P.O. Box 1149, Flagstaff, AZ 86002-1149; University of Washington, Box 351580, Seattle, WA 98195, USA

The SDSS completed its originally planned phase of operations — SDSS-I — on 30 June 2005 after five years of operation. The goal initially set was to cover 10,000 square degrees of sky, but at the time the production survey began, the Five Year Baseline was developed to provide a more realistic metric against which the progress was evaluated. This decreased the target area to 8,387 square degrees (7,642 square degrees in the northern sky and 745 square degrees in the southern sky). The imaging carried out over 5 years has sustained the planned pace. At the end of the survey 97% of the baseline area were observed for the northern-sky baseline and 99% of southern-sky baseline were completed. Spectroscopic surveys, however, are somewhat behind the schedule. Only 74% of the baseline area were observed for the north (100% for the south). This is due to unusually poor weather conditions in the spring of 2003 and in the winter of 2004. The time consuming spectroscopic runs were severely affected. Otherwise, all the operations have been working smoothly (98% is the mean uptime fraction), producing the data as expected. Software has undergone extensive fine tunings and all the data were re-reduced for a number of times, which are now made public as *The Data Release of the Sloan Digital Sky Survey I to V (DR1-DR5)*, the last one comprising 8000 square degrees of imaging and 5740 square degrees of spectroscopic surveys done to 30 June 2005. This database contains 215 million objects including 1,049,000 objects with spectroscopic information. These numbers include 675,000 galaxies and 91,000 quasars obtained with the uniform selection criteria.

The SDSS has entered a new phase, SDSS-II, continuing through June, 2008. SDSS-II will carry out three distinct surveys — the Sloan Legacy Survey, SEGUE (The Sloan Extension for Galactic Understanding and Exploration), and the Sloan Supernova Survey — to address fundamental questions about the nature of the Universe, the origin of galaxies and quasars, and the formation and evolution of our own Galaxy, the Milky Way.

The Sloan Legacy Survey is the continuation of SDSS-I to complete spectroscopic survey to fill the gap in the Northern Galactic Cap which was not observed during SDSS-I due to poor weather conditions. Constructing the largest possi-

ble single contiguous survey volume will improve the following three main results: the determination of the power spectrum, the photometric calibration, and the legacy which SDSS will supply to the astronomical world. The goal is contiguous region of 7,808 square degrees in both imaging and spectroscopy. By the second quarter of 2006, 97% of imaging and 81% of spectroscopy have been completed.

SEGUE is mining the stellar content of the Milky Way in order to create a detailed 3-dimensional map of the Galaxy. SEGUE will image 3,320 square degrees mostly at $|b| < 30^\circ$ and obtain spectra of 240,000 stars in the disk and spheroid, revealing the age, composition and phase space distribution of stars within the various Galactic components. These stellar excavations will provide essential clues to the structure, formation, and evolution of our Galaxy. By the second quarter of 2006, 68% of imaging and 37% of spectroscopy have been completed.

The Sloan Supernova Survey is a time-domain survey involving repeat imaging of the same region of the sky (the SDSS Southern equatorial stripe; about 2.5 degree wide by ~ 120 degree long) every other nights over the course of three 3-month campaigns (Sep-Nov). A primary scientific motivation is to detect and measure multi-band light-curves for ~ 200 Type Ia supernovae in the redshift range $z = 0.1 - 0.3$. This sample, with excellent photometric calibration, should provide insights into systematics of SNe Ia as calibrated standard candles. The survey of the first two years (2005-2006) have been finished successfully and found 322 spectroscopically confirmed SNe Ia in the redshift range between 0.05 and 0.40. About 85% of SNe Ia are discovered before maximum light. Follow-up spectra were taken at various telescopes through collaboration including MDM(2.4m), NOT(2.6m), APO(3.5m), NTT(3.6m), KPNO(4m), WHT(4.2m), Subaru(8.2m), HET(9.2m), Keck(10m), and SALT(10m).

The prime scientific goals of the SDSS are focused on extragalactic themes, such as the large-scale structure of galaxies over a very large volume of the Universe, and detailed characterisations of the galaxy properties and those of quasars.

The clustering of galaxies observed in the SDSS, when mapped in three dimensional space, looks very similar to that expected in the model of the Universe dominated by cold dark matter (CDM) with density fluctuations starting from nearly scale-invariant adiabatic perturbations, as predicted in the model of inflation. As a quantitative measure this density field is characterised by the statistic called the power spectrum, the squared amplitude of the Fourier modes of fluctuations, which is written,

$$P(k) = |\delta_k|^2 = \int d^3r \xi(r) e^{-ik \cdot r} \quad (1)$$

where $\xi(r)$ is the two-point correlation function of galaxies. The important result is an accurate derivation of this power spectrum from galaxy clustering over the scale from 10 to 200 Mpc, and the demonstration that it joins smoothly the spectrum derived from the temperature field imprinted on the cosmic microwave background measured by *Wilkinson Microwave Anisotropy Probe* (WMAP) (see Fig. 1). Combined with WMAP that explores the Universe at $z \approx 1000$, this lends the most convincing support to the standard model of struc-

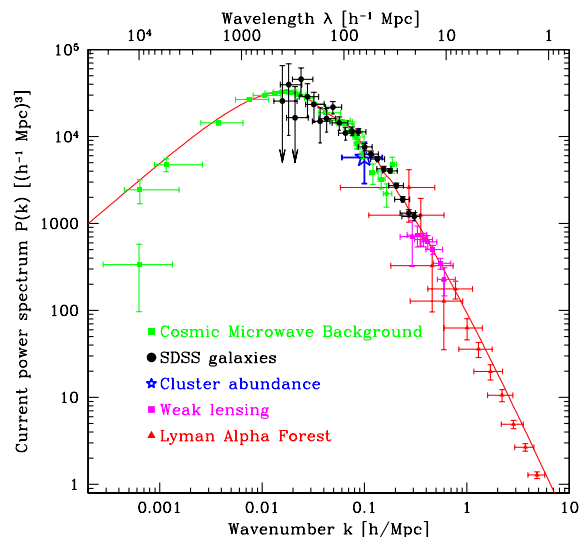


Fig. 1. The power spectrum of galaxy clustering scaled to the present epoch (SDSS galaxies) plotted with four other independent measures, extending four decades on spatial resolution, and demonstrating remarkable consistency. These data provide fundamental constraints on cosmological models. Figure is taken from Tegmark et al. *Astrophys. J.* **606**, 702 (2004).

ture formation in the Universe based on the Λ CDM model. Moreover, the large-scale structure data of SDSS reduced the parameter degeneracies that exist within the CMB analyses; the combined data of WMAP and SDSS yield the cosmological parameters $\Omega_m = 0.29 \pm 0.04$, $\Omega_\Lambda = 0.71 \pm 0.04$ and $H_0 = 71 \pm 4 \text{ km s}^{-1} \text{ Mpc}^{-1}$ at the year of 2004. Two years later, 3-year WMAP data was released. It includes the new measurement of the low- l polarization power spectrum, which detects the reionization signature and determines the corresponding optical depth. This measurement breaks the severe degeneracy in the 1-year WMAP data and causes the dramatic tightening of the constraints on various important cosmological parameters. Now the value added by other datasets is clearly reduced. However, the information from large scale structure of galaxies give substantial improvements by cutting error bars.

SDSS has applied another selection of galaxies — the selection of luminous red galaxies (LRG). Approximately 10% of SDSS galaxies belong to this category. The advantage of this selection is to allow us to explore much deep sky. The sight increases from $600h^{-1} \text{ Mpc}$ ($z = 0.2$) to $1200h^{-1} \text{ Mpc}$ ($z = 0.4$), quadrupling the survey volume compared with the main galaxy sample. The constraints on cosmological parameters obtained by combining 3-year WMAP data and SDSS LRG measurements are $\Omega_m = 0.239 \pm 0.018$, $\Omega_\Lambda = 0.761 \pm 0.018$ and $H_0 = 73 \pm 2 \text{ km s}^{-1} \text{ Mpc}^{-1}$. This set is taken as an authoritative in the astronomy community.

Baryonic acoustic oscillations (BAO) is a reminiscence of the sound wave oscillation in the pre-recombination era, which is most dramatically seen in CMB multipoles. In real space this leads to a peak in the two-point correlation function $\xi(r)$ at about $r_s = 100h^{-1} \text{ Mpc}$. In Fourier space this process leads to oscillations in the power spectrum. The wavelength of these oscillations will be $k_s = 2\pi/r_s = 0.06h \text{ Mpc}^{-1}$. Eisen-

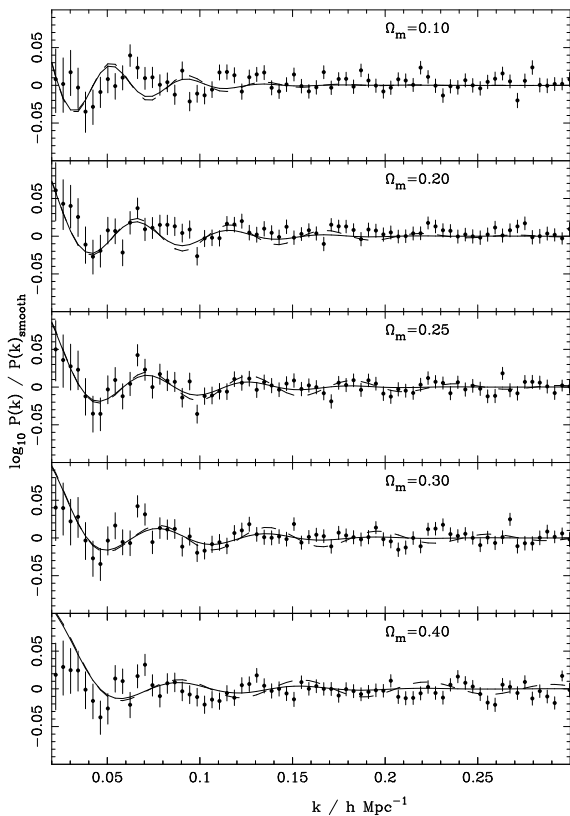


Fig. 2. Ratio of the power spectra calculated from the SDSS to the overall shape of the measured power spectra (filled circles with 1 errors). Solid lines represents the BAO predicted by a CDM model with matter densities given in each panel and $h = 0.73$, and a 17% baryon fraction. As can be seen, the observed oscillations approximately match those predicted for $0.2 \leq \Omega_m \leq 0.3$. Figure is taken from Percival et al. *Astrophys. J.* **657**, 51 (2007).

stein et al. (2005) has detected this acoustic peak in correlation function of SDSS LRG and determine the curvature of the Universe to 1% accuracy, $\Omega_\Lambda + \Omega_m = 1.01 \pm 0.01$, which is comparable to the latest WMAP3+SDSS LRG analysis. The analysis of the main galaxies and LRGs in the SDSS DR5 sample determines $\Omega_m = 0.256 \pm 0.029$ using the dependence of r_s on the matter density Ω_m (Fig. 2). This value of the matter density is derived from the localtions of BAO in the galaxy power spectrum and in the CMB. This is an extermely clean geometrical cosmological measurement, as the physics of the BAO production is well understood. With larger samples and a wider redshift range, the BAO “standard ruler” can be used to constrain the comsmology at high precision through the co-moving distance-redshift relation. Forthcoming surveys will be designed to exploit this effect.

Although CDM models seem to be very successful on large scales, one of the most serious challenges facing CDM models is the so-called “missing satellite” problem. CDM models predicts at least 1-2 orders of manitude more low-mass sub-halos at the present epoch compared to the observed abundance of dwarf galaxies surrounding the Milky Way and M31. All-sky photographic surves cover most of the sky, but are limited to surface brightnesses of ~ 25.5 mag arcsec $^{-2}$. The selection effects are also difficult to model with accuracy.

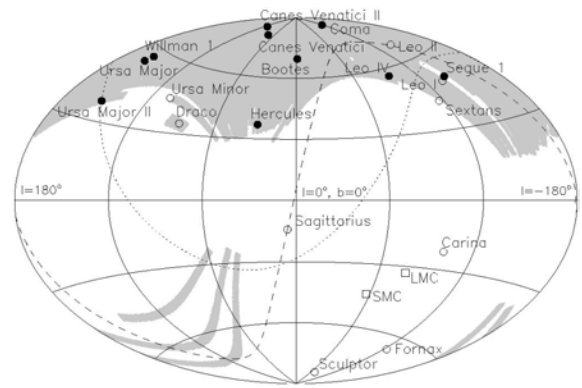


Fig. 3. Locations of Milky Way satellites in Galactic coordinates. Filled circles are satellites discovered by SDSS, and open circles are previously known Milky Way dSphs. Figure is taken from Belokurov et al. *Astrophys. J.* **654**, 897 (2007).

The SDSS makes it possible to carry out a systematic survey for satellite galaxies, which are detectable through overdensity of stars in position-color-magnitude space. A total of 10 new Milky Way satellites with effective surface brightness $\mu_V \geq 28$ mag arcsec $^{-2}$ have been discovered in SDSS data (Fig. 3) in addition to the previously known 9 Milky Way dwarf spheroidals. Some preliminary studies of these indicate that they may be dark matter dominated. We need more investigation to see if these are the “missing satellites”.

Gravitational lensing is also a subject to which the SDSS is making a significant contribution in a number of ways. The SDSS is one of the first few that observed a weak effect of gravitational lensing of galaxy images by foreground galaxies. The lensing effect appears as distorted images of galaxies due to the gravitational shear field, but it is only on the order of a few percent, compared with the order of unity effect of randomly oriented galaxies that have intrinsically different shapes. Millions of galaxies are needed to extract this small signal from noise of the order of unity. With the SDSS galaxy sample, this distortion was unambiguously detected, showing that the mass concentration around galaxies behaves as $r^{-0.8}$ as a function of distance r , consistently with the famous $r^{-1.8}$ law of the galaxy-galaxy correlation. Another effect of gravitational lensing by foreground galaxies is a magnification of distant sources, *cosmic magnification*. Graviational magnification has two effects. First, the flux received from distant sources is increased, resulting in a relatively deeper apparent magnitude limited survey. Second, the solid angle is stretched, diluting the surface density of source images on the sky. The net result of these competing effects is an induced cross-correlation between between physically separated populations that depends on how the loss of sources due to dilution is balanced by the gain of sources due to flux magnification. Using $\sim 200,000$ quasars and 13 million galaxies, cosmic magnification has been detected for the first time at 8σ level (Fig. 4).

The large quasar sample of the SDSS also provides an excellent platform to search for classical strong gravitational lenses of quasar images, i.e., splitting of images. 16 lenses are found from 46000 quasar images. Among the novel cases

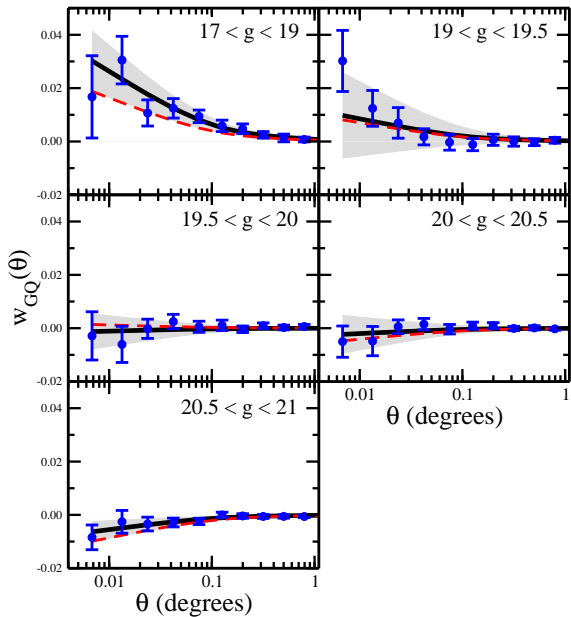


Fig. 4. Measurement of $w_{GQ}(\theta)$, cross-correlation between foreground galaxies and distant quasars, as a function of quasar g -band magnitude. The dark solid curve is the fitting model. Figure is taken from Scranton et al. *Astrophys. J.* **633**, 589 (2005).

that deserve special scientific discussion, we quote the large-separation lensed quasar, SDSS J1004+4112 of four images with their maximum separation being 14.6 arcsec and SDSS J1029+2623 with two images with their separation of 22.5 arcsec (Figure 5). These are the case where split lensed images are further enhanced by a cluster of galaxies. A statistical analysis to infer cosmological and mean galaxy parameters from the lens sample yielded $\Omega_m = 0.26 \pm 0.15$, $\Omega_\Lambda = 0.74 \pm 0.15$, consistent with the values derived from WMAP and SDSS power spectrum analysis.

As it became apparent already at Imaging First Light, the SDSS project has made unrivalled contributions to our understanding of high redshift quasars from its commissioning phase. By now the project has found 19 quasars with redshift higher than 5.7 (*i*- dropout quasars) from ~ 6600 square degrees — Among them 8 are with $z > 6$: there are no $z > 6$ quasars reported from other projects. The highest redshift is 6.42, which means that the light was emitted only 0.84 Gyr after the Big Bang. These high z quasars, together with a sample for lower z , show the abundance of luminous quasars declining exponentially with redshift from $z \approx 3$ towards early epochs. This is a significant constraint on the model of quasar formation at high redshifts.

Also important aspect with high redshift quasars is that they allowed us to observe a change of the ionisation state of the intergalactic medium (IGM) in a high redshift universe. We know that a free electron and a proton recombine to form a neutral hydrogen atom at $z \approx 1000 - 1500$. We also know that IGM was again highly reionised before $z \approx 3$. When and how the reionisation took place is a matter of significant interest

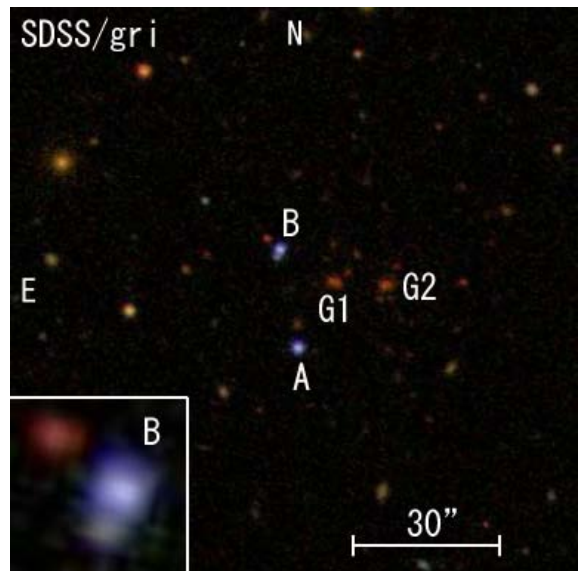


Fig. 5. *gri* composite SDSS image of SDSS J1029+2623. The quasar images (blue stellar objects) are indicated by A and B. G1 and G2 (red extended objects) are likely to be member galaxies of a lensing cluster at $z \sim 0.55$. Figure is taken from Inada et al. *Astrophys. J. (Letters)* **653**, L97 (2006).

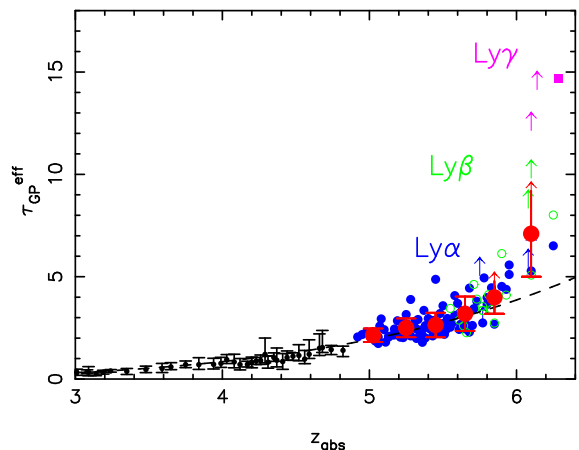


Fig. 6. Evolution of optical depth combined with the $\text{Ly}\alpha$, $\text{Ly}\beta$, and $\text{Ly}\gamma$ results. At $z > 5.5$, the best-fit evolution has $\tau_{\text{GP}}^{\text{eff}} \approx (1+z)^{10.9}$, indicating an accelerated evolution. Figure is taken from Fan et al. *Astron. J.* **132**, 117 (2006).

from the point of view of galaxy formation. The SDSS quasar spectra show the flux shortwards the Lyman α line rapidly vanishing at $z \geq 6$ (called the Gunn-Peterson trough), indicating the change of state of the IGM at this redshift (Figure 6). Cosmic reionisation is also evident from the WMAP 3-year data and its epoch $z_r = 8 \pm 2$ is consistent with SDSS result if we consider the error of optical depth determined from WMAP data. A problem newly created is the question whether the star formation activity, as inferred from faint galaxy observations, is sufficient to ionise the entire IGM at $z \approx 6$.

Besides high redshift quasars, a large number of quasars are collected and their properties are being studied. We have released four catalogues of quasars, the fourth one con-

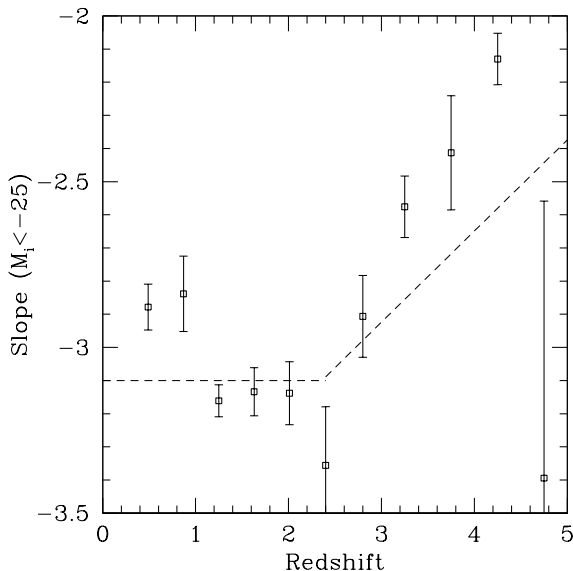


Fig. 7. Bright-end slope of the Quasar Luminosity Function as a function of redshift determined from a linear least-squares fit to the $M_i(z=2) < -25$. The slope of the luminosity function significantly flattens with redshift $z > 3$. Figure is taken from Richards et al. *Astron. J.* **131**, 2766 (2006).

taining 77,429 quasars in 5740 square degrees. The long-awaited quasar luminosity function (the work requires proper understanding of the selection function) was determined for well-defined and homogeneous sample consisting of 15,343 quasars within an effective area of 1622 square degrees. Derived luminosity function has a flatter bright-end slope at high redshift than at low redshift (Fig. 7). This slope change must be accounted for in models of the evolution of accretion onto supermassive black holes.

Theory Group

CMB constraints on the fine structure constant

[Spokesperson : T. Kanzaki]

ICRR, Univ. of Tokyo, Kashiwa, Chiba 277-8582

In collaboration with the members of ICRR.

We study constraints on time variation of the fine structure constant α from cosmic microwave background (CMB) taking into account simultaneous change in α and the electron mass m_e which might be implied in unification theories. We obtain the constraints $-0.097 < \Delta\alpha/\alpha < 0.034$ at 95% C.L. using WMAP data only, and $-0.042 < \Delta\alpha/\alpha < 0.026$ combining with the constraint on the Hubble parameter by the HST Hubble Key Project.

Bibliography

- [1] K. Ichikawa, T. Kanzaki and M. Kawasaki, *Phys. Rev. D* **74** (2006) 023515

Cosmological Constraints on Gravitino LSP Scenario with Sneutrino NLSP

[Spokesperson : T. Kanzaki]

ICRR, Univ. of Tokyo, Kashiwa, Chiba 277-8582

In collaboration with the members of ICRR, Tohoku Univ. and Harvard-Smithsonian Center.

We study the scenario where a sneutrino is the next lightest supersymmetric particle (NLSP) and decays into a gravitino and standard model particles. The daughter particles such as neutrinos and quarks cause electro- and hadronic showers and affect big-bang nucleosynthesis. It is found that despite a small branching ratio, four-body processes including quarks in the final state give the most stringent constraint on the sneutrino abundance for gravitino mass of 1 – 100 GeV. Pion production by high energy neutrinos is important when the sneutrinos decay at ~ 1 sec. We also discuss the thermal leptogenesis in the sneutrino NLSP scenario.

Bibliography

- [1] T. Kanzaki, T. Kawasaki, K. Kohri and T. Moroi, *hep-ph/0609246*.

Graviton emission from a Gauss-Bonnet brane

[Spokesperson : K. Konya]

ICRR, Univ. of Tokyo, Kashiwa, Chiba 277-8582

We study the emission of gravitons by a homogeneous brane with the Gauss-Bonnet term into an Anti de Sitter five dimensional bulk spacetime. It is found that the graviton emission depends on the curvature scale and the Gauss-Bonnet coupling and that the amount of emission generally decreases. Therefore nucleosynthesis constraints are easier to satisfy by including the Gauss-Bonnet term.

Bibliography

- [1] K. Konya, *hep-th/0701257*.

New Two-loop Contributions to Hadronic EDMs in the MSSM

[Spokesperson : M. Nagai]

ICRR, Univ. of Tokyo, Kashiwa, Chiba 277-8582

In collaboration with the members of ICRR and Technion.

Flavor-changing terms with CP-violating phases in the quark sector may contribute to the hadronic electric dipole moments (EDMs). However, within the Standard Model (SM), the source of CP violation comes from the unique CKM phase, and it turns out that the EDMs are strongly suppressed. This implies that the EDMs are very sensitive to non-minimal flavor violation structures of theories beyond the SM. In this paper, we discuss the quark EDMs and CEDMs (chromoelectric dipole moments) in the MSSM with general flavor-changing terms in the squark mass matrices. In particular, the charged-Higgs mediated contributions to the down-quark

EDM and CEDM are evaluated at two-loop level. We point out that these two-loop contributions may dominate over the one-loop induced gluino or Higgsino contributions even when the squark and gluino masses are around few TeV and $\tan\beta$ is moderate.

Bibliography

- [1] J. Hisano, M. Nagai and P. Paradisi, Phys. Lett. B **642**, 510 (2006).

Electric Dipole Moments in PseudoDirac Gauginos

[Spokesperson : M. Nagai]

ICRR, Univ. of Tokyo, Kashiwa, Chiba 277-8582

In collaboration with the members of ICRR.

The SUSY CP problem is one of serious problems in construction of realistic supersymmetric standard models. We consider the problem in a framework in which adjoint chiral multiplets are introduced and gauginos have Dirac mass terms induced by a U(1) gauge interaction in the hidden sector. This is realized in hidden sector models without singlet chiral multiplets, which are favored from a recent study of the Polonyi problem. We find that the dominant contributions to electron and neutron electric dipole moments (EDMs) in the model come from phases in the supersymmetric adjoint mass terms. When the supersymmetric adjoint masses are suppressed by a factor of ~ 100 compared with the Dirac ones, the electron and neutron EDMs are suppressed below the experimental bound even if the SUSY particle masses are around 1 TeV. Thus, this model works as a framework to solve the SUSY CP problem.

Bibliography

- [1] J. Hisano, M. Nagai, T. Naganawa and M. Senami, Phys. Lett. B **644**, 256 (2007).

Non-perturbative effect on thermal relic abundance of dark matter

[Spokesperson : M. Nagai]

ICRR, Univ. of Tokyo, Kashiwa, Chiba 277-8582

In collaboration with the members of ICRR and KEK.

We point out that thermal relic abundance of the dark matter is strongly altered by a non-perturbative effect called the Sommerfeld enhancement, when constituent particles of the dark matter are non-singlet under the $SU(2)_L$ gauge interaction and much heavier than the weak gauge bosons. Typical candidates for such dark matter particles are the heavy wino- and higgsino-like neutralinos. We investigate the non-perturbative effect on the relic abundance of dark matter for the wino-like neutralino as an example. We show that its thermal abundance is reduced by 50% compared to the perturbative result. The wino-like neutralino mass consistent with the observed dark matter abundance turns out to be $2.7 \text{ TeV} < m < 3.0 \text{ TeV}$.

Bibliography

- [1] J. Hisano, S. Matsumoto, M. Nagai, O. Saito and M. Senami, Phys. Lett. B **646**, 34 (2007).

Late-time Affleck-Dine baryogenesis after thermal inflation

[Spokesperson : K. Nakayama]

ICRR, Univ. of Tokyo, Kashiwa, Chiba 277-8582

In collaboration with the members of ICRR.

Thermal inflation can solve serious cosmological problems such as overproduction of gravitinos and moduli. However, it also dilutes the preexisting baryon asymmetry. We investigate a possibility that Affleck-Dine mechanism works after thermal inflation and generate the baryon number at an acceptable level using lattice calculation. We find that a proper amount of baryon number can be generated for appropriate model parameters.

Bibliography

- [1] M. Kawasaki and K. Nakayama, Phys. Rev. D **74**, 123508 (2006).

Affleck-Dine baryogenesis in anomaly-mediated supersymmetry breaking

[Spokesperson : K. Nakayama]

ICRR, Univ. of Tokyo, Kashiwa, Chiba 277-8582

In collaboration with the members of ICRR.

It has been known that in anomaly-mediated SUSY breaking model Affleck-Dine baryogenesis does not work due to trapping of Affleck-Dine field into charge-breaking minima. We show that when finite-temperature effect is properly taken into account and if reheating temperature is relatively high, the problem of falling into charge breaking global minima can be avoided and hence Affleck-Dine baryogenesis works. Moreover, for the LH_u flat direction we obtain a constraint on the mass of neutrino.

Bibliography

- [1] M. Kawasaki and K. Nakayama, JCAP **0702**, 002 (2007).

Increasing the effective number of neutrinos with decaying particles

[Spokesperson : K. Nakayama]

ICRR, Univ. of Tokyo, Kashiwa, Chiba 277-8582

In collaboration with the members of ICRR and DESY.

We present models of decaying particles to increase the effective number of neutrinos N_ν after big bang nucleosynthesis but before the structure formation begins. We point out that our scenario not only solves the discrepancy between the constraints on N_ν from these two epochs, but also provides a possible answer to deeper inconsistency in the estimation of the matter power spectrum amplitude at small scales, represented

by σ_8 , between the WMAP and some small scale matter power measurements such as the Lyman- α forest and weak lensing. We consider (a) saxion decay into two axions; (b) gravitino decay into axino and axion; (c) Dirac right-handed sneutrino decay into gravitino and right-handed neutrino.

Bibliography

- [1] K. Ichikawa, M. Kawasaki, K. Nakayama, M. Senami and F. Takahashi, JCAP **0705**, 008 (2007).

Implication of Dark Energy Parametrizations on the Determination of the Curvature of the Universe

[Spokesperson : T. Sekiguchi]

ICRR, Univ. of Tokyo, Kashiwa, Chiba 277-8582

In collaboration with the members of ICRR and Saga Univ..

We investigate how the nature of dark energy affects the determination of the curvature of the universe from recent observations. For this purpose, we consider the constraints on the matter and dark energy density using observations of type Ia supernovae, baryon acoustic oscillation peak and cosmic microwave background with several types of dark energy equation of state. Although it is usually said that the combination of current observations favors a flat universe, we found that a relatively large parameter space allows the universe to be open for a particular model of dark energy. We also discuss what kind of dark energy model or prior allow a non-flat universe.

Bibliography

- [1] K. Ichikawa, M. Kawasaki, T. Sekiguchi and T. Takahashi, JCAP **0612**, 005 (2006).

Dark matter in universal extra dimension model

[Spokesperson : M. Senami]

ICRR, Univ. of Tokyo, Kashiwa, Chiba 277-8582

Departmento of Micro Engineering, Kyoto University, Kyoto, 606-8501

In collaboration with the members of ICRR and Saitama Univ..

Relic abundance of dark matter is investigated in the minimal universal extra dimension model and the extension with right-handed neutrinos. The relic abundance in the minimal universal extra dimension model has been calculated very accurately. By including right-handed neutrino, the neutrinos get Dirac mass term. In addition to this success, this solve KK graviton problems. Contribution from KK right-handed neutrino to the relic abundance of KK dark matter has also been studied.

Bibliography

- [1] M. Kakizaki, S. Matsumoto and M. Senami, Phys. Rev. D **74**, 023504 (2006); S. Matsumoto, J. Sato, M. Senami

and M. Yamanaka, Phys. Lett. B **647**, 466 (2007); Phys. Rev. D **76**, 043528 (2007).

Power Spectrum of the Density Perturbations From Smooth Hybrid New Inflation Model

[Spokesperson : T. Takayama]

ICRR, Univ. of Tokyo, Kashiwa, Chiba 277-8582

In collaboration with the members of ICRR, Aoyama Gakuin Univ. and RESCEU.

We numerically investigate density perturbations generated in the smooth hybrid new inflation model, a kind of double inflation model that is designed to reproduce the running spectral index suggested by the WMAP results. We confirm that this model provides the running spectral index within 1σ range of the three year WMAP result. In addition, we find a sharp and strong peak on the spectrum of primordial curvature perturbation at small scales. This originates from amplification of fluctuation in the first inflaton fields due to parametric resonance, which takes place in the oscillatory phase between two inflationary regime. Formation probability of primordial black holes (PBHs) is discussed as a consequence of such peak.

Bibliography

- [1] M. Kawasaki, T. Takayama, M. Yamaguchi and J. Yokoyama, Phys. Rev. D **74**, 043525 (2006) [arXiv:hep-ph/0605271].

Baryogenesis via left-right asymmetry generation by Affleck-Dine mechanism in Dirac neutrino model

[Spokesperson : T. Takayama]

ICRR, Univ. of Tokyo, Kashiwa, Chiba 277-8582

In collaboration with the member of Kyoto Univ.

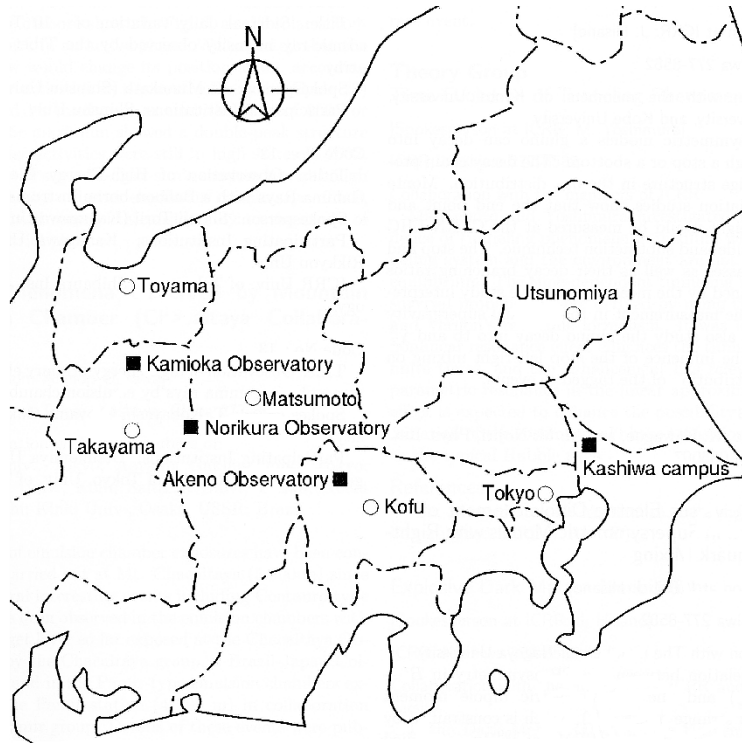
A baryogenesis scenario in supersymmetric standard models with Dirac neutrinos proposed by Abel and Page is reconsidered with introducing intermediate scale physics to stabilize the runaway potential along a right-handed sneutrino direction. In contrary with previous results, the baryon number asymmetry can be explained even for higher reheating temperature without entropy production if the lightest neutrino mass is small and/or thermal effects induce early oscillation. We discuss the solution to the problem of dark matter overproduction by the right-handed sneutrino decay by $SU(2)_R$ gauge interaction.

Bibliography

- [1] M. Senami and T. Takayama, Phys. Rev. D **75**, 105004 (2007) [arXiv:hep-ph/0701103].

OBSERVATORIES and A RESEARCH CENTER

Location of the Institute and the Observatories in Japan



Norikura Observatory

Location: Nyukawa-mura, Ohno-gun, Gifu Prefecture 506-2100
 N 36°06', E 137°33', 2770 m a.s.l.
 Telephone (Fax): +263-33-7456
 Telephone (satellite): 090-7721-5674
 Telephone (car): 090-7408-6224

Akeno Observatory

Location: Akeno-mura, Kitakoma-gun, Yamanashi Prefecture 407-0201
 N 35°47', E 138°30', 900 m a.s.l.
 Telephone / Fax: +551-25-2301 / +551-25-2303

Kamioka Observatory

Location: 456 Higashi-mozumi, Kamioka-cho, Hida-shi, Gifu Prefecture 506-1205
 N 36°25'26", E 137°19'11", 357.5 m a.s.l.
 Telephone / Fax: +578-85-2116 / +578-85-2121

Research Center for Cosmic Neutrinos

Location: 5-1-5 Kashiwanoha, Kashiwa, Chiba Prefecture 277-8582
 Telephone / Fax: +4-7136-3138 / +4-7136-3115

NORIKURA OBSERVATORY

[Director of Norikura Observatory : Masato Takita]
ICRR, Univ. of Tokyo, Kashiwa, Chiba 277-8582

Introduction

Norikura Observatory (36.10°N and 137.55°E) was founded in 1953 and attached to ICRR in 1976. It is located at 2770 m above sea level, and is the highest altitude manned laboratory in Japan. Experimental facilities of the laboratory are made available to all the qualified scientists in the field of cosmic ray research and associated subjects. The AC electric power is generated by the dynamo and supplied throughout the observatory. In 1996, two dynamos of 70 KVA each were replaced with the new ones. The observatory can be accessed easily by car and public bus in summer (July-September). The 50th anniversary of Norikura Observatory was celebrated in 2003.

The feasibility of the automatic operation of Norikura Observatory during winter period has been tested since winter 2004 in order to study the possibilities to reduce maintenance and labor costs without seriously damaging to the use of researches. A long-distance (~40km) wireless LAN system (11M bps) was set up in 2003. Two new easy-to-handle and easy-to-maintain dynamos of 115 KVA each were installed in 2004 as well. The unmanned operation of Norikura Observatory was successful in the first winter, during which the battery backed-up solar panels and/or wind power generators kept supplying the electricity to the wireless LAN and on-going cosmic-ray experiments.

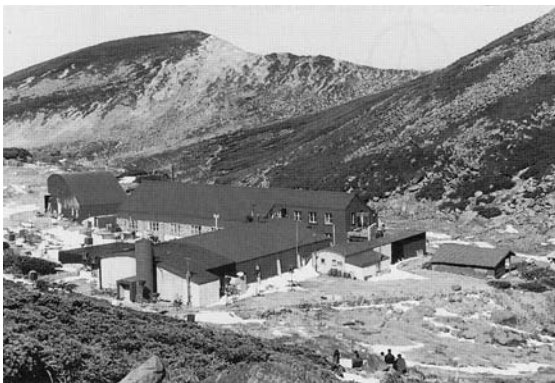


Fig. 1. Norikura Observatory.

Present major scientific interests of the laboratory is focused on the modulation of high energy cosmic rays in the interplanetary space associated with the solar activity and the generation of energetic particles by the solar flares, both of which require long-term monitoring. This research has been carried out by the group of universities, where ICRR provides them with laboratory facility. A part of the facility has been open for the environmental study at high altitude such as the aerosol removal mechanism in the atmosphere or for the botanical study of the high altitude environment.

Cosmic Ray Physics

For the modulation study[2], two small experiments have been operated continuously for a long time. One is a neutron monitor operated to study the correlation of solar activity and the cosmic ray flux. The other is a high counting muon telescope consisting of 36 m² scintillation counters to study the time variation of cosmic rays with energies of 10–100 TeV over 20 years. The neutron monitor data are open to researchers worldwide as a world observation network point (WDC). The 5 years from 2000 corresponded to the solar maximum (2000) to a declining phase in the solar cycle 23. The sun spot number in 2004 is approximately one fourth of the those at maximum. Nonetheless, there occurred active cosmic-ray phenomena associated with Coronal Mass Ejection (CME). As regards solar cosmic rays, although many ground level enhancement (GLE) phenomena took place every year, such GLEs were observed only by neutron monitors in Japan, as the maximum cosmic-ray energy was several GeV in the GLEs and the magnetic rigidity cutoff in Japan is approximately 10 GeV for charged particles initiating secondary muons. The sunspot numbers in the solar cycle 23 was smaller than those in the previous cycle 22, indicating less solar activities of cycle 23. Although the GLEs above 10 GeV were not observed in cycle 23, the total number of GLEs were greater in cycle 23 than in cycle 22. This suggests that the charged particle acceleration associated with CME was less frequent in the cycle 23 than in the cycle 22. On the other hand, Forbush decreases in galactic cosmic rays caused by CME in the Sun were observed frequently in cycle 23, though the solar activities have been in a declining phase since 2000. The worldwide observation of Forbush decreases may contribute significantly to space weather study.

In addition, space weather observation is actively made by a 25 m² muon hodoscope at Norikura Observatory[1], [2],[3],[4],[5], [6],[7],[8]. A loss cone anisotropy is observed by a ground-based muon hodoscope in operation at Norikura Observatory in Japan for 7 hours preceding the arrival of an interplanetary shock at Earth on October 28, 2003. Best fitting a model to the observed anisotropy suggests that the loss cone in this event has a rather broad pitch-angle distribution with a half-width about 50° from the interplanetary magnetic field (IMF). According to numerical simulations of high-energy particle transport across the shock, this implies that the shock is a "quasi-parallel" shock in which the angle between the magnetic field and the shock normal is only 6°. It is also suggested that the leadtime of this precursor is almost independent of the rigidity and about 4 hour at both 30 GV for muon detectors and 10 GV for neutron monitors (see paper [7]).

The Sun is the nearest site to the Earth capable of accelerating particles up to high energies. When the Sun becomes active, flares are frequently observed on its surface. The flare accelerates the proton and ion to high energy and they are detected on the Earth soon after the flare. Among the particles

generated by the flare, high energy neutrons provide the most direct information about the acceleration mechanism as they come straight from the flare position to the Earth without deflected by the magnetic field.

In 1990, Nagoya group constructed a solar neutron telescope consisting of scintillators and lead plates, which measures the kinetic energy of incoming neutrons up to several hundred MeV. This telescope observed high energy neutrons associated with a large flare occurred on the 4th of June, 1991. The same event was simultaneously detected by the neutron monitor and the high counting muon telescope of Norikura Observatory. This is the most clear observation of solar neutrons at the ground level in almost ten years since the first observation at Jungfraujoch in 1982.

A new type of the large solar neutron telescope (64 m² sensitive area) was constructed by Nagoya group in 1996. It consists of scintillators, proportional counters and wood absorbers piled up alternately. This takes a pivotal role among a worldwide network of ground based solar neutron telescopes of the same type in Yangbajing in Tibet, Aragatz in Armenia, Gornergrat in Switzerland, Chacaltaya in Bolivia and Mauna Kea in Hawaii. The Sun is being watched for 24 hours using this network.

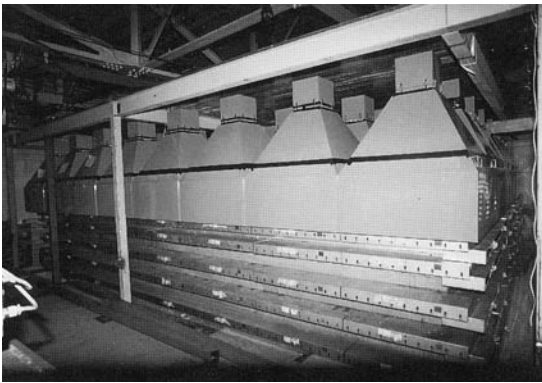


Fig. 2. New Solar-Neutron Telescope of Nagoya Group.

The Sun reached the maximum activity in 2000 and the active phase continued for the next few years. All the telescopes in Norikura Observatory, neutron telescope, neutron monitor, muon telescope and muon hodoscope, have been operated almost continuously through the solar cycle 23 in order to obtain comprehensive information on the solar flare phenomena. Important hints for understanding the mechanism of cosmic-ray acceleration near the solar surface will be obtained by these measurements, especially by energy spectra measured by the timing information of arriving neutrons and muons.

Furthermore, the relation between the electric fields induced by thunderclouds is studied recently[10]. The electric fields with thunderclouds change the intensity of secondary cosmic rays observed on the ground. This effect has been investigated using several detectors located at Norikura Observatory where excesses of 1 % and more of the average counting rate are observed when the observatory is covered with thunderclouds. A frequency analysis of the time series of days with such excesses for the period 26 October 1990 to 15 January shows the expected summer maximum in the rate

of occurrence and, surprisingly, a 26-day variation. An electric field mill was installed to help determine the relationship between the intensity variations and the strength and direction of the field near the detector system: the excess is usually observed when a negative electric field (accelerating negative charges downward) greater than 10 kV/m is present in the atmosphere above the observatory. Based on Monte Carlo simulations, it is predicted that excess counting rates measured without charge discrimination will be expected as a consequence of the excess of positive muons among the secondary cosmic rays.

In addition to the long-term cosmic-ray observations mentioned above, various kinds of short-dated experiments are carried out every year taking an advantage of the high altitude of the observatory. A few examples include a search for super heavy particles with plastic plates, a precise measurement of atmospheric gamma rays and muons, collection of cosmic dusts contained in the snow and the performance study of the balloon borne cosmic ray experiments.

Environmental Study

One of the interesting topics is atmospheric environment especially relating with atmospheric aerosol particles and water soluble gases. Because of its height, AC power supply, accommodation facility, and accessibility of cargos, the cosmic ray observatory at Mt. Norikura provides a very unique opportunity for atmospheric observation, especially for free-tropospheric conditions. (The atmosphere lower than a few kilometer is highly affected by the ground. This height level is named as 'atmospheric boundary layer'. The height of the boundary layer is about 4 km in daytime and about 2 km in nighttime around Norikura area. The atmosphere higher than this atmospheric boundary layer is called 'free troposphere'.) Originally, atmospheric observation at the cosmic ray observatory was initiated to study cosmogenic radionuclides with Prof. Suzuki at Shizuoka University. During early stage of the research at Mt. Norikura, a local effect of air contamination was recognized. To reduce air contamination from diesel exhausts and other activities around the observatory, an atmospheric observation hut (6 m²) was installed at the west end (windward) of the observatory in September 1999. From year 2000, continuous monitoring (mostly mid-May to mid-October) of meteorology was started, number-size distribution of aerosols, dew point, aerosol chemical composition, ozone and radon concentrations, and column amount of aerosols from sky radiometer and ceilometer. Monitoring of ozone and radon concentrations was extended during 2 winters from 2001 to 2003. During summer season, also collected were rain, fog, water-condensed aerosol samples. These samples combined with other parameters were used in several thesis (master) works and provided useful information about future seeds of hygroscopic study of aerosols. During the past 5 years, the following results[11],[12],[13] were obtained at Mt. Norikura.

(1) Polluted air pumping effects over central Japanese Alps in summer

Under the clear sky conditions in summer, polluted air

from mountain valley area is lifted up about 4km of altitude (1km above the mountain top) over Mt. Norikura. The height of observatory is within the atmospheric boundary layer in the daytime, and is out of (higher than) the atmospheric boundary layer in nighttime. The ratio of aerosol volume concentration for daytime (polluted valley wind) to nighttime (clean free-tropospheric) conditions was about 10. The air pumping effects over central Japanese Alps carry about 10 time higher concentration of aerosols to the free-troposphere over Japan in summer. Under the high-pressure system centered over the northwest Pacific in typical summer condition, backward air trajectories were originated from the northwest Pacific to Mt. Norikura and forward trajectories returned to the north Pacific with some deviations to east Russia and the Kurile Islands. The air pumping effects over mountain area provide a strong pollution source mechanism to the free-troposphere over the western Pacific region including East Asia.

(2) Seasonal variation of aerosol chemistry in free troposphere

An automated aerosol sampler was installed at the site in September 2000 to obtain seasonal aerosol samples. The sampler collected aerosols from mid-May to mid-October in 2001 and 2002. Results of its analysis showed seasonal changes in major and minor constituents of aerosols associating with changes of dominant air mass type over Japan.

(3) Vertical profiles of aerosols and clouds near the top of the atmospheric boundary layer

Ceilometer (lidar with small output energy) was installed in summer 2002, and was operated in 4 summer seasons. The aerosol and cloud profiles near the top of the atmospheric boundary layer have been observed. Some events of Asian dust, and of smoke from Siberian forest fire at lower free troposphere have been detected.

Botanical Study

It is predicted that ecosystems in high-latitudes and alpine regions are sensitive to global climatic warming. The significant increasing trends in air temperature are found in the Hida Mountains, where Mt. Norikura is located. Thus, effects of climatic change caused by global warming on alpine ecosystems must be urgently studied in the alpine region of central Japan. The Hida Mountains, strongly influenced by cold-air masses from Siberia in winter, receive some of the heaviest snowfall in the world. Due to heavy snowfall, dynamics of alpine ecosystems may be peculiar to the Hida Mountains. However, few studies have been made because of difficulty in approach to the alpine study site. The inter-university research program of ICRR, gave an opportunity to make an intensive study all year around in the alpine region on Mt. Norikura[14],[15].

(1) Tree line dynamics

The tree form of evergreen sub-alpine fir (*Abies mariesii*) is studied at the upper distribution limit (2500m above sea level) on Mt. Norikura. Leader stems degenerate above the maximum snowpack line (3-4m high), whereas branches below the snowpack line grow densely. In winter, leaves

above snowpack line were severely damaged by environmental stresses, such as abrasion by wind-blown snow particles, desiccation, photoinhibition. Longevity of leaves was shortened to 4-5 years due to high mortality rate in winter. In contrast, leaves below snowpack line were protected from environmental stresses and their longevity was 11 years. As a result, biomass below the snowpack line takes more than 80 with climate change should have unfavorable effects on tree line *Abies mariesii*.

(2) Alpine region

Pinus pumila, an alpine prostrated pine, is dominant in the alpine regions (2500~3000m above sea level). At wind-protected sites, *Pinus pumila* grows vigorously with the tree height of 1-2m. They were buried in snowpack throughout the winter. At the wind-exposed ridge, growth is suppressed with the tree height of 0.2-0.5m. Throughout the winter, the surface of the pine community was exposed due to strong wind at the ridge. Leeward leaves were sound, because pine stems with high elasticity were prostrated and buried in snow. Thus, alpine pine can catch and accumulate snow to protect itself. This feature may be advantageous to alpine trees in comparison with sub-alpine trees (*Abies mariesii*). On the other hand, at the windward side (western), cuticular layer covering epidermal cells of leaf was abraded probably due to wind-blown snow and ice particles. By spring, abraded leaves at the windward side were dead caused by desiccation and photoinhibition. Even *Pinus pumila* community could reduce its habitat in small snowfall condition caused by global warming.

Impact of global warming due to so-called greenhouse gases like CO₂, CH₄ and others on vegetation ecology is among the most serious environmental issues. To investigate how plants response to global warming, an experiment of greenhouse effect on vegetation has been continued at a high mountain, Mt. Norikura (3,025 m a.s.l.), central Japan, since 1997. Five open-top chambers which are small greenhouses with a size of maximum open-top diameter, the maximum basal diameter and the height of the chamber were 47 cm, 85 cm and 30 cm, respectively, were set over alpine plant communities consisting of small woody plants and herbaceous vegetation. At places inside and outside of the chambers, seasonal changes in vegetation growth and phenology were observed every month. Using automatic data-recorders, some climate elements such as air and ground temperatures, humidity and rainfall have been observed every hour. Some results through the experiment were quite remarkable. Due to the temperature enhancement of about 0.8 for air temperature and about 0.3 for ground temperature, plant growth rates and phenological changes showed notable differences between inside and outside of the chambers. The responses to warming, however, were different by different plant species. The results suggest[16],[17] that dominant species in plant community should be replaced by the species with a high physiological response to warming and with a growing form extending tree crown.

Bibliography

- [1] “Precursors of geomagnetic storms observed by the muon detector network”, K. Munakata, J. W. Bieber, S. Yasue, C. Kato, M. Koyama, S. Akahane, K. Fujimoto, Z. Fujii, J. E. Humble, and M. L. Duldig, *J. Geophys. Res.*, Vol. 105, No.A12, pp. 27,457-27,468 (2000).
- [2] “Solar cycle variations of modulation parameters of galactic cosmic-rays in the heliosphere”, K. Munakata, H. Miyasaka, I. Sakurai, S. Yasue, C. Kato, S. Akahane, M. Koyama, D. L. Hall, Z. Fujii, K. Fujimoto, S. Sakakibara, J. E. Humble, and M. L. Duldig, *Adv. Space Res.*, Vol.29, No.10, pp.1527-1532 (2002).
- [3] “A 1.7 year quasi-periodicity in cosmic ray intensity variation observed in the outer heliosphere”, C. Kato, K. Munakata, S. Yasue, K. Inoue, and F. B. McDonald, *J. Geophys. Res.*, Vol.18, No.A10, p.1367, doi:10.1029/2003JA009897 (2003).
- [4] “Exploration of the heliosphere by cosmic rays”, K. Munakata, published as the chapter 2 of *Advances in Solar-Terrestrial Physics*, pp.101-116, edited by H. Oya, published by TERRAPUB, Tokyo (2004).
- [5] “Cosmic-ray modulation in the heliosphere: global and near-earth measurements and modeling”, K. Munakata, Rapporteur paper in 28th *International Cosmic Ray Conference*, Vol.8, edited by T. Kajita et al., pp.251-276, Univ. Acad. Press, Tokyo (2004).
- [6] “Geometry of an interplanetary CME on October 29, 2003 deduced from cosmic rays”, T. Kuwabara, K. Munakata, S. Yasue, C. Kato, S. Akahane, M. Koyama, J. W. Bieber, P. Evenson, R. Pyle, Z. Fujii, M. Tokumaru, M. Kojima, K. Marubashi, M. L. Duldig, J. E. Humble, M. Silva, N. Trivedi, W. Gonzalez and N. J. Schuch, *Geophys. Res. Lett.*, Vol.31, L19803, doi:10.1029/2004GL020803 (2004).
- [7] “A ‘loss-cone’ precursor of an approaching shock observed by a cosmic-ray muon hodoscope on October 28, 2003”, K. Munakata, T. Kuwabara, S. Yasue, C. Kato, S. Akahane, M. Koyama, Y. Ohashi, A. Okada, T. Aoki, H. Kojima and J. W. Bieber, *Geophys. Res. Lett.*, Vol.32, L03S04, doi:10.1029/2004GL021469, 2005.
- [8] “CME-geometry and cosmic-ray anisotropy observed by a prototype muon detector network”, K. Munakata, T. Kuwabara, J. W. Bieber, P. Evenson, R. Pyle, S. Yasue, C. Kato, Z. Fujii, M. L. Duldig, J. E. Humble, M. R. Silva, N. B. Trivedi, W. D. Gonzalez and N. J. Schuch, *Adv. Space Res.*, doi:10.1016/j.asr.2003.05.064, 2005, in press.
- [9] “Acceleration below Thunder Clouds at Mount Norikura”, by the Tibet hybrid experiment”, Y. Muraki *et al.*, Proceedings in the 28th International Cosmic Ray Conference, (31 July - 7 August 2003, Tsukuba, Japan), Vol.7, pp 4177-4180.
- [10] “Effects of atmospheric electric fields on cosmic rays”, Y. Muraki *et al.*, *Phys. Rev. D*, **69**, 123010–1-13 (2004).
- [11] K. Osada, M. Kido, C. Nishita, K. Matsunaga, Y. Iwasaka, M. Nagatani, H. Nakada, Changes in ionic constituents of free tropospheric aerosol particles obtained at Mt. Norikura (2770 m a. s. l.), central Japan, during the Shurin period in 2000, *Atmos. Environ.*, 36, 5469-5477, 2002.
- [12] “Atmospheric diffusion process based on time change of ^{222}Rn vertical profile”, K. Yoshioka, *Journal of Aerosol Research, Japan*, 17, 267-275, 2002 (in Japanese).
- [13] “Free-tropospheric aerosols based on airplane and mountain observations”, K. Osada, *Journal of Aerosol Research, Japan*, 15, 335-342, 2000 (in Japanese).
- [14] “Diurnal changes in needle gas exchange in alpine *Pinus pumila* during snow-melting and summer seasons”, A. Ishida, T. Nakano, S. Sekikawa, E. Maruta, T. Masuzawa, *Ecological Research* 16, 107-116 (2001).
- [15] “Effects of high light and low temperature during harsh winter on needle photodamage of *Abies Mariesii* growing at the forest limit on Mt. Norikura in Central Japan”, J. Yamazaki, A. Ohashi, Y. Hashimoto, E. Negishi, S. Kumagai, T. Kubo, T. Oikawa, E. Maruta, *Plant Science* 165, 257-264, (2003).
- [16] “Chemistry of surface water at a volcanic summit area, Norikura, central Japan: Multivariate statistical approach”, K. Anazawa and H. Ohmori, *Chemosphere*, 45, 807-816, (2001).
- [17] “Experimental research on vegetation response to artificial warming on a mid-latitude high mountain, central Japan”, H. Ohmori, J.H. Iguchi, T. Ohta, A. Terazono and K. Hikita, *Geogr. Rev. Japan*, 77, 301-320, (2004).

AKENO OBSERVATORY

Observatory

The Observatory is in Akeno town of Hokuto-city situated 20 km west of Kofu and 130 km west of metropolitan Tokyo. The location is at the longitude of 138.5°E and the latitude of 35.5°N. The altitude is ~ 900 m above sea level.

It was established in 1977 as a research center for air shower studies in the very high energy region. The Observatory has been administered by the ICRR as a facility of joint-university-use. An important part of observatory's scientific outputs originates from the university collaborators.

From 1 km² Array to AGASA

The Akeno Air Shower Experiment started in 1979 with an array covering 1 km² area (1 km² array). The array was enlarged to 20 km² in 1985 and was gradually expanded to Akeno Giant Air Shower Array (AGASA) of approximately 100 km² area by 1990. The observation by AGASA continued for 13 years until the beginning of 2004.

One of the distinctive features of Akeno experiments is that the measurement was made over five decades of energies well covering 10¹⁵ eV - 10²⁰ eV by using both the surface detector (for electromagnetic component) and the shielded detector (for muon component). This feature is well demonstrated in Fig.2; the spectra from Akeno 1 km² for 10^{14.7} eV - 10^{18.7} eV [1, 2] and AGASA for 10^{18.6} eV - 10^{20.3} eV [3] are plotted by open squares and solid circles in red. The wide energy coverage was accomplished by the arrays of scintillation detectors of various inter-detector spacings from 3 m to 1 km and with different triggering conditions.

The analysis had been made with similar algorithm under the same definition of single particle throughout the energy range covered. A difference exists however for the conversion method to the primary energy; the total number of electrons N_e is used for 1 km² array and the local density at 600 m from the shower core $S(600)$ is used for AGASA. A shift of $\sim 10\%$ in energy is seen between AGASA and 1 km² array around 10^{18.5} eV. This is due to the difference of energy conversion methods employed by two experiments.

The parameter N_e^{\max} at the maximum of shower development is well known as one of the best primary energy estimators which does not depend sensitively on the interaction model or primary composition. The observed N_e at Akeno was converted to N_e^{\max} experimentally with the longitudinal shower development curves determined with constant intensity cut method of integral N_e spectra measured at Mt. Chacaltaya and at Akeno[1]. The result around the *knee* is consistent with all-particle spectra extrapolated from the direct measurements and those of recent results from Tibet[4] and KASCADE[5].

However, as seen in Fig.2, there are large discrepancies among experiments in the highest energy region. It should be noted that the systematic deviation among experiments already starts at 10¹⁷ eV. New data coming from TA and Pierre



Fig. 1. Aerial View of Akeno Observatory and 1 km² Array Area

Auger will have to be understood in a consistent manner with existing lower energy data.

Research and Development

Facilities of Akeno Observatory have been used for a variety of air shower studies, detector developments and associated researches. Activities of recent 6 years (2000 - 2005) are listed below.

- Study of EHECRs by AGASA by M.Teshima^{a,b}, N.Hayashida^a and AGASA collaboration (2000-2005).
- Research and Development of Telescope Array Detectors by Y.Arai^c, M.Chikawa^d, M.Fukushima^a, K.Hashimoto^e, K.Honda^e, N.Inoue^f, F.Kakimoto^g, S.Ogino^{g,h}, H.Sagawa^a, M.Sasaki^a, Y.Tanakaⁱ, S.Yoshida^j and TA collaboration (2000-2005).
- Observation of UHECRs with Lead-Burger Detector by K.Honda^e et al. (2000-2003).
- Observation of Air Shower Core for $E > 10^{16}$ eV by H.Sakuyama^k and N.Suzuki^k et al. (2000-2004).
- Test Measurement of HE Cosmic Rays using Wide Angle Refractive Optics by H.Shimizu^l, S.Ebisuzaki^l and EUSO collaboration (2001-2005).
- Energy Calibration of AGASA Event with Schmidt Type Air Fluorescence Telescope (CRIS) by S.Yoshida^j et al. (2002).
- Measurement of Galactic Cosmic Ray Flux with Large Muon Telescope by S.Kawakami^h et al. (2000-2005).
- Study of Cosmic Evolution by Quick Observation of GRBs by S.Kawai^g et al. (2003-2005).

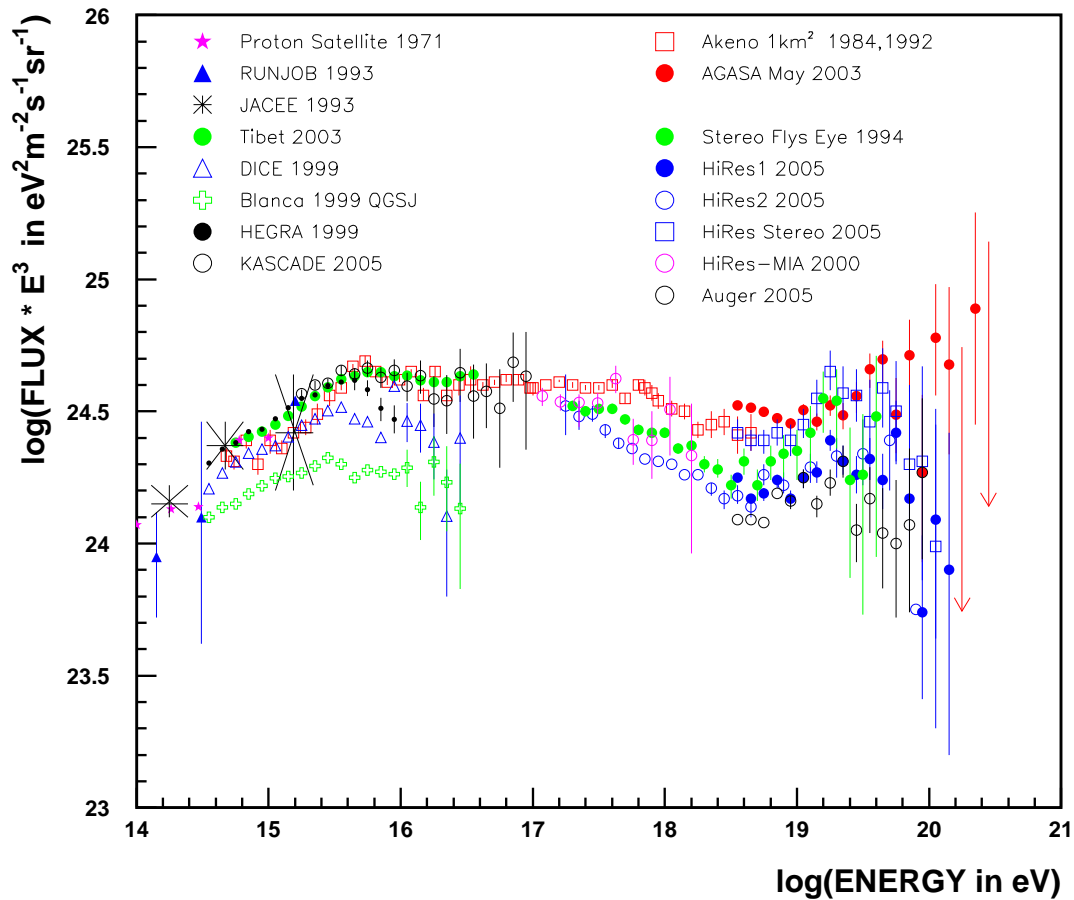


Fig. 2. Energy Spectra of Cosmic Rays between 10^{14} eV and $10^{20.3}$ eV. The data marked as “Auger 2005” and “HiRes Stereo 2005” were presented in the 29th ICRC in 2005, Pune and are preliminary [6].

- On-line Observation of GRBs by Wide Angle Optical Telescope by T.Tamagawa¹ et al. (2003-2005).
- Chemical Composition of Primary Cosmic Rays for 10^{17} eV < E < 10^{18} eV by M.Nagano^m et al. (2003).
- Research and Development for High Resolution All Sky Cosmic Ray Telescope by Y.Arai^c, M.Ieiri^c, R.Ogawaⁿ, M.Sasaki^a, Y.Tanaka¹, Y.Watanabe^g et al. (2003-2005).
- Effect of Cloud for Cosmic Ray Observation from Space by M.Nagano^m et al. (2005).

a: Institute for Cosmic Ray Research, University of Tokyo
 b: Max Planck Institute for Physics, Muenchen
 c: Institute of Particle and Nuclear Studies, KEK, Tsukuba
 d: Kinki University, Osaka
 e: Yamanashi University, Kofu
 f: Saitama University, Saitama
 g: Tokyo Institute of Technology, Tokyo
 h: Osaka City University, Osaka
 i: Nagasaki Institute of Applied Science, Nagasaki
 j: Chiba University, Chiba

k: Meisei University, Tokyo
 l: Riken Institute of Physical and Chemical Research, Tokyo
 m: Fukui University of Technology, Fukui
 n: Toho University, Tokyo

This manuscript was prepared by M.Nagano and M.Fukushima.

Bibliography

- [1] M. Nagano et al., J. Phys. G: Nucl. Phys. **10**, 1295 (1984).
- [2] M. Nagano et al., J. Phys. G: Nucl. Phys. **18**, 423 (1992).
- [3] M. Takeda et al., Astropart. Phys. **19**, 447 (2003).
- [4] M. Takita et al., ICRR Annual Report (2005) p.23.
- [5] T. Antoni et al., astro-ph/0505413 v1 (2005) accepted for publication in Astroparticle Physics.
- [6] S. Yoshida, Slides in Rapporteur Talk at the 29th Int. Cosmic Ray Conf. (2005).

KAMIOKA OBSERVATORY

Kamioka observatory is located at 1000m underground (2700 m.w.e.) in the Kamioka Mine, Gifu prefecture, about 200 km west of Tokyo. The observatory was established in 1995 in order to operate Super-Kamiokande. The underground laboratories are located in Mt.Ikeno-yama and it is possible to access the experimental site through a 1.7 km horizontal tunnel in the mountain. The observatory also has surface research offices and a dormitory which are located just west of the mountain. The Super-Kamiokande experiment discovered neutrino oscillations through the observations of atmospheric and solar neutrinos and it was confirmed by the K2K accelerator neutrino experiment. The future long baseline neutrino experiment using the J-PARC high intensity proton accelerator (the T2K experiment) will inject neutrino beam to the Super-Kamiokande detector from 2009.

The low cosmic ray flux and low seismic noise environment in the underground site enables us to construct various experiments. There are 100 m long laser interferometers in the underground observatory which are aiming to study gravitational waves and geophysics (details are described in the section of the gravitational wave group). Using the low background environment in Kamioka Mine, dark matter and double beta experiments are also being prepared. The XMASS group has performed R&D study for the dark matter search and the construction of the 800kg liquid xenon detector will start in 2007. The R&D study of a tracking type detector by the Kyoto University group (NEWAGE experiment) also has been performed. For double beta decay, the CANDLE experiment (Osaka Univ.) is planned to be located in the Kamioka observatory. In order to accommodate those newly coming experiments, a new experimental area has been excavated since 2007.

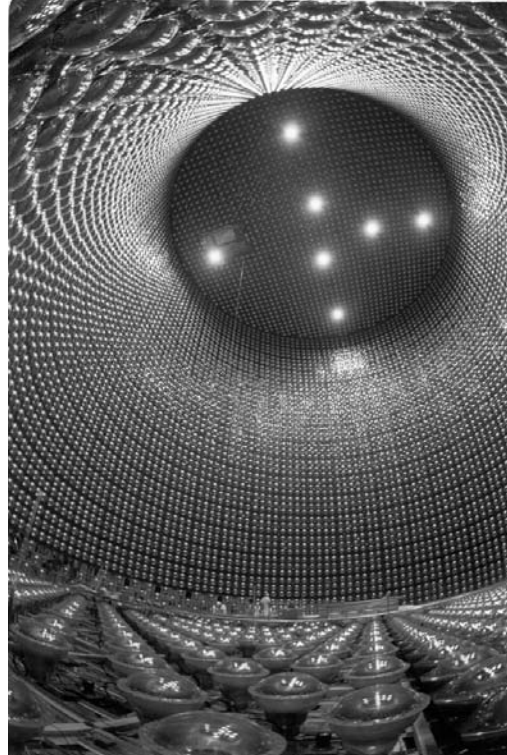


Fig. 2. Super-Kamiokande detector.

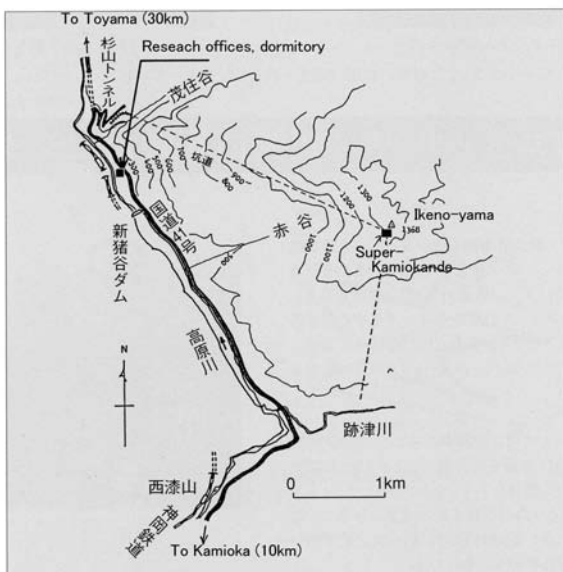


Fig. 1. Map of Kamioka observatory.



Fig. 3. 100 m baseline laser interferometers for gravitational wave and geophysics in Kamioka mine.

RESEARCH CENTER FOR COSMIC NEUTRINOS

Research Center for Cosmic Neutrinos was established in April 1999. The main objective of this center is to study neutrinos based on data from various observations and experiments.

In order to promote the studies of neutrino physics, it is important to provide the opportunity for discussions on theoretical ideas and experimental results on neutrino physics. Therefore, one of the most important, practical jobs of this center is the organization of neutrino related meetings. In the fiscal year 2006, we organized two domestic neutrino meetings. In one of the domestic meetings, we discussed new results from neutrino experiments, and independently cosmic microwave background radiation and their implications. In the other workshop, we discussed non-standard neutrino interactions.

It is important that the general public knows the achievements in the present science. Because of this reason, we had a public lecture on neutrinos at Kashiwa in April 2006. Two active scientists related to neutrino physics lectured on various aspects of neutrino physics.

This Center is also in charge of the computer system and the related network system for the inter-university research programs of ICRR together with the members of the computer committee in ICRR. The systems were operated with a very high efficiency without any serious problem in FY 2006. We formed a committee to discuss the specifications for the new computer system in this fiscal year. The new system will be installed in Jan. 2008.

Since 2004, this Center has been acting as the body for accepting the ICRR inter university programs related to the Underground lab in the Kashiwa campus. The lab. is currently equipped with 4 Ge detectors mainly for the measurements of cosmic radioactive isotopes. The scientific activities that are related to this lab. is described elsewhere.

Finally, the scientific staffs in this center are actively working in the Super-Kamiokande and K2K experiments. These research activities are described in the section of Neutrino and Astroparticle Division. In addition to the Super-Kamiokande and K2K experiments, research activities in this Center include the calculation of the flux of atmospheric neutrinos, studies of neutrino interactions, designing the intermediate detector for the T2K experiment and studying future neutrino detector (Hyper-Kamiokande) and neutrino oscillation experiment in the second phase of the T2K experiment.



Fig. 1. Public lecture held in Kashiwa in April 2006.

APPENDICES

A. ICRR International Workshops

B. ICRR Seminars

C. List of Publications

- (a) **Papers Published in Journals**
- (b) **Conference Papers**
- (c) **ICRR Report**

D. Doctoral Theses

E. Public Relations

- (a) **ICRR News**
- (b) **Public Lectures**
- (c) **Visitors**

F. Inter-University Researches

G. List of Committee Members

- (a) **Board of Councillors**
- (b) **Executive Committee**
- (c) **Advisory Committee**

H. List of Personnel

A. ICRR International Workshops

Twenty Years after SN1987A

Date: February 23-25, 2007

Place: Hilton Waikoloa, Hawaii

(The conference is sponsored by the Kamioka Observatory (ICRR, University of Tokyo), the University of California, Irvine, and the University of Hawaii.)

Outline

On February 23, 1987 detectors on Earth recorded a pulse of neutrinos emitted by SN1987A. This historic event was the first and only detection of neutrinos from outside of our solar system. We have planned a conference at the Hilton Waikoloa near Kona on the Big Island of Hawaii on February 23 to 25, 2007, the 20th anniversary of this event. The conference will review what we have learned about supernovae in the past twenty years and what could be learned from a future supernova. Talks will be by invitation only. Scientific topics include: the history of SN1987A, theoretical developments in understanding supernovae and their environments, neutrino properties and what we can learn about them from a supernova, and present and planned neutrino detectors. Further information about the conference, registration and accommodations will be available on the conference website: <http://sn1987a-20th.physics.uci.edu/>

International Advisory Committee

John Beacom (Ohio State), Venya Berezhinsky (INFN, Gran Sasso), Adam Burrows (Arizona), Sterling Colgate (LANL), Maurice Goldhaber (BNL), Wick Haxton (UW), Hans Thomas Janka (MPI Garching), Manfred Lindner (T.U. Munich), Art McDonald (Queen's Univ.), Kenichi Nomoto (U. of Tokyo), Katsuhiko Sato (U. of Tokyo), Gary Steigman (Ohio State), Atsuto Suzuki (KEK), Yoichiro Suzuki (ICRR), Yoji Totsuka (U. of Tokyo), Craig Wheeler (U. of Texas, Austin), Lincoln Wolfenstein (CMU), Stan Woosley (UCSC).

Local Organization Committee

Masayuki Nakahata (ICRR) Co-chair, Hank Sobel (UCI) Co-chair, Yoshiyuki Fukuda (MUE), Yusuke Koshio (ICRR), William Kropp (UCI), Rolf Peter Kudritzki (UH), John Learned (UH), Yoshihisa Obayashi (ICRR), Sandip Pakvasa (UH), Kate Scholberg (Duke), Michael Smy (UCI), Atsushi Takeda (ICRR), Yasuo Takeuchi (ICRR), Mark Vagins (UCI).

Participants

40 from Japan, 48 from USA, 5 from Germany, 3 from Italy, 2 from Korea, 1 from Canada, 1 from Switzerland, 1 from Russia, 1 from Poland.

B. ICRR Seminars

Date	Lecturer	Title
May 9, 2006	Katsushi ARISAKA (UCLA)	“ Current Status and Future Prospect of Pierre-Auger ”
May 11, 2006	Susumu INOUE (NAOJ)	“ Ultrahigh Energy Cosmic Rays and Gamma-rays from Clusters of Galaxies ”
May 25, 2006	Katsuaki ASANO (NAOJ)	“ High energy CRs, neutrinos, and photons from GRBs ”

Date	Lecturer	Title
Jun 1, 2006	Yasunori FUJII (Advanced Research Institute for Science and Engineering, Waseda University)	“ On the reported time-variability of alpha, particularly on the so-called meteorite constraint ”
Jun 20, 2006	Ryo YAMAZAKI (Hiroshima University)	“ TeV Gamma-Rays from Old Supernova Remnants ”
Jul 4, 2006	Koichi HAMAGUCHI (Univ.Tokyo)	“ Gravitino in the early universe and in the future colliders ”
Jul 13, 2006	Yasunobu UCHIYAMA (ISAS/JAXA)	“ Multifrequency Observations of AGN Relativistic Jets and Their Implications to the Origin of Ultra-High Energy Cosmic-rays ”
Aug 2, 2006	Tsunehiko KATO (NAOJ)	“ Dynamics of collisionless shocks and particle acceleration mechanism ”
Sep 14, 2006	Yuriy BUNKOV (CRTBT-CNRS 38042 Grenoble, France)	“ ”Project ULTIMA” (Particle detector with working temperature 100 μ K) ”
Nov 22, 2006	Hideaki TAKABE (Osaka University)	“ Laboratory Astrophysics with Large-scale Intense Lasers - Present Status of the World and Our Prospect at ILE, Osaka University ”
Dec 1, 2006	Kohta MURASE (Yukawa Institute, Kyoto University)	“ High Energy Emission from Gamma-Ray Bursts ”
Dec 7, 2006	Kari ENQVIST (University of Helsinki)	“ Inflation within Minimally Supersymmetric Standard Model ”
Dec 21, 2006	Herv De KERRET (CNRS)	“ Double Chooz; Reactor theta-13 experiment in France ”
Jan 11, 2007	Takanori SAKAMOTO (NASA/GSFC)	“ Gamma-ray burst observation in the Swift era ”
Jan 23, 2007	Pyungwon KO (KIAS and ICRR)	“ Bs-Bs bar oscillation, Bs \rightarrow $\mu\mu$ and dark matter physics within MSSM ”
Jan 29, 2007	Alok C. GUPTA (Yunnan Astronomical Observatory, China)	“ Variability Study of Radio-Loud and Radio-Quiet AGNs ”
Mar 15, 2007	Marco CASOLINO (INFN, National Institute of Nuclear Physics and Dept. of Physics, University of Roma Tor Vergata)	“ The Cosmic Ray Experiment Pamela: launch, status and perspectives ”
Mar 22, 2007	Mutsumi SUGIZAKI (SLAC)	“ Image Deconvolution for Suzaku XIS CCD Imagers ”

C. List of Publications — 2006 fiscal year

(a) Papers Published in Journals

1. "Study of TeV Neutrinos with Upward Showering Muons in Super-Kamiokande", The Super-Kamiokande Collaboration (S. Desai et al.), Submitted to Astroparticle Physics, hep-ex/arXiv:0711.0053v1.
2. "Observation of the Anisotropy of 10 TeV Primary Cosmic Ray Nuclei Flux with the Super-Kamiokande-I Detector", The Super-Kamiokande Collaboration (G. Guillian et al.), Phys.Rev. D 75, 062003 (2007).
3. "Search for Supernova Neutrino Bursts at Super-Kamiokande", The Super-Kamiokande Collaboration (M. Ikeda et al.), Astrophys J. 669 (2007) 519.
4. "Search for neutral Q-balls in super-Kamiokande II", By Super-Kamiokande Collaboration (Y. Takenaga et al.). Aug 2006. 5pp. Published in Phys.Lett. B647:18-22, 2007.
5. "A Measurement of atmospheric neutrino flux consistent with tau neutrino appearance", By Super-Kamiokande Collaboration (K. Abe et al.). Jul 2006. 6pp. Published in Phys.Rev.Lett. 97:171801, 2006.
6. "Search for Diffuse Astrophysical Neutrino Flux Using Ultrahigh Energy Upward-Going Muons in Super-Kamiokande I", By Super-Kamiokande Collaboration (Molly E.C. Swanson et al.). Jun 2006. 10pp. Published in Astrophys.J. 652:206-215, 2006.
7. "Measurement of Neutrino Oscillation by the K2K Experiment", By K2K Collaboration (M.H. Ahn et al.). Jun 2006. 40pp. Published in Phys.Rev. D74:072003, 2006.
8. "High energy neutrino astronomy using upward-going muons in Super-Kamiokande-I", By Super-Kamiokande Collaboration (K. Abe et al.), Jun 2006. 8pp. Published in Astrophys.J. 652:198, 2006.
9. "Three flavor neutrino oscillation analysis of atmospheric neutrinos in Super-Kamiokande", By Super-Kamiokande Collaboration (J. Hosaka et al.). APS-123-QED, Apr 2006. 13pp. Published in Phys.Rev. D74:032002, 2006.
10. "Solar neutrino measurements in Super-Kamiokande-I", The Super-Kamiokande Collaboration (J. Hosaka et al.), Phys. Rev. D 73, 112001 (2006).
11. "An Improved search for $\nu_\mu \rightarrow \nu_e$ oscillation in a long-baseline accelerator experiment", By K2K Collaboration (S. Yamamoto et al.). Mar 2006. 5pp. Published in Phys.Rev.Lett. 96:181801, 2006.
12. T. Kajita "Discovery of neutrino oscillations", Rept. Prog. Phys. 69, 1607-1635 (2006).
13. T. Kajita, H. Minakata, S. Nakayama and H. Nunokawa "Resolving eight-fold neutrino parameter degeneracy by two identical detectors with different baselines" Phys. Rev. D 75, 013006 (2007).
14. T. Sanuki et al. "Study of cosmic ray interaction model based on atmospheric muons for the neutrino flux calculation" Phys. Rev. D 75, 043005 (2007).
15. M. Honda et al. "Calculation of atmospheric neutrino flux using the interaction model calibrated with atmospheric muon data" Phys. Rev. D 75, 043006 (2007).
16. "CANGAROO-III Observations of the Supernova Remnant RX J0852.0-4622", Enomoto, R. et al., Astrophys. J., 652, 1268-1276 (2006).
17. "Erratum: Detection of diffuse TeV gamma-ray emission from the nearby starburst galaxy NGC 253", Itoh, C. et al., Astron. Astrophys., 462, 67-71 (2007).
18. "Study on Machining of Large Acrylic Lens," Katsuta,T., Yokomizo,S., Sasaki, M., Journal of the Japan Society of Precision Engineering, **73**, No.2, 215-219 (Feb., 2007).
19. "Variation of Sun shadow in the solar cycle 23 observed with the Tibet air shower array", Advances in Space Research, 38, 936-941 (2006).
20. "Anisotropy and Corotation of Galactic Cosmic Rays", Science, 314, 439-443 (2006).
21. "Primary proton spectrum around the knee observed by the Tibet air-shower experiment", Advances in Space Research, 37, 1938-1943 (2006).

22. "Flux upper limits of diffuse TeV gamma rays from the Galactic plane using the effective area of the Tibet-II and -III arrays", *Advances in Space Research*, 37, 1932-1937 (2006).
23. "Are protons still dominant at the knee of the cosmic-ray energy spectrum?", *Physics Letters B*, 632, 58-64 (2006).
24. "Manufacture of a 10-km-scale radius-of-curvature surface by use of a thin-film coating technique", S. Miyoki, et al., *Optics Letters* 30, 1399 (2005)
25. "Present status of CLIO in 2004", T. Uchiyama, et al., *Int. J. Mod. Phys. A20*, 7066 (2005)
26. "Burst wave analysis of TAMA300 data with the ALF filter", T. Akutsu, et al., *Class. Quantum Grav.* 22, S1303 (2005)
27. "Limits on gravitational wave emission from selected pulsars using LIGO data", Abotto and LIGO Scientific Collaboration, *Phys. Rev. Lett.* 94, 181103 (2005)
28. "First all-sky upper limits from LIGO on the strength of periodic gravitational waves using the Hough transform", B. Abotto and LIGO Scientific Collaboration, *Phys. Rev. D72*, 102004 (2005)
29. "Search for gravitational waves from primordial black hole binary coalescences in the galactic halo", B. Abotto and LIGO Scientific Collaboration, *Phys. Rev. D72*, 082002 (2005)
30. "Search for gravitational waves from galactic and extra-galactic binary neutron stars", B. Abotto and LIGO Scientific Collaboration, *Phys. Rev. D72*, 082001 (2005)
31. "Upper limits from the LIGO and TAMA detectors on the rate of gravitational-wave bursts", LIGO Scientific Collaboration and TAMA Collaboration, *Phys. Rev. D72*, 122004 (2005)
32. "Upper limits on gravitational-wave bursts in LIGO's second science run", B. Abotto and LIGO Scientific Collaboration, *Phys. Rev. D72*, 062001 (2005)
33. "A search for gravitational waves associated with the gamma ray burst GRB030329 using the LIGO detectors", B. Abotto and LIGO Scientific Collaboration, *Phys. Rev. D72*, 042002 (2005)
34. "Veto analysis for gravitational wave burst signals in TAMA300 data using ALF filter", T. Akutsu, et al., *Class. Quantum Grav.* 23, S23 (2006)
35. "The CLIO project", S. Miyoki, et al., *Class. Quantum Grav.* 23, S231 (2006)
36. "The status of LCGT", K. Kuroda and the LCGT Collaboration, *Class. Quantum Grav.* 23, S215 (2006)
37. "Influence of radio frequency harmonics to TAMA300 sensitivity", N. Nakagawa, et al., *J Phys. Conf. series* 32, 99 (2006)
38. "Cryogenic systems of the Cryogenic Laser Interferometer Observatory", T. Uchiyama, et al., *J Phys. Conf. series* 32, 259 (2006)
39. "Measurement of vibration of the top of the suspension in a cryogenic interferometer with operating cryocoolers", K. Yamamoto, et al., *J Phys. Conf. series* 32, 418 (2006)
40. "Development of an automatic birefringence measuring device of mirror substrates for gravitational wave detectors", M. Tokunari, et al., *J Phys. Conf. series* 32, 432 (2006)
41. "Rayleigh scattering, absorption, and birefringence of large-size bulk single-crystal sapphire", Z Yan, et al. *Appl. Optics* 45, 2631 (2006)
42. "Experimental effort to detect gravitational waves", K. Kuroda and LCGT Collaboration, *Progress on Theor. Phys. Suppl.* 163, 54 (2006)
43. "Development of a radiation pressure noise interferometer", A Okutomi, et al., *J Phys. Conf. series* 32, 327 (2006)
44. "Measurement of the mechanical loss of a cooled reflective coating for gravitational wave detection", K. Yamamoto, et al., *Phys. Rev. D74*, 022002 (2006)
45. "Joint LIGO and TAMA300 Search for Gravitational Waves from Inspiralling Neutron Star Binaries", LIGO Scientific Collaboration and TAMA Collaboration, *Physical Review D73*, 102002 (2006)
46. "Search for gravitational waves from binary black-hole inspirals in LIGO data", B. Abotto and LIGO Scientific Collaboration, *Phys. Rev. D73*, 062001 (2006)

47. "Dark energy evolution and the curvature of the universe from recent observations", Ichikawa, K. et al., *Physical Review D*, 73, 083526 (2006)
48. "The Sloan Digital Sky Survey Quasar Survey: Quasar Luminosity Function from Data Release 3", Richards, G. T. et al., *Astronomical Journal*, 131, 2766 (2006)
49. "Constraining the Evolution of the Ionizing Background and the Epoch of Reionization with $z \sim 6$ Quasars. II. A Sample of 19 Quasars", Fan, X. et al., *Astronomical Journal*, 132, 117 (2006)
50. "CMB constraints on the simultaneous variation of the fine structure constant and the electron mass", Ichikawa, K. et al., *Physical Review D*, 74, 023515 (2006)
51. "Limit on the neutrino mass from the WMAP three-year data", Fukugita, M. et al., *Physical Review D*, 74, 027302 (2006)
52. "Primordial Helium Abundance: A Reanalysis of the Izotov-Thuan Spectroscopic Sample", Fukugita, M. et al., *Astrophysical Journal*, 646, 691 (2006)
53. "The Sloan Digital Sky Survey Quasar Lens Search. I. Candidate Selection Algorithm", Oguri, M. et al., *Astronomical Journal*, 132, 999 (2006)
54. "The rest-frame optical colours of 99000 Sloan Digital Sky Survey galaxies", Smolčić, V., et al., *Monthly Notices of the Royal Astronomical Society*, 371, 121 (2006)
55. "Implications of cosmic strings with time-varying tension on the CMB and large scale structure", Ichikawa, K. et al., *Physical Review D*, 74, 063526 (2006)
56. "The History of Cosmological Star Formation: Three Independent Approaches and a Critical Test Using the Extragalactic Background Light", Nagamine, K. et al., *Astrophysical Journal*, 653, 881 (2006)
57. "Luminosity Functions of Lyman Break Galaxies at $z \sim 4$ and $z \sim 5$ in the Subaru Deep Field", Yoshida, M. et al., *Astrophysical Journal*, 653, 988 (2006)
58. "SDSS J1029+2623: A Gravitationally Lensed Quasar with an Image Separation of 22.5''", Inada, N., et al. *Astrophysical Journal*, 653, L97 (2006)
59. "Implications of dark energy parametrizations for the determination of the curvature of the universe", Ichikawa, K. et al., *Journal of Cosmology and Astro-Particle Physics*, 12, 5 (2006)
60. "Cosmological constraints from the SDSS luminous red galaxies", Tegmark, M. et al., *Physical Review D*, 74, 123507 (2006)
61. "Dark energy parametrizations and the curvature of the universe", Ichikawa, K. et al., *Journal of Cosmology and Astro-Particle Physics*, 2, 1 (2007)
62. "Measuring the Matter Density Using Baryon Oscillations in the SDSS", Percival, W. J. et al., *Astrophysical Journal*, 657, 51 (2007)
63. "The Shape of the Sloan Digital Sky Survey Data Release 5 Galaxy Power Spectrum", Percival, W. J. et al., *Astrophysical Journal*, 657, 645 (2007)
64. "CMB constraints on the fine structure constant", K. Ichikawa, T. Kanzaki and M. Kawasaki, *Phys. Rev.* **D74**, 023515 (2006).
65. "511 keV line and diffuse gamma rays from moduli", S. Kasuya, M. Kawasaki, *Physical Review* **D73** 063007 (2006)
66. "Primordial Helium Abundance: A Reanalysis of the Izotov-Thuan Spectroscopic Sample", M. Fukugita, M. Kawasaki, *Astrophysical Journal* **646** 691 (2006)
67. "Gravitino overproduction in inflaton decay", M. Kawasaki, F. Takahashi and T. T. Yanagida, *Physics Letters* **B638** 8 (2006)
68. "Limit on the neutrino mass from the WMAP three year data", M. Fukugita, K. Ichikawa, M. Kawasaki and O. Lahav, *Physical Review* **D74** 027302 (2006)
69. "Towards the robustness of the Affleck-Dine baryogenesis" S. Kasuya and M. Kawasaki, *Physical Review* **D74** 063507 (2006)

70. "The gravitino overproduction problem in inflationary universe", M. Kawasaki, F. Takahashi and T. T. Yanagida, *Physical Review D* **74** 043519 (2006)
71. "Inflaton Decay through Supergravity Effects", M. Endo, M. Kawasaki, F. Takahashi and T. T. Yanagida, *Physical Letters B* **642** 518 (2006)
72. "Early reionization by decaying particles in light of three year WMAP", S. Kasuya and M. Kawasaki, *JCAP* **0702** 010 (2007)
73. "Gauss-Bonnet brane-world cosmology without Z_2 -symmetry", K. Konya, *Class. Quantum Grav.* **24** 2761 (2007).
74. "Graviton emission from a Gauss-Bonnet brane", K. Konya, *Phys. Rev.* **D75** 104003 (2007).
75. "New two-loop contributions to hadronic EDMs in the MSSM", J. Hisano, M. Nagai and P. Paradisi, *Phys. Lett. B* **642**, 510 (2006).
76. "Electric dipole moments in pseudoDirac gauginos", J. Hisano, M. Nagai, T. Naganawa and M. Senami, *Phys. Lett. B* **644**, 256 (2007).
77. "Non-perturbative effect on thermal relic abundance of dark matter", J. Hisano, S. Matsumoto, M. Nagai, O. Saito and M. Senami, *Phys. Lett. B* **646**, 34 (2007).
78. "Late-time Affleck-Dine baryogenesis after thermal inflation," M. Kawasaki and K. Nakayama, *Phys. Rev. D* **74**, 123508 (2006).
79. "Affleck-Dine baryogenesis in anomaly-mediated supersymmetry breaking," M. Kawasaki and K. Nakayama, *JCAP* **0702**, 002 (2007).
80. "Increasing the effective number of neutrinos with decaying particles," K. Ichikawa, M. Kawasaki, K. Nakayama, M. Senami and F. Takahashi, *JCAP* **0705**, 008 (2007).
81. "Implication of dark energy parametrizations on the determination of the curvature of the universe", K. Ichikawa, M. Kawasaki, T. Sekiguchi and T. Takahashi, *JCAP* **0612**, 005 (2006).
82. "Constraining SuperWIMPy and Warm Subhalos with Future Submillilensing", J. Hisano, K.T. Inoue, T. Takahashi, *Phys. Lett. B* **643**, 141 (2006).
83. "Universality of strength for Yukawa couplings with extra down-type quark singlets", K. Higuchi, M. Senami and K. Yamamoto, *Phys. Lett. B* **638**, 492 (2006).
84. "Non-perturbative effect on thermal relic abundance of dark matter", S. Matsumoto, J. Sato, M. Senami and M. Yamanaka, *Phys. Lett. B* **647**, 466 (2007).
85. "Solving cosmological problem in universal extra dimension models by introducing Dirac neutrino", S. Matsumoto, J. Sato, M. Senami and M. Yamanaka, *Phys. Lett. B* **647**, 466 (2007).
86. "Relic abundance of dark matter in the minimal universal extra dimension model", M. Kakizaki, S. Matsumoto and M. Senami, *Phys. Rev. D* **74**, 023504 (2006).
87. "Power Spectrum of the Density Perturbations From Smooth Hybrid New Inflation Model", M. Kawasaki, T. Takayama, M. Yamaguchi and J. Yokoyama, *Phys. Rev. D* **74**, 043525 (2006).
88. "Baryogenesis via left-right asymmetry generation by Affleck-Dine mechanism in Dirac neutrino model", M. Senami and T. Takayama, *Phys. Rev. D* **75**, 105004 (2007).

(b) Conference Papers

1. J. Kameda, "Summary of Searches for exotic phenomena with Super-Kamiokande", Workshop on Exotic Physics with Neutrino Telescope Upsala, Sweden, 20-22 Sep 2006, Proceeding of the First Workshop on Exotic Physics with Neutrino Telescopes Uppsala University, January 2007 ISBN978-91-506-1913-3, astro-ph/0701333 p9-13
2. H. Nishino, K. Awai, Y. Hayato, K. Kaneyuki, K. Okumura, M. Shiozawa, A. Takeda, Y. Arai, K. Ishikawa, A. Minegishi, "Development of New Data Acquisition Electronics for the Large Water Cherenkov Detector", IEEE Nuclear Science Symposium Conference Record 2006, (San Diego, California, Oct.29-Nov.4, 2006), Vol.1, pp124-127

3. M. Nakahata, " Search for Supernova neutrinos at Super-Kamiokande", Proceedings of the International workshop on Energy Budget in the High Energy Universe, edited by K. Sato and J. Hisano, October, 2006.
4. Y. Takenaga, "Search for neutral Q-balls in Super-Kamiokande II", Workshop on Exotic Physics with Neutrino Telescopes, Uppsala, Sweden, Sep 20-22, 2006, ISBN 978-91-506-1913-3 astro-ph/0701333 (2007)
5. Y. Obayashi, "SUPER-KAMIOKANDE: The Status of Neutrino Oscillations", in Conference Proceedings Vol. 93 "Frontier Objects in Astrophysics and Particle Physics" (Vulcano, Italy, May 22-27, 2006), F. Giovannelli & G. Mannocchi (eds.), SIF, Bologna 2007, ISBN 978-88-7438-034-3, p571-582
6. A. Takeda, "XMASS experiment", Proceedings of "International Workshop on the Identification of Dark Matter (IDM2006)", (2006) pp243-247, World Scientific.
7. H. Sekiya, "Background Reduction in Super-Kamiokande Detector for Solar Neutrino", in AIP Conference Proceedings Vol. 897 "Topical Workshop on Low Radioactivity Techniques" (Aussois, France, 1-4 October 2006), Pia Loaiza (eds.), Melville, New York 2007, ISBN 978-0-7354-0402-1, pp73-78
8. T. Kajita "Future neutrino oscillation physics in Japan", Proceedings of the Neutrino Oscillation Workshop (Nucl. Phys. B (Proc. Suppl.) 168, 155-160 (2007).)
9. T. Kajita "Updating the Future Long Baseline Experiment with the Kamioka-Korea two Detector Setup" Proceedings of Twelfth International Workshop on Neutrino Telescopes (2007), pp211-221.
10. M. Mori, "Recent Results from CANGAROO" SCIENCE WITH THE NEW GENERATION OF HIGH ENERGY GAMMA-RAY EXPERIMENTS, The Variable Gamma-Ray Sources: Their Identifications and Counterparts, Isola d'Elba, Italy 20 - 22 June 2006 (eds. M.M. Massai, N. Omodai and G. Spandre, World Scientific, Singapore, 2007)
11. T. Tanimori, "Recent Results from CANGAROO TeV gamma-ray observations" The Extreme Universe in the Suzaku Era, Kyoto, Japan, December 4-8, 2006 (to be published)
12. K. Nishijima, "Detection of VHE gamma-ray flare from PKS 2155-304" *ibid.*
13. M. Mori, "Recent results from CANGAROO-III" Locating PeV Cosmic-Ray Accelerators: Future Detectors in Multi-TeV Gamma-Ray Astronomy, Adelaide, Australia, December 6-8, 2006
14. T. Yoshikoshi, " Simulations and R & D Studies for 100 TeV Gamma-Ray Astrophysics with a Large Effective Area IACT Array", *ibid.*
15. T. Kifune, "Nearby galaxies, 10^{20} eV cosmic rays and the 10TeV10km² project" *ibid.*
16. M. Mori, "Recent results from CANGAROO" International Workshop on "Cosmic-rays and High Energy Universe", Aoyama Gakuin Univ., Shibuya, Tokyo, Japan, March 5-6, 2007 (to be published)
17. "All-sky Survey High Resolution Air-Shower Detector (Ashra)," Sasaki, M., Proceeding of International Workshop on Energy Budget in the High Energy Universe (ICRR, Kashiwa), edit. by Sato, K. and Hisano, J., 197-204 (March, 2007).
18. A. Okutomi et al., " Development of a radiation pressure noise interferometer ", The 6th Elardo Amaldi Conference on Gravitational Waves 2005, Okinawa, Japan, June 20-24, 2005. (to be published in Journal of Physic : Conference Series)
19. K. Yamamoto et al., " Measurement of vibration of the top of the suspension in a cryogenic interferometer with operating cryocoolers ", The 6th Elardo Amaldi Conference on Gravitational Waves 2005. (to be published in Journal of Physic : Conference Series)
20. T. Uchiyama et al., " Cryogenic systems of the Cryogenic Laser Interferometer Observatory ", The 6th Elardo Amaldi Conference on Gravitational Waves 2005. (to be published in Journal of Physic : Conference Series)
21. T. Suzuki et al., " Application of sapphire bonding for suspension of cryogenic mirrors ", The 6th Elardo Amaldi Conference on Gravitational Waves 2005. (to be published in Journal of Physic : Conference Series)
22. M. Kakizaki, S. Matsumoto and M. Senami, "Cosmological constraint on the minimal universal extra dimension model", 14th International Conference on Supersymmetry and the Unification of Fundamental Interactions, (12-17 Jun 2006, Irvine, California), AIP Conf. Proc. **903** (2007) 483.
23. M. Nagai, "Detection possibilities of thermally produced wino dark matter", 14th International Conference on Supersymmetry and the Unification of Fundamental Interactions (SUSY06), (12-17 Jun 2006, Irvine, California, USA), AIP Conf. Proc. **903**, 575 (2007).

24. “Baryogenesis via left-right asymmetry generated by Affleck-Dine mechanism in Dirac neutrino model”, M. Senami and T. Takayama, International Workshop on Neutrino Masses and Mixings: Toward Unified Understanding of Quark and Lepton Mass Matrices (NMM2006), (17-19 Dec 2006, Shizuoka, Japan), Int. J. Mod. Phys. E **16**, 1513 (2007).

D. Doctoral Theses

“Vertex Operators in Supersymmetric matrix models”, Osamu Saito, Ph.D. Thesis, Theory, May 2007.

E. Public Relations

(a) ICRR News

ICRR News is a newspaper published quarterly in Japanese to inform the Institute’s activities. This year’s editors were K.Okumura and M.Ohashi. It includes :

1. reports on investigations by the staff of the Institute or made at the facilities of the Institute,
2. reports of international conferences on topics relevant to the Institute’s research activities,
3. topics discussed at the Institute Committees,
4. list of publications published by the Institute [ICRR-Report, ICRR-Houkoku(in Japanese)],
5. list of seminars held at the Institute,
6. announcements,
7. and other items of relevance.

The main topics in the issues in 2006 fiscal year were :

No.60 (May 31, 2006)

- The 10th anniversary of the Super-Kamiokande. Masato Shiozawa.
- The tour of SK. Hideo Itoh.
- Report of the Symposium on Future Projects in Cosmic Ray Physics hosted by CRC. Saburo Kawakami. Studies of cosmic rays in the highest energy region
High energy gamma rays
High energy electrons and gamma rays
High energy neutrinos
- ICRR seminars and Reports.

No.61 (November 30, 2006)

- Report on the visit to the site of the Telescope Array experiment. Hideo Itoh.
- Report on the ICRR Open House in JFY2006. Naoki Yasuda.
- Notice of Call for ICRR Inter-University Researches in JFY2007.
- ICRR-Seminar/Report.
- Self-introduciton.

- Staff reassignmen.

No.62 (March 30, 2007)

- Study meetings towards the Symposium on ICRR Future Projects. Masaki Mori.
- Report on the meeting for presenting the results of Inter-University Researches in the JFY2006. Masatake Ohashi.
- Science Cafe in the US-Japan Joint Physics Society Meeting. Hideo Itoh.
- ICRR-Seminar.

(b) Public Lectures

- "Public Lecture on Neutrino",
April 22 2006, Kashiwa, Chiba,
"Observing the Earth using Neutrinos", K.Inoue (Tohoku University).
"Expecting New Physics from New Neutrino Experiments", T.Kajita (ICRR, University of Tokyo).

(c) Visitors

KAMIOKA Observatory (Total: 191 groups, 3933 people)

- Mr. Yoshino (Ministerial aid of Ministry of Education, Culture, Sports, Science and Technology) April 17, 2006.
- Mr. Matsuda (Minister of policy for science and technology), June 5, 2006.
- Mr. Kosaka (Minister of Ministry of Education, Culture, Sports, Science and Technology) June. 10, 2006.
- Mr. Takeda, Mr. Hara, Mr. Oato, Mr. Shimada and Mr. Nozaki (National Institution for Academic Degrees and University Evaluation) August 30, 2006.
- Mr. Ishii (Governor of Toyama prefecture) October 10, 2006.
- Mr. Mori (City mayor of Toyama city) November 14, 2006.
- Mr. Oiso (National Diet Library) January 24, 2007.
- Mr. Tsuchino (City mayor of Takayama city) February 2, 2007.
- Mr. Yamada (City mayor of Gero city) February 2, 2007.
- Mr. Taniguchi (City mayor of Shirakawa city) February 2, 2007.
- Mr. Funasaka (City mayor of Hida city) February 2, 2007.
- Yumeno Tamago Jyuku (Science camp for Junior High School Students)
- Yumeno Tamago Jyuku (Hida academy for High School Students)
- MEXT Super Science High School(SSH) project: total 1 schools

F. Inter-University Researches

Researcher Numbers

	Application Numbers	Adoption Numbers	Researchers Numbers
<hr/> <hr/> Facility Usage <hr/> <hr/>			
Kamioka Observatory	34	34	559
Norikura Observatory	7	7	45
Akeno Observatory	5	5	82
Research Center for Cosmic neutrinos	1	1	5
Emulsion and Air Shower Facilities in Kashiwa	3	3	60
Low-level Radio-isotope Measurement Facilities in Kashiwa	6	6	30
Gravitational Wave Facilities in Kashiwa	4	4	31
Over Sea Facilities	12	12	104
Other	19	19	253
<hr/> <hr/>			
Collaborative Researches <hr/> <hr/>			
Cosmic Neutrino Researches	42	42	599
High Energy Cosmic Ray Researches	39	39	417
Theoretical Researches or Rudimental Researches	10	10	153
<hr/> <hr/>			
Others <hr/> <hr/>			
Conferences	4	4	31
Special Activity on Abroad	0	0	0

Research Titles

1. Study of the solar neutrino flux
2. Study of solar neutrino energy spectrum
3. Precise measurement of Day/Night effect for ^8B solar neutrinos
4. Study for Supernova monitor
5. Study of Supernova Relic Neutrinos
6. Study of atmospheric neutrinos and neutrino oscillations
7. Study of flavor identification of atmospheric neutrinos
8. Study on 3-flavor Oscillation Effect in Atmospheric Neutrinos
9. Study of simulation for atmospheric neutrino
10. Study of upward going muons
11. Precise calculation of the atmospheric neutrino flux
12. Search for Nucleon Decay
13. search for proton decay via $e^+\pi^0$ mode
14. Study of nucleon decay $p \rightarrow \nu K$
15. Energy calibration for Super-Kamiokande
16. Development of high-sensitivity radon detector

17. Sidereal daily variation of 10TeV galactic cosmic-ray intensity observed by the Super-Kamiokande
18. R&D of J-PARC-Kamioka Long Baseline Experiment T2K
19. Study of neutrino-nucleus interactions for accurate neutrino oscillation experiments
20. Neutrino interaction study using accelerator data
21. Neutrino workshop
22. Development of detectors for astroparticles by using liquid Xenon
23. Direct dark matter search with liquid xenon detector
24. Direction-sensitive dark matter search experiment
25. Study of ambient gamma-ray and neutron flux at Kamioka mine
26. A study on emission spectrum of liquid xenon
27. R&D of a 1 Mton water Cherenkov Hyper-Kamiokande
28. Study for the electron neutrino appearance search in the T2K experiment
29. Study for lowering backgrounds of radioisotopes in large volume detectors
30. The construction of dark matter detector by simulation
31. Study for double beta decay of ^{48}Ca
32. Development of InP detector for measurement of solar ν
33. Calibration test of High energy electron telescope for spacecraft
34. Study of High Energy Cosmic Neutrinos
35. Commissioning and First Observation of TA
36. Study of absolute energy calibration air shower by compact Electron LINAC
37. R&D of a new atmospheric monitoring system
38. Calibrations of the mirrors for the TA experiment
39. Experimental Study of High-energy Cosmic Rays in the Tibet AS γ experiment
40. Study of the composition of cosmic-rays at the knee
41. A study on variation of interplanetary magnetic field with the cosmic-ray shadow by the sun
42. Sidereal daily variation of 10TeV galactic cosmic-ray intensity observed by the Tibet air shower array
43. Observation of high-energy cosmic-ray electrons with emulsion chambers
44. Observation of celestial very-high-energy gamma-rays in Australia
45. CANGAROO-III Observation of gamma-rays in the southern sky
46. R&D of mirrors and optical sensors for TeV telescopes of the next generation
47. Observation of TeV gamma-ray spectra from galactic objects
48. Search for High Energy Gamma-ray Emission from Star Forming Regions and Theoretical Research
49. Emission mechanism of TeV Gamma-rays from HESS UnID sources
50. Study of the formation and the evolution of the Universe with prompt observations of gamma-ray bursts
51. Observation of Galactic Cosmic ray intensities by the large muon telescope
52. Observation of solar neutrons in solar cycle 24

53. Space weather observation using muon hodoscope at Mt.Norikura
54. A Study of the Radiation Damage to Polyimide film
55. Study for fluctuation of radiation intensity in thunderstorm
56. Continuous observation of microbarographs at high mountains
57. Ecophysiological studies of alpine plants
58. Study of the interaction of cloud with aerosol at Mt.Norikura
59. Bolivian Air Shower Joint Experiment
60. All-sky Survey High Resolution Air-shower detector Ashra
61. Observation of UHE cosmic rays and TeV gamma rays with Ashra detector
62. Development of image transmission system using optical fiber for Ashra
63. Absolute Calibration of the IceCube Digital Optical Modules (DOMs)
64. Study on High Energy Cosmic-Ray Acceleration Objects by Balloon Observation
65. Symposium for CRC's Future Projects
66. Workshop on 'New experiment for a study of ultra-high energy cosmic-ray interaction in $E_0 \geq 10^{17}$ eV'
67. Workshop on "'High Energy Gamma-ray Astrophysics''
68. Real-time data analysis in the Telescope Array experiment
69. Study of Galactic Diffuse Gamma Rays
70. Time Variability of Extra galactic gamma-ray objects
71. Development of immediate data analysis system for GANGAROO-III
72. Research for degradation of image sensor used in Ashra
73. Experimental study of cosmic ray interactions in the knee and the highest energy regions
74. Evolution of the universe and particle physics
75. R&D and Design of large-scale cryogenic gravitational wave telescope (IX)
76. Development of a sapphire mirror suspension for LCGT (III)
77. Study of effective thermal shielding method for the LCGT cryostat
78. quality measurement of sapphire test mass for LCGT (II)
79. Sensitivity enhancement of interferometergravitational wave detector by light squeezing (III)
80. Gravitational Wave Research in Kamioka (VI)
81. digital Control of CLIO and Its Analysis
82. observation of gravitational wave from pulsars by CLIO
83. Study for the Earth's normal modes with the superconducting gravimeter observations
84. Continuous Measurement of Underground Laboratory Environment
85. Deposition Rate/Flux of Natural Radioactive Nuclides ^7Be and ^{210}Pb
86. Detection of variability in cosmic rays with cosmogenic nuclide Be-7 and/or Na-22
87. Detection of low level radioisotopes in tree rings
88. Comprehensive Researches on Cosmic Dusts
89. Chemical study for Antarctic micrometeorites
90. Measurements of ^{26}Al radioactivities for minor amount of Antarctic meteorite
91. Development of the IceCube Detector Simulation

G. List of Committee Members

(a) Board of Councillors

SUZUKI, Yoichiro	ICRR, University of Tokyo
KURODA, Kazuaki	ICRR, University of Tokyo
KAJITA, Takaaki	ICRR, University of Tokyo
FUKUSHIMA, Masaki	ICRR, University of Tokyo
YAMAMOTO, Masayuki	University of Tokyo
OKAMURA, Sadanori	University of Tokyo
TAKASAKI, Tadafumi	KEK
EGUCHI, Toru	YITP, Kyoto university
MIYAMA, Shoken	National Astronomical Observatory
SATO, Fumitaka	Konan University
EJIRI, Hiroyasu	Osaka University
MURAKI, Yasushi	The Open University of Japan
OHTA, Itaru	Utsunomiya University
INOUE, Hajime	Institute of Space and Astronautical Science
KOMAMIYA, Yukio	ICEPP, University of Tokyo

(b) Advisory Committee

SUZUKI, Yoichiro	ICRR, University of Tokyo
TORII, Shoji	Waseda University
MURAKI, Yasushi	Konan University
TANIMORI, Toru	Kyoto University
KAWAKAMI, Saburo	Osaka City University
YANAGIDA, Manabu	University of Tokyo
NAGAE, Tomohumi	KEK
NISHIKAWA Koichiro	KEK
NAKAMURA, Takashi	Kyoto University
MINOWA, Makoto	University of Tokyo
KURODA, Kazuaki	ICRR, University of Tokyo
FUKUGITA, Masataka	ICRR, University of Tokyo
FUKUSHIMA, Masaki	ICRR, University of Tokyo
MORI, Masaki	ICRR, University of Tokyo
NAKAHATA, Masayuki	ICRR, University of Tokyo
TAKITA, Masato	ICRR, University of Tokyo

(c) User's Committee

KAJINO, Fumiyoshi	Konan University
NISHIJIMA, Kyoshi	Tokai University
TORII, Shoji	Waseda University
TANIMORI, Toru	Kyoto University
MATSUBARA, Yutaka	Nagoya University
KANDA, Nobuyuki	Osaka University
SAKURAI, Takahisa	Yamagata University
ITO, Yoshitaka	Nagoya University
OHASHI, Masataka	ICRR, University of Tokyo
YOSHIKOSHI, Takanori	ICRR, University of Tokyo
SHIOZAWA, Makoto	ICRR, University of Tokyo
KANEYUKI, Kenji	ICRR, University of Tokyo
TAKITA, Masato	ICRR, University of Tokyo
HISANO, Junji	ICRR, University of Tokyo

H. List of Personnel

Director SUZUKI Yoichiro

Vice-Director KURODA Kazuaki

Kamioka Observatory (Neutrino and Astroparticle Division)

Scientific Staff SUZUKI Yoichiro, NAKAHATA Masayuki, MORIYAMA Shigetaka,
TAKEUCHI Yasuo, SHIOZAWA Masato, HAYATO Yoshinari
MIURA Makoto, OBAYASHI Yoshihisa, KOSHIO Yusuke,
KAMEDA Jun, TAKEDA Atsushi, ABE Ko,
SEKIYA Hiroyuki, YAMADA Satoru,

Chief Secretary AKIMOTO Masatoshi,

Technical Staff MIZUHATA Minoru, KANBE Tomio, KUMAMARU Seiichi,
NAKAJIMA Tetsue,

Research Fellows OGAWA Hiroshi, WATANABE Hideki,
Secretary OKURA Youko, MAEDA Yukari, OKADA Eri,

Research Center for Cosmic Neutrinos (Neutrino and Astroparticle Division)

Scientific Staff KAJITA Takaaki, KANEYUKI Kenji, OKUMURA Kimihiro,

Technical Staff SHINOHARA Masanobu,

Research Fellows NAKAYAMA Shoei, HIGUCHI Itaru, HONDA Morihiro,

Secretary FUKUDA Yoko, KITSUGI Atsuko,

High Energy Cosmic Ray Division

Scientific Staff FUKUSHIMA Masaki, MORI Masaki, TAKITA Masato,
ENOMOTO Ryoji, YOSHIKOSHI Takanori, HAYASHIDA Naoaki,
SASAKI Makoto, TAKEDA Masahiro, OHNISHI Munehiro,
OHISHI Michiko, HATANO Yoshikazu

ASAOKA Yoichi, SAKURAI Nobuyuki,
Technical Staff AOKI Toshifumi, KOBAYASHI Takahide,

Research Fellows OZAWA Shunsuke, UDO Shigeharu, TOKUNOU Hisao,
SHIBATA Tatsunobu, YAMAKAWA Toshie, SHIOMI Atsushi,
KONDO Yoshimi, KAWATA Kazumasa, HUANG Jing,
WANG Xiao, NONAKA Toshiyuki, TATSUMI Fusako,
YAN Zhitao, FABRICE Cohen,

Secretary SAWANO Sumiko, KOKUBUN Yayoi,

Akeno Observatory (High Energy Cosmic Ray Division)

Scientific Staff SAGAWA Hiroyuki,

Technical Staff TORII Reiko, OHOKA Hideyuki, KAWAGUCHI Masami,

Norikura Observatory (High Energy Cosmic Ray Division)

Technical Staff YAMAMOTO Kuniyuki, AGEMATSU Yoshiaki, USHIMARU Tsukasa,

ISHITSUKA Hideki, SHIMODAIRA Hideaki,

Astrophysics and Gravity Division

Scientific Staff FUKUGITA Masataka, KURODA Kazuaki, KAWASAKI Masahiro,
OHASHI Masatake, YASUDA Naoki, HISANO Junji,
MIYOKI Shinji, UCHIYAMA Takashi,

Research Fellows YAMAMOTO Kazuhiro, OKADA Atsushi, ICHIKAWA Kazuhide,

Secretary SENAMI Masato,

SAKAI Akiko,

Graduate
Students

TAKETA Akimichi (D1),
 IKEDA Daisuke (M2),
 KIUCHI Ryuta (D2),
 AITA Yuichi (D2),
 EGUCHI Makoto (M1),
 MINAMINO Akihiro (D3),
 IIDA Takashi (M2),
 ISHIHARA Chizue (M2),
 KONDO, Kazuhiro (D3),
 TOKUNARI Masao (D3),
 NAKAGAWA Noriyasu (D1),
 KONISHI Kohki (M2),
 KONYA Kenichiro (D2),
 KANZAKI Toru (D1),
 NAKAYAMA Kazunori (M2)
 SUGIYAMA Shohei (M1),

KIDO Eiji (M2),
 YAMAKAWA Yuichi (M1)
 YUKAWA Yohei (D1),
 OKUMURA Akira (D2),
 CHONAN Tsutomu (M1),
 TAKENAGA Yumiko (D2),
 MITSUKA Gaku (D1),

KASAHARA Kunihiko (D3),
 AKUTSU, Tomomi (D2),
 KIRIHARA Hiroyuki (M2),
 NAGAI Minoru (D2),
 TAKAHASHI Hiroyuki (M2),
 SAITO Osamu (D2),
 NAGANAWA Tatsuya (M2),

HIYAMA Kazunori (M2),

SAKO Takashi (M2),
 NODA Koji (D1),

UESHIMA Kota (M2),
 NISHINO Haruki (D1),

OKUTOMI Akira (D3),
 KAMAGASAKO Shogo (D1),
 AGATSUMA Kazuhiro (M2),

TAKAYAMA Tsutomu (D1),
 SEKIGUCHI Toyokazy (M2),
 IMAI Yuta (M1),

Administration
Division Staff

NAGANEO Nobuyoshi,
 IIDA Nobuyuki
 TASHIRO Megumi,
 MATSUMOTO Kenichi
 MARUMORI Yasuko

SASADA Noriaki,
 AKIMOTO Mari,
 AKIYAMA Makiko,
 KITA Aiko,

YAMAMOTO Tetsuya,
 IRIE Makoto,
 SAITO Akiko,
 KATO Yasuhiro,